Biological and Medical Physics, Biomedical Engineering

Bharat Bhushan

Biophysics of Skin and Its Treatments

Structural, Nanotribological, and Nanomechanical Studies

Springer

Biophysics of Skin and Its Treatments

More information about this series at http://www.springer.com/series/3740

BIOLOGICAL AND MEDICAL PHYSICS, BIOMEDICAL ENGINEERING

The fields of biological and medical physics and biomedical engineering are broad, multidisciplinary and dynamic. They lie at the crossroads of frontier research in physics, biology, chemistry, and medicine. The Biological and Medical Physics, Biomedical Engineering Series is intended to be comprehensive, covering a broad range of topics important to the study of the physical, chemical and biological sciences. Its goal is to provide scientists and engineers with textbooks, monographs, and reference works to address the growing need for information.

Books in the series emphasize established and emergent areas of science including molecular, membrane, and mathematical biophysics; photosynthetic energy harvesting and conversion; information processing; physical principles of genetics; sensory communications; automata networks, neural networks, and cellular automata. Equally important will be coverage of applied aspects of biological and medical physics and biomedical engineering such as molecular electronic components and devices, biosensors, medicine, imaging, physical principles of renewable energy production, advanced prostheses, and environmental control and engineering.

Bharat Bhushan

Biophysics of Skin and Its Treatments

Structural, Nanotribological, and Nanomechanical Studies

Springer

Bharat Bhushan
Nanoprobe Laboratory for Bio- &
Nanotechnology and Biomimetics
The Ohio State University
Columbus, OH
USA

ISSN 1618-7210 ISSN 2197-5647 (electronic)
Biological and Medical Physics, Biomedical Engineering
ISBN 978-3-319-45706-2 ISBN 978-3-319-45708-6 (eBook)
DOI 10.1007/978-3-319-45708-6

Library of Congress Control Number: 2016949581

Printed on acid-free paper

This Springer imprint is published by Springer Nature
The registered company is Springer International Publishing AG
The registered company address is: Gewerbestrasse 11, 6330 Cham, Switzerland

To my grandkids Sahana,
Ashwin, and Joya

Preface

Skin is the outer layer covering human or animal body and is a complex biological structure. Its function is to protect the body from physical and environmental assaults and to provide sensation, heat regulation, water resistance, and so on. Environmental conditions, such as dry and cold weather, can reduce the moisture content of skin and increase the skin roughness and physical discomfort. Skin is damaged as it goes through daily activities. Skin also ages with time. For healthy and beautiful human skin, cleaning and maintenance of skin is a daily process. Various beauty care products involve surface interaction between the product and the skin surface they are applied to. Skin cream is used to improve the skin health and create a smooth, soft, and flexible surface with moist perception by altering the surface roughness, adhesion, friction, elasticity, and surface charge of the skin surface. Rheology of skin cream as a function of cream thickness and strain rate and the binding interaction between skin cream and skin surface and operating environment are some of the important factors affecting the smooth feel and repair of the skin surface. The vibrations generated during the rubbing are a function of friction at the interface and govern the tactile perception of skin texture by the brain.

Atomic force microscopy (AFM) and nanoindentation have recently become important tools for studying micro-/nanoscale properties in beauty care, including human hair, hair conditioner, skin, and skin cream. In this book, we present an overview of the structural, nanotribological, and nanomechanical properties of skin with and without cream treatment as a function of operating environment. Relevant mechanisms are discussed. The result of a triboelectrification study of skin with and without cream treatment is presented. Next, an overview of attempts to develop a synthetic skin for research purposes is presented. Finally, data on tactile response of skin with and without cream treatment are presented.

This is the first book on nanotribological and nanomechanical properties of skin and skin treatment. The book is written for a novice in the field. It should serve as a reference book for researchers, practitioners, and users.

The author would like to thank his former students and senior colleagues who contributed to the research reported in the book. These include Prof. Shirong Ge, Dr. Wei Tang, Dr. Si Chen, and Shuyang Ding. The author would also like to thank Renee L. Ripley for many important contributions during the preparation of the manuscript.

Powel, OH, USA Bharat Bhushan

Contents

About the Author

Dr. Bharat Bhushan received an M.S. in mechanical engineering from the Massachusetts Institute of Technology in 1971; an M.S. in mechanics and a Ph.D. in mechanical engineering from the University of Colorado at Boulder in 1973 and 1976, respectively; an MBA from Rensselaer Polytechnic Institute at Troy, NY in 1980; Doctor Technicae from the University of Trondheim at Trondheim, Norway, in 1990; a Doctor of Technical Sciences from the Warsaw University of Technology at Warsaw, Poland, in 1996; and Doctor Honouris Causa from the National Academy of Sciences at Gomel, Belarus, in 2000 and University of Kragujevac, Serbia, in 2011. He is a registered professional engineer. He is presently an Ohio Eminent Scholar and The Howard D. Winbigler Professor in the College of Engineering, and the Director of the Nanoprobe Laboratory for Bio- & Nanotechnology and Biomimetics (NLB^2) and affiliated faculty in John Glenn College of Public Affairs at the Ohio State University, Columbus, Ohio. In 2013–2014, he served as an ASME/AAAS Science and Technology Policy Fellow, House Committee on Science, Space and Technology, United States Congress, Washington, DC. His research interests include fundamental studies with a focus on scanning probe techniques in the interdisciplinary areas of bio-/nanotribology, bio-/nanomechanics, and bio-/nanomaterials characterization and applications to bio-/nanotechnology, and biomimetics. He is an internationally recognized expert of bio-/nanotribology and bio-/nanomechanics using scanning probe microscopy and is one of the most prolific authors. He is considered by some a pioneer of the tribology and mechanics of magnetic storage devices. He has authored 8 scientific books, 90+ handbook chapters, 800+ scientific papers (Goggle Scholar h-index—105+ with 50k+ citations; Web of Science h-index—80+; ISI Highly Cited Researcher in Materials Science since 2007 and in Biology and Biochemistry, 2013; ISI Top 5% Cited Authors for Journals in Chemistry, 2011), and 60+ technical reports. He has also edited 50+ books and holds 20 US and foreign patents. He

is a coeditor of Springer NanoScience and Technology Series and coeditor of Microsystem Technologies, and member of Editorial Board of PNAS. He has given more than 400 invited presentations on six continents and more than 200 keynote/plenary addresses at major international conferences.

Dr. Bhushan is an accomplished organizer. He organized the Ist Symposium on Tribology and Mechanics of Magnetic Storage Systems in 1984 and the Ist Int. Symposium on Advances in Information Storage Systems in 1990, both of which are now held annually. He organized two international NATO institutes in Europe. He is the founder of an ASME Information Storage and Processing Systems Division founded in 1993 and served as the founding chair during 1993–1998. His biography has been listed in over two dozen Who's Who books including Who's Who in the World. He has received more than two dozen awards for his contributions to science and technology from professional societies, industry, and US government agencies including Life Achievement Tribology Award and Institution of Chemical Engineers (UK) Global Award. His research was listed as the top ten science stories of 2015. He is also the recipient of various international fellowships including the Alexander von Humboldt Research Prize for Senior Scientists, Max Planck Foundation Research Award for Outstanding Foreign Scientists, and Fulbright Senior Scholar Award. He is a foreign member of the International Academy of Engineering (Russia), Byelorussian Academy of Engineering and Technology, and the Academy of Triboengineering of Ukraine; an honorary member of the Society of Tribologists of Belarus and STLE; a fellow of ASME, IEEE, and the New York Academy of Sciences; and a member of ASEE, Sigma Xi, and Tau Beta Pi.

Dr. Bhushan has previously worked for Mechanical Technology Inc., Latham, NY; SKF Industries Inc., King of Prussia, PA; IBM, Tucson, AZ; and IBM Almaden Research Center, San Jose, CA. He has held visiting professorship at University of California at Berkeley; University of Cambridge, UK; Technical University Vienna, Austria; University of Paris, Orsay; ETH Zurich, EPFL Lausanne; University of Southampton, UK; University of Kragujevac, Serbia; Tsinghua University, China; Harbin Institute, China; and KFUPM, Saudi Arabia. https://nlbb.engineering.osu.edu/

Chapter 1
Introduction

Skin is the outer layer covering a human or animal body. It is the largest organ and for humans covers an average surface area of 1.5–2 m^2. Its function is to protect the body from physical and environmental assaults, and to provide sensation, heat regulation, water resistance, and other such functions. Skin ages over time, resulting in changes in skin properties. The skin aging process is the result of two biological processes called intrinsic aging, where changes accumulate over a lifetime, and extrinsic aging, attributed to environmental influences. Aging is a degeneration of tissue (such as degradation of mechanical properties as a result of decreases in collagen) and loss of lipids (responsible for creating a water barrier), and leads to various issues such as sagging skin and wrinkles. In addition to aging, skin also is damaged as it goes through various daily activities. Environmental conditions, such as dry and cold weather, can reduce the moisture content of skin temporarily, and can induce epidermal hyperplasia, mast cell degranulation, cytokine secretion, increased skin roughness, and physical discomfort (Harding et al. 2000; Leyden and Rawlings 2002; Tang and Bhushan 2010; Bhushan 2012; Bhushan et al. 2012).

For healthy and beautiful human skin, cleaning and maintenance of skin is a daily process. The demand for skin care products that prevent or relieve skin damage has created a $2 billion dollar industry in the U.S. alone, as of 2015. As commonly-used skin care products, skin cream and moisturizer increase the moisture content in the outer layer of skin. This hydration creates a smooth, soft, moist, and flexible surface, and alters the tribological properties (surface roughness, adhesion, friction, and wear) and mechanical properties (elastic modulus, hardness, and viscous damping) of the skin surface. Hydration changes the surface feel or tactile perception of cream treated skin when it touches a surface. Beauty care science is interested in the way in which skin cream changes the tribological and mechanical properties, tactile perception, and the effect of the operating environment of skin, as these properties are closely tied to product performance and, ultimately, guide consumers' likes or dislikes of the product (Bhushan et al. 2010,

B. Bhushan, *Biophysics of Skin and Its Treatments*, Biological and Medical Physics, Biomedical Engineering, DOI 10.1007/978-3-319-45708-6_1

2012; Tang and Bhushan 2010; Tang et al. 2010a, b; Bhushan and Tang 2011; Bhushan 2012; Chen and Bhushan 2013).

For a primer to tribology, see Appendix A.

1.1 Tribological and Mechanical Properties and Triboelectric Effects

The tribological and mechanical properties of human skin were reported as early as the 1950s (Naylor 1955). Since then, many studies have focused on evaluating the frictional properties of skin and the factors affecting friction. Friction is resistance to sliding in a contact, and is a measure of tactile perception (Bhushan 2001, 2013a, b). There are various factors that affect friction between skin and an object that comes into contact with it. For example, friction between skin and wet fabric is reported to be higher than that with dry fabric. To study the effects of age, sex, and anatomical region on frictional properties, various studies on human skin have been carried out (Cua et al. 1990; Sivamani et al. 2003b; Kwiatkowka et al. 2009). Cua et al. (1990) reported significant differences in friction within various anatomical regions—forehead, arm, palm, abdomen, back, thigh, and ankle.

Skin is affected easily by the environment. A high temperature and low humidity environment will increase the rate of transepidermal water loss, cause dehydration of the stratum corneum, and cause scaling, cracking, and electrostatic charging of skin surface. On the other hand, a high humidity environment hydrates the skin surface and creates soft, smooth, flexible, and healthy-looking skin with lower electrostatic charge build up. It is established that the state of skin hydration affects friction (Highley et al. 1977; Nacht et al. 1981; Cua et al. 1990; Gerhardt et al. 2008; Kwiatkowska et al. 2009). Dry skin exhibits lower friction than moist skin. With the application of water or moisturizer on a skin surface or in a humid environment, a positive linear correlation exists between skin moisture and the coefficient of friction. As compared to male skin, female skin shows higher moisture sensitivity and a higher coefficient of friction.

Studies have been carried out in order to quantify the efficiency of skin care products to study their effect on friction (EI-Shimi 1977; Cua et al. 1990; Zhang and Mak 1999; Koudine et al. 2000; Sivamani et al. 2003a, b; Tang et al. 2008, 2015; Bhushan 2012; Bhushan et al. 2012). Skin treatment increases the moisture content in the outer skin layer. The hydration creates a smooth, soft, and elastic surface leading to higher real area of contact, adhesion, and friction, which results in a change in tactile perception. Thus, after treatment, the skin surface is perceived as sticky or greasy, but because this change improves moistness, softness, and elasticity, the treated skin is perceived as more comfortable than virgin skin.

Since solid surfaces are not microscopically smooth, many interactions between skin-skin and other surfaces in contact take place at micro/nanoasperities with linear dimension ranging from a few hundred nm to hundreds of μm (Bhushan 2001, 2013a, b). Therefore, the study of the coefficient of friction and adhesive force on the nanoscale is useful because it allows for a better understanding of the

mechanisms behind how the skin cream interacts with skin. Atomic force microscopes (AFM) and nanoindenters have made it possible to study the tribological and mechanical properties of skin and evaluate the effect of cream on the nanoscale (Bhushan and Li 2003; Bhushan 2008, 2010a, b, 2011, 2012, 2013a, b). The AFM uses a sharp tip with a radius typically less than 10 nm, which allows the simulation of single asperity contact for measurement of the film thickness, friction, adhesion, and wear. A nanoindenter uses a sharp tip with a radius typically on the order of 50–100 nm, which allows measurement of mechanical properties on the nanoscale, relevant for individual asperity contacts.

Rat skin and pig skin are commonly used as substitutes for human skin for cosmetic research (Bhushan et al. 2010, 2012; Tang and Bhushan 2010; Tang et al. 2010a, b). In cosmetic science, synthetic skins are also used in place of human tissue. Various synthetic skins have been used for cosmetic research (Bhushan and Tang 2011; Chen and Bhushan 2013). Nanotribological and macrotribological data for skins with and without cream treatment as well as at various temperatures and humidities has been reported by Tang and Bhushan (2010), Tang et al. (2010a, b), and Bhushan et al. (2012). Nanomechanical data of various skins with and without cream treatments have been reported by Bhushan et al. (2010, 2012). These data are useful in bridging the gap between the nano- and macroscale data, as well as to gain an understanding of the mechanisms behind how skin cream interacts with skin.

It is well known that friction force is quantized with the number of molecular layers in very thin liquid films (Israelachvili et al. 1988). Cream rheology is expected to be a function of its thickness as well as the sliding velocity (shear thinning) and normal load during its application (Liu and Bhushan 2003; Tambe and Bhushan 2005; Tao and Bhushan 2007). Tang and Bhushan (2010), Tang et al. (2010a), and Bhushan et al. (2012) studied the effect of the effect of cream thickness, normal load, and velocity on the nanotribological properties of skin with and without cream treatment.

The mechanical properties of skin are of importance to prevent damage and maintain good feel. For example, mechanical properties influence skin's resistance to laceration during impact injury (Karlson 1982). They are important indicators of pathological situations. Precise knowledge of the mechanical properties of skin is also of interest to plastic surgeons in designing the size, shape, and orientation of skin grafts (Lanir and Fung 1974b). The mechanical properties of skin are affected by the level of hydration (Aubert et al. 1985; Murray et al. 1996; Dobrev 2000). Extensibility and viscoelasticity are markedly influenced by the water content of the stratum corneum, which is the top layer of skin. The main objective of the application of skin cream is to assist the stratum corneum in restoring lost moisture. Many macroscale studies have focused on the mechanical properties of skin with and without skin treatment such as elastic-plastic deformation behavior, hardness, Young's modulus of elasticity, time dependent creep, and relaxation properties (Lanir and Fung, 1974a, b; Dombi et al. 1993; Piérard et al. 1999; Őzyazgan et al. 2002, Del Prete et al. 2004; Sanders 1973; Diridollou et al. 1998; Pan et al. 1998; Falanga and Bucalo 1993). Nanoscale studies using an AFM and nanoindenter have

focused on the mechanical properties of skin with and without cream treatments (Yuan and Verma 2006; Kendall et al. 2007; Bhushan et al. 2010, 2012).

As skin is the outer layer of our body, it is the first line of defense against external objects. However, it often fails in contact with sharp objects (scratch action). AFM has been used to perform scratch tests on skin by Bhushan et al. (2010). The experiments have been performed to understand how skin with a cream film fails at light loads, and how the skin cream acts as a protective coating. In addition, in situ deformation experiments with an AFM to follow the progress on morphological changes and deformation in skin subjected to tensile loading have been carried out by Tang et al. (2010b).

In addition to change in the mechanical and tribological properties of skin by moistening and softening skin surface, skin cream also can reduce the electrostatic charges on skin surface. The stratum corneum of skin is a good insulator with high electrical resistance, around hundreds of kilo-ohms (Johnson and Corah 1963). Due to the high electrical resistance, charges on the skin surface are difficult to dissipate, especially in a low humidity environment. These electrostatic charges usually cause unpleasant and unhealthy effects, such as electric shocks, dry skin, headaches, and tiredness (Jonassen 1998). Skin cream is known to affect the electrical properties of skin. Understanding the mechanisms behind charge buildup and how to control it is a focal point in designing effective skin cream products.

The effect of skin cream on the electrical properties of skin surface on the macroscale has been studied (Blichmann et al. 1989; Lodén and Lindberg 1991; Sivamani et al. 2003a). Surface potential studies on the skin surface with and without skin cream and different humidity levels on the nanoscale have been carried out using AFM-based Kelvin probe method by Tang et al. (2010a, b). Nanoscale data allows for a better understanding of the mechanisms behind how skin cream interacts with skin and affects the electrical properties of skin. Since the charge is proportional to the contact surface potential (Son and Lee 2008), the change of surface potential can reflect the change of surface charge.

Macroscale rubbing is a general method to charge a sample surface and quantitatively evaluate the static charge during rubbing. Since there are also many microspherical particles in the environment interacting with skin surface and inducing static charge on the microscale, the triboelectrification of skin using microscale rubbing have also been used. Many investigations have reported the dependence of the charging behavior on friction, velocity, normal load, and rubbing time for insulator material, such as polymer, human hair, and animal skin (Wåhlin and Bäckström 1974; Ohara 1978; Ohara et al. 1990; Greason et al. 2004; Seshadri and Bhushan 2008b; Tang et al. 2010a, b).

1.2 Tactile Perception

Humans traditionally are described as possessing five senses (sight, smell, taste, hearing, and touch), each of which has a corresponding receptor organ (eyes, nose, tongue, ears, and skin, respectively). Tactile perception (also known as “somatic

sense" or "touch") is accomplished by the skin. Tactile perception of the surface as being soft and smooth is important in many applications, such as touch with skin or fabrics (Katz 1989; Hollins et al. 1998; Scheibert et al. 2009). Smooth skin is perceived as young skin. Therefore, most humans want smooth skin because it makes them look and feel younger. Though we describe tactile perception as a single sensation, it is the result of nervous response to the external stimuli causing stretch of the skin, pressure on the skin, temperature, and vibrations. To arrive at the perception that skin is smooth, our brains integrate data on skin's stretch, pressure, temperature, and vibrations.

When human skin touches human skin (whether between two people or when one person touches their own skin), the condition of the skin of both sides of the touch is of importance to the perception of that touch. Skin that is perceived as smooth is more pleasing to touch, and is more pleasing to have touch. As an example, if fingers touch a face, it is more pleasing to the owner of the face if the fingers are not rough, and it is more pleasing to the owner of the fingers if the face is smooth.

The perception and integration of the four sub-sensations of stretch, pressure, temperature, and vibration into a single sense of touch is affected by the interfacial condition between the skin receiving the stimulus and the object causing the stimulus. When skin is hydrated and an external stimulus is applied, those four sub-sensations can be perceived more acutely. When skin is dry, they may be perceived less acutely. This is important to the skin's functions of thermoregulation, injury prevention, general comfort, and other functions. Skin creams can increase the skin's hydration, and therefore its perception of external stimuli, providing faster and more critical responses.

When one applies skin cream to the body, interfacial friction results in vibrations carried by nerves to the brain. The brain perceives skin smoothness during the application of skin cream by sensing, among other things, skin vibrations. Therefore, a more direct measure of the degree of skin smoothness is to measure interface vibrations created during application and touch. Vibration data, which correlate to friction data, are presented.

1.3 Application of Skin Cream, Tactile Perception, and Role of Tribology

When skin cream is applied to the skin surface, the primary penetration pathway of cream compounds is through the intercellular lipids of the stratum corneum, though it does not exclude the possibility that the compounds can pass into the corneocytes (Bronaugh and Maibach 1999; Morganti et al. 2001); see Fig. 1.1. In terms of percutaneous absorption, the compounds of skin cream dissolve/partition into the surface lipids of the stratum corneum, diffuse through the lamellar domains of the stratum corneum, partition from the stratum corneum into the more hydrophilic

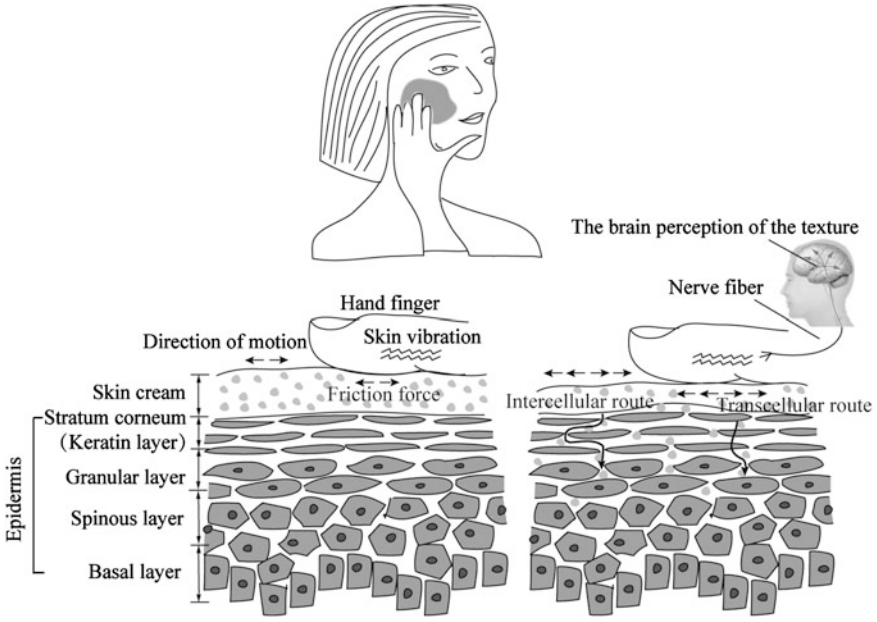

Fig. 1.1 Schematics illustrating the application process of skin cream, as well as the route of penetration of skin cream, and the relationship between skin vibration and brain perception of the skin texture (adapted from Tang and Bhushan 2010)

viable epidermis, and diffuse through the epidermis and dermis (Morganti et al. 2001). Through these interactions with skin, an efficient skin cream can cause a drastic change in tactile perception.

Figure 1.1 also schematically illustrates the application process of skin cream, along with the mechanisms behind the interaction that make friction important to the tactile perception of skin cream (Tang and Bhushan 2010). Skin cream is usually applied at a frequency of 1–10 Hz. Adhesion and friction properties are governed by the physical and chemical properties of both the skin and the rubbing surface. The vibrations in the process of rubbing are highly dependent on the friction and adhesion properties, as well as the dynamic viscosity of skin cream at the relevant film thickness and shear rate (Giasson et al. 1997; Luengo et al. 1997; Vicente et al. 2006). For moist, soft, and smooth skin after cream treatment, the friction and adhesion of skin would be higher than that for a dry, hard, and rough skin (EI-Shimi 1977; Nacht et al. 1981; Egawa et al. 2002; Bhushan 2012; Bhushan et al. 2012).

Usually there are three phases of tactile perception in the application process of skin cream: “slippery,” “sticky,” and “smooth or moist,” corresponding to the three phases of friction. In the initial phase, when skin cream is first applied, the cream film is relatively thick, and there is less asperity contact. The contact with the skin surface operates essentially in the hydrodynamic or mixed lubrication regime,

so the coefficient of friction is low, and the skin feels slippery. In the second phase, as the cream film becomes thinner and is absorbed, the contact with the skin transitions into the boundary lubrication regime. Meanwhile, the skin is moistened and softened by the cream, which results in high adhesive force and friction force, so the skin feels sticky prior to complete absorption. In the third phase, water evaporates from the skin, along with other physical and chemical changes resulting from the absorption of skin cream. In this phase, the coefficient of friction and adhesive force reduce such that skin no longer feels sticky, but not to pre-application levels, so skin instead feels smooth. The duration of the third phase is highly related to the quality of cream and the operating environment. For a high-performance cream, high friction may last for over a day, while for a low-performance cream, it may last for less than an hour. Tribological and mechanical studies provide a straightforward and valuable way to investigate how the properties of skin are altered with various skin care products.

The vibrations generated during the rubbing affect the tactile perception of the skin by the brain (Katz 1989; Hollins et al. 1998; Scheibert et al. 2009). Many studies show that there is a correlation between changes in the sensory perception and friction of skin (Tang et al. 2015; Ding and Bhushan 2016).

1.4 Organization of the Book

In this book, we present an overview of surface roughness, friction, adhesion, dynamic viscosity, and wear resistance (durability) of skin with and without cream treatment. The effect of cream thickness, velocity, normal load, temperature, and humidity on the adhesion, friction, nanomechanical properties, and surface charging of skin with and without cream treatment using an AFM and nanoindenter are summarized. Next, nanotribological and nanomechanical data on two relatively inexpensive synthetic skins with and without cream treatment is presented. Finally, data on tactile perception of skin with and without cream treatment is presented.

References

Aubert, L., Anthoine, P., Rigal, J. D., & Leveque, J. L. (1985). An in vivo assessment of the biomechanical properties of human skin modifications under the influence of cosmetic products. *International Journal of Cosmetic Science, 7*, 51–59.

Bhushan, B. (2001). *Modern Tribology Handbook, vol. 1—Principles of Tribology; vol. 2—Materials, Coatings, and Industrial Applications*. Boca Raton, Florida: CRC Press.

Bhushan, B. (2008). Nanoscale characterization of human hair and hair conditioners. *Progress in Materials Science, 53*, 585–710.

Bhushan, B. (Ed.). (2010a). *Springer Handbook of Nanotechnology* (3rd ed.). Heidelberg, Germany: Springer.

Bhushan, B. (2010b). *Biophysics of Human Hair—Structural, Nanomechanical and Nanotribological Studies*. Heidelberg, Germany: Springer.

Bhushan, B. (2011). *Nanotribology and Nanomechanics I—Measurement Techniques and Nanomechanics, II—Nanotribology, Biomimetics, and Industrial Applications* (3rd ed.). Heidelberg, Germany: Springer.

Bhushan, B. (2012). Nanotribological and nanomechanical properties of skin with and without skin cream treatment using atomic force microscopy and nanoindentation. *Journal of Colloid and Interface Science, 367*, 1–33.

Bhushan, B. (2013a). *Principles and Applications of Tribology* (2nd ed.). New York: Wiley.

Bhushan, B. (2013b). *Introduction to Tribology* (2nd ed.). New York: Wiley.

Bhushan, B., Chen, S., & Ge, S. (2012). Friction and durability of virgin and damaged skin with and without skin cream treatment using atomic force microscopy. *Beilstein Journal of Nanotechnology, 3*, 731–746.

Bhushan, B., & Li, X. (2003). Nanomechanical characterisation of solid surfaces and thin films. *International Materials Reviews, 48*, 125–164.

Bhushan, B., & Tang, W. (2011). Surface, tribological and mechanical characterization of synthetic skins for cosmetic science. *Journal of Applied Polymer Science, 120*, 2881–2890.

Bhushan, B., Tang, W., & Ge, S. (2010). Nanomechanical characterization of skin and skin cream. *Journal of Microscopy, 240*, 135–144.

Blichmann, C. W., Serup, J., & Winther, A. (1989). Effects of single application of a moisturizer: Evaporation of emulsion water, skin surface temperature, electrical conductance, electrical capacitance, and skin surface (emulsion) lipids. *Acta Dermato Venereologica, 69*, 327–330.

Bronaugh, R. L., & Maibach, H. I. (1999). *Percutaneous Absorption: Drugs—Cosmetics—Mechanisms—Methodology* (3rd ed.). New York: Marcel Dekker.

Chen, S., & Bhushan, B. (2013). Naonomechanical and nanotribological characterization of two synthetic skins with and without skin cream treatment using atomic force microscopy. *Journal of Colloid and Interface Science, 398*, 247–254.

Cua, A. B., Wilhelm, K. L., & Maibach, H. I. (1990). Frictional properties of human skin: Relation to age, sex, and anatomical region, stratum corneum hydration and transepidermal water loss. *British Journal of Dermatology, 123*, 473–479.

Del Prete, Z., Antoniucci, S., Hoffman, A., & Grigg, P. (2004). Viscoelastic properties of skin in Mov-13 and Tsk mice. *Journal of Biomechanics, 37*, 1491–1497.

Ding, S., & Bhushan, B. (2016). Tactile perception of skin and skin cream by friction induced vibrations. *Journal of Colloid and Interface Science*, *481*, 131–143.

Diridollou, S., Berson, M., Vabre, V., Black, D., Karlsson, B., Auriol, F., et al. (1998). An in vivo method for measuring the mechanical properties of the skin using ultrasound. *Ultrasound in Medicine and Biology, 24*, 215–224.

Dobrev, H. (2000). Use of cutometer to assess epidermal hydration. *Skin Research and Technology, 6*, 239–244.

Dombi, G. W., Haut, R. C., & Sullivan, W. G. (1993). Correlation of high-speed tensile strength with collagen content in control and lathyritic rat skin. *Journal of Surgical Research, 54*, 21–28.

Egawa, M., Oguri, M., Hirao, T., Takahashi, M., & Miyakawa, M. (2002). The evaluation of skin friction using a frictional feel analyzer. *Skin Research and Technology, 8*, 41–51.

EI-Shimi, A. F. (1977). In vivo skin friction measurements. *Journal of the Society of Cosmetic Chemists, 28*, 37–51.

Falanga, V., & Bucalo, B. (1993). Use of a durometer to assess skin hardness. *Journal of the American Academy of Dermatology, 29*, 47–51.

Gerhardt, L. C., Strassle, V., Lenz, A., Spencer, N. D., & Derler, S. (2008). Influence of epidermal hydration on the friction of human skin against textiles. *Journal of the Royal Society, Interface, 5*, 1317–1328.

Giasson, S., Israelachvili, J., & Yoshizawa, H. (1997). Thin film morphology and tribology study of mayonnaise. *Journal of Food Science, 62*, 640–646.

Greason, W. D., Oltean, I. M., Kucerovsky, Z., & Ieta, A. C. (2004). Triboelectric charging between polytetrafluoroethylene and metals. *IEEE Transactions on Industry Applications, 40*, 442–450.

Harding, C. R., Watkinson, A., & Rawlings, A. V. (2000). Dry skin, moisturization, and corneodesmolysis. *International Journal of Cosmetic Science, 22*, 21–52.

Highley, D. R., Cooney, M., DenBeste, M., & Wolfram, L. J. (1977). Frictional properties of skin. *Journal of Investigative Dermatology, 69*, 303–305.

Hollins, M., Bensmaïa, S. J., & Risner, S. R. (1998). The Duplex theory of tactile texture perception. In S. Grondin & Y. Lacouture (Eds.), *Proceedings of the Fourteenth Annual Meeting of the International Society for Psychophysics* (Fechner Day 98.) (pp. 115–120). Quebec, Canada: The International Society for Psychophysics.

Israelachvili, J. N., McGuiggan, P. M., & Homola, A. M. (1988). Dynamic properties of molecularly thin liquid films. *Science, 240*, 189–191.

Johnson, L. C., & Corah, N. L. (1963). Racial differences in skin resistance. *Science, 139*, 766–767.

Jonassen, N. (1998). *Electrostatics*. New York: Chapman & Hall.

Karlson, T. A. (1982). The influence of hospital-treated facial injuries from vehicles. *Journal of Trauma, 22*, 303–310.

Katz, D. (1989). *The World of Touch* (L. E. Krueger & Lawrence Erlbaum Associates, Inc., Trans.). Hillsdale, New Jersey.

Kendall, M. A. F., Chong, Y. F., & Cock, A. (2007). The mechanical properties of the skin epidermis in relation to targeted gene and drug delivery. *Biomaterials, 28*, 4968–4977.

Koudine, A. A., Barquins, M., & Anthoine, P. H. (2000). Frictional properties of skin: Proposal of a new approach. *International Journal of Cosmetic Science, 22*, 11–20.

Kwiatkowska, M., Franklin, S. E., Hendriks, C. P., & Kwiatkowski, K. (2009). Friction and deformation behaviour of human skin. *Wear, 267*, 1264–1273.

Lanir, Y., & Fung, Y. C. (1974a). Two-dimensional mechanical properties of rabbit skin-II. Experimental results. *Journal of Biomechanics, 7*, 171–182.

Lanir, Y., & Fung, Y. C. (1974b). Two-dimensional mechanical properties of rabbit skin. I. Experimental system. *Journal of Biomechanics, 7*, 29–34.

Leyden, J. J., & Rawlings, A. V. (Eds.). (2002). *Skin Moisturization*. New York: Marcel Dekker.

Liu, H., & Bhushan, B. (2003). Nanotribological characterization of molecularly thick lubricant films for applications to MEMS/NEMS by AFM. *Ultramicroscopy, 97*, 321–340.

Lodén, M., & Lindberg, M. (1991). The influence of a single application of different moisturizers on the skin capacitance. *Acta Dermato Venereologica, 71*, 79–82.

Luengo, G., Tsuchiya, M., Heuberger, M., & Israelachvili, J. (1997). Thin film rheology and tribology of chocolate. *Journal of Food Science, 62*, 767–772.

Morganti, P., Ruocco, E., Wolf, R., & Ruocco, V. (2001). Percutaneous absorption and delivery systems. *Clinics in Dermatology, 19*, 489–501.

Murray, B. C., & Wickett, R. R. (1996). Sensitivity of cutometer data to stratum corneum hydration level. A preliminary study. *Skin Research and Technology, 2*, 167–172.

Nacht, S., Close, J., Yeung, D., & Gans, E. H. (1981). Skin friction coefficient: Changes induced by skin hydration and emollient application and correlation with perceived skin feel. *Journal of the Society of Cosmetic Chemists, 32*, 55–65.

Naylor, P. F. D. (1955). The skin surface and friction. *British Journal of Dermatology, 67*, 239–248.

Ohara, K. (1978). Temperature and frictional speed dependence of frictional electrification between polymer films: Contribution of molecular motion of polymers to frictional electrification. *Journal of Electrostatics, 4*, 233–246.

Ohara, K., Tonouchi, T., & Uchiyama, S. (1990). Frictional electrification of thin films deposited by the Langmuir-Blodgett method. *Journal of Physics. D. Applied Physics, 23*, 1092–1096.

Őzyazgan, I., Liman, N., Dursun, N., & Gunes, I. (2002). The effects of ovariectomy on the mechanical properties of skin in rats. *Maturitas, 43*, 65–74.

Pan, L., Zan, L., & Foster, F. S. (1998). Ultrasonic and viscoelastic properties of skin under transverse mechanical stress in vitro. *Ultrasound in Medicine and Biology, 24*, 995–1007.

Piérard, G. E., Nizet, J. L., & Adant, J. P. (1999). Tensile properties of relaxed excised skin exhibiting striae distensae. *Journal of Medical Engineering & Technology, 23*, 69–72.

Sanders, R. (1973). Torsional elasticity of human skin in vivo. *Pflügers Archiv, 342*, 255–260.

Scheibert, J., Leurent, S., Prevost, A., & Debrégeas, G. (2009). The role of fingerprints in the coding of tactile information probed with a biomimetic sensor. *Science, 323*, 1503–1506.

Seshadri, I. P., & Bhushan, B. (2008). Effect of rubbing and load on nanoscale charging characteristics of human hair characterized by AFM based Kelvin probe. *Journal of Colloid and Interface Science, 325*, 580–587.

Sivamani, R. K., Goodman, J., Gitis, N. V., & Maibach, H. I. (2003a). Friction coefficient of skin in real-time. *Skin Research and Technology, 9*, 235–239.

Sivamani, R. K., Wu, G., Gitis, N., & Maibach, H. (2003b). Tribological testing of skin products: Gender, age, and ethnicity on the volar forearm. *Skin Research and Technology, 9*, 299–305.

Son, J. Y., & Lee, G. (2008). Writing nanotriboelectric charge bits on insulator surface. *Applied Physics Letters*, *93*, 173105-1–173105-2.

Tambe, N. S., & Bhushan, B. (2005). Friction model for the velocity dependence of nanoscale friction. *Nanotechnology, 16*, 2309–2324.

Tang, W., & Bhushan, B. (2010). Adhesion, friction and wear characterization of skin and skin cream using atomic force microscope. *Colloid Surface B, 76*, 1–15.

Tang, W., Bhushan, B., & Ge, S. (2010a). Friction, adhesion and durability and influence of humidity on adhesion and surface charging of skin and various skin creams using atomic force microscopy. *Journal of Microscopy, 239*, 99–116.

Tang, W., Bhushan, B., & Ge, S. (2010b). Triboelectrification studies of skin and skin cream using Kelvin probe microscopy. *Journal of Vacuum Science and Technology A, 28*, 1018–1028.

Tang, W., Ge, S., Zhu, H., Cao, X., & Li, N. (2008). The influence of normal load and sliding speed on frictional properties of skin. *Journal of Bionic Engineering, 5*, 33–38.

Tang, W., Zhang, J., Chen, S., Chen, N., Zhu, H., Ge, S., et al. (2015). Tactile perception of skin and skin cream. *Tribology Letters, 59*, 24.

Tao, Z., & Bhushan, B. (2007). Velocity dependence and rest time effect on nanoscale friction of ultrathin films at high sliding velocities. *Journal of Vacuum Science and Technology A, 25*, 1267–1274.

Vicente, J., Spikes, H. A., & Stokes, J. R. (2006). Viscosity ratio effect in the emulsion lubrication of soft EHL contact. *Journal of Tribology, 128*, 795–800.

Wåhlin, A., & Bäckströml, G. (1974). Sliding electrification of teflon by metals. *Journal of Applied Physics, 45*, 2058–2064.

Yuan, Y., & Verma, R. (2006). Measuring microelastic properties of stratum corneum. *Colloids Surfaces B: Biointerfaces, 48*, 6–12.

Zhang, M., & Mak, A. F. T. (1999). In vivo friction properties of human skin. *Prosthetics and Orthotics International, 23*, 135–141.

Chapter 2
Skin and Skin Cream

2.1 Skin

The skin is a highly complex organ that controls heat and water loss, as well as prevents admission of undesirable chemicals and microorganisms. In general, skin is composed of three distinct layers: subcutis (also called hypodermis), dermis, and epidermis (Sutton 1962; Bender 1991; Elsner et al. 1994, 2002; Pugliese 1996; Wilhelm et al. 1997; Harding et al. 2000; Lodén and Maibach 2000; Shai et al. 2001; Baumann 2002; Förster 2002; Leyden and Rawlings 2002; Fuchs and Raghavam 2002; Tang and Bhushan 2010). A schematic of skin structure is shown in Fig. 2.1. The subcutis lies under the dermis, and consists of adipose tissue or fat cells with a collagen partition. Its primary function is insulation and shock absorption. It is abundant in collagen and fat, which acts as an energy reservoir. The dermis lies below the epidermis and supports it structurally and nutritionally. It is a 3–5 mm thick layer composed of collagen, elastin, glycosaminoglycans (GAGs), salts, and water. It contains blood vessels, nerves, hair follicles, arrector pili muscle, sweat glands, and sebaceous glands. The epidermis is the outer layer of skin. It contains four distinct cellular layers: basal layer, spinous layer, granular layer, and stratum corneum (Tang and Bhushan 2010). Cells proliferate in the basal layer of the epidermis. Upon leaving the basal layer, cells start to differentiate and migrate upwards through the spinous layer and granular layer, finally reaching the stratum corneum, from which it is shed. The stratum corneum is the outermost layer of the skin and is 10–20 μm thick. It comes in contact with cosmetic products, fabrics, and a variety of other surfaces (Tang and Bhushan 2010). It is the most important layer to tribologists.

Figure 2.2a shows the structure, nerves, and receptors in skin (Gardner et al. 2000). Beneath the epidermis there are mechanoreceptors and nerve endings that detect stimuli from the skin surface. A breakthrough in our understanding of the

B. Bhushan, *Biophysics of Skin and Its Treatments*, Biological and Medical Physics, Biomedical Engineering, DOI 10.1007/978-3-319-45708-6_2

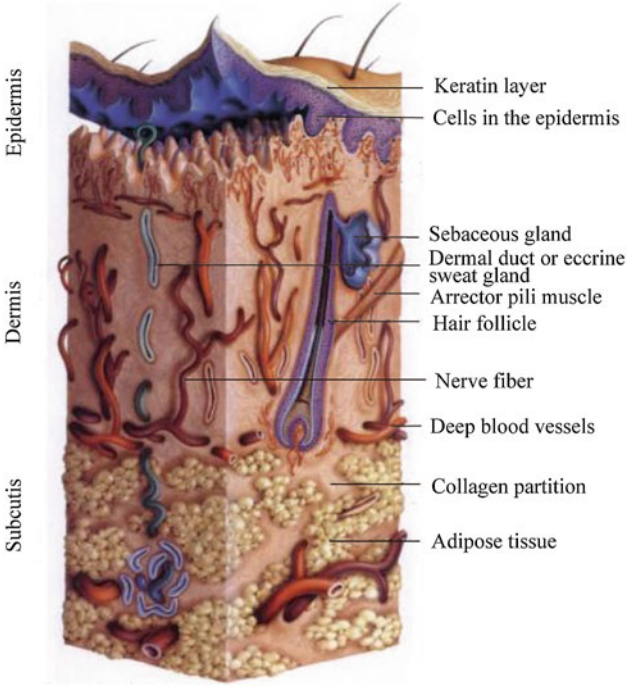

Fig. 2.1 Schematic of skin structure with different layers: subcutis, dermis, and epidermis (Shai et al. 2001)

coding of roughness perception has been made with the experimental confirmation of Katz's historical proposition of the existence of two independent coding channels that are specific for the perception of fine and coarse textures (Katz 1989; Hollins et al. 2001; Hollins and Bensmaïa 2007). Fine textures (<200 μm) are mediated by the rapidly adapting (RA) mechanoreceptors comprising the Meissner's corpuscle and Pacinian corpuscle. Coarse textures (with features of lateral dimensions larger than about 200 μm) are mediated by the slowly adapting (SA) mechanoreceptors, which include the Merkel disk receptor and Ruffini ending (Lederman and Taylor 1972). They are differentiated into classes, depending on their receptive fields (Gardner et al. 2000) shown in Fig. 2.2b: Type I with small receptive fields, and Type II with large fields. The superficial dermis and subcutaneous tissue each contain a RA and SA mechanoreceptor. The superficial dermis contains both Type I mechanorecepters, the Meissner's corpuscle (RA I) and the Merkel Disk (SA I), whereas the subcutaneous tissue contains the Type II mechanoreceptors, the Pacinian corpuscle (RA II) and the Ruffini ending (SA II). These mechanoreceptors detect skin stretch, compressive stress, vibration, and stretch direction, respectively. The function of these mechanoreceptors and related features are presented in Table 2.1 (Dargahi and Najarian 2004; Francomano et al. 2013).

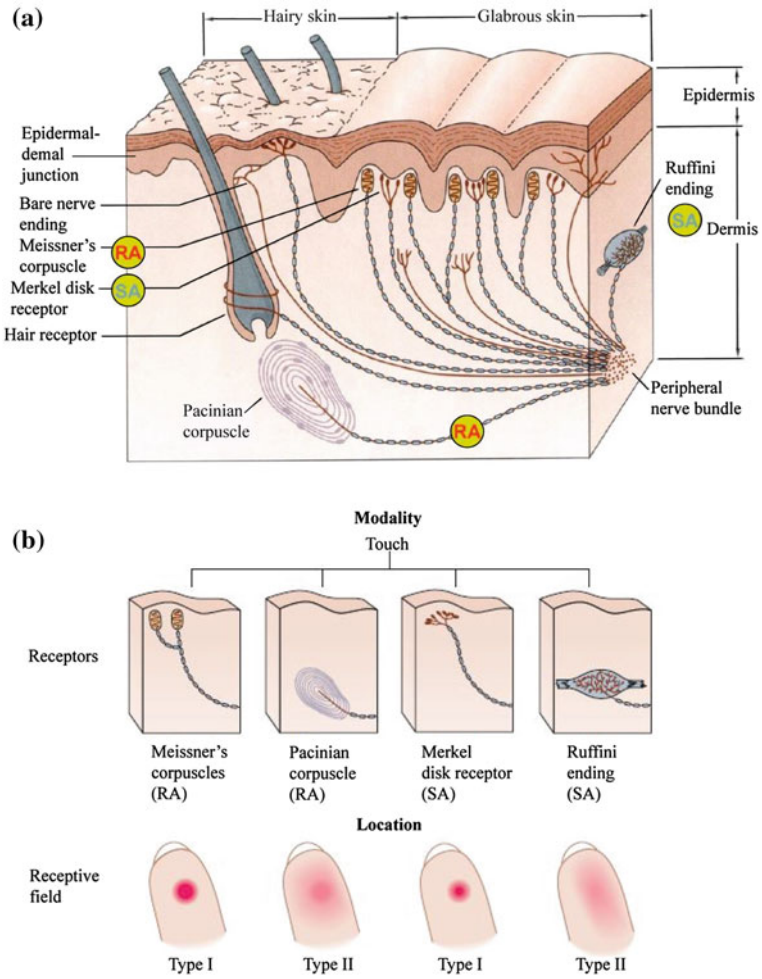

Fig. 2.2 Schematic of **a** skin structure with epidermis and dermis layers, and different mechanoreceptors: Meissner's corpuscle, Pacinian corpuscle, Merkel disk, and Ruffini ending, and **b** modality and location of various receptors (adapted from Gardner et al. 2000; Dargahi and Najarian 2004)

Rat skin and pig skin are common models used for human skin in health and cosmetic sciences. Figure 2.3 shows the epidermis and dermis of rat skin, indicating four layers of epidermis (Tang and Bhushan 2010) and pig skin (Lawson et al. 2007). The figure also shows the chemical structure of the major components of the stratum corneum. Corneocytes with lipid bilayers exist in the stratum corneum. Undamaged skin is covered with a thin, hydrophobic lipid layer on its outer layer containing triglycerides, diglycerides, fatty acids, wax esters, squalene, cholesterol, and cholesterol esters (Downing et al. 1969). The intercellular lipids act as a water

Table 2.1 The function of mechanoreceptors and related features (adapted from Dargahi and Najarian 2004; Francomano et al. 2013)

Receptor types	Class	Receptive field (mm^2)	Receptors per cm^2	Frequency range (Hz)	Detected parameter
Meissner's corpuscle	RA type I	1–100	140	10–60	Skin stretch
Pacinian corpuscle	RA type II	10–1000	21	50–1000	Vibration
Merkel disk	SA type I	2–100	70	0–30	Compressive stress
Ruffini endings	SA type II	10–500	49	0–15	Skin stretch direction

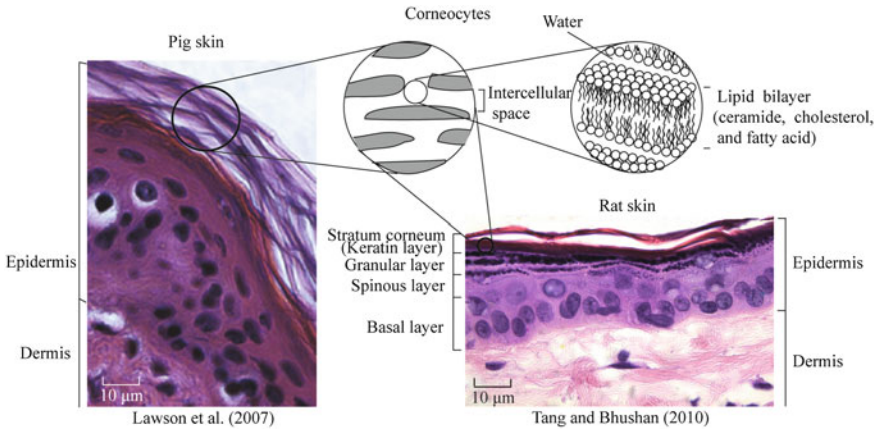

Fig. 2.3 Histology of pig skin (*left*) (Lawson et al. 2007) and rat skin (*right*) (Tang and Bhushan 2010). Also shown is the chemical structure of the major components of the stratum corneum. The intercellular lipids present act as a water barrier

barrier and play an essential role in the establishment or maintenance of water-retention capacity in the stratum corneum (Elias and Friend 1975; Imokawa et al. 1989; Harding et al. 2000).

Figure 2.4 shows the chemical structure of the major lipid components of the stratum corneum (Förster 2002). The variations in the levels and types of stratum corneum lipids lead directly to poor skin condition (Rawlings et al. 1994). For example, atopic dermatitis and acne are associated with low levels of ceramide-1 linoleate (Imokawa et al. 1991), while xerosis, especially in winter, is associated with an increase of fatty acids and a reduction of ceramides (Rawlings et al. 1993). Water is also a crucial factor to the stratum corneum barrier function and structure (Leyden and Rawlings 2002). In soft and flexible skin, the water content of the

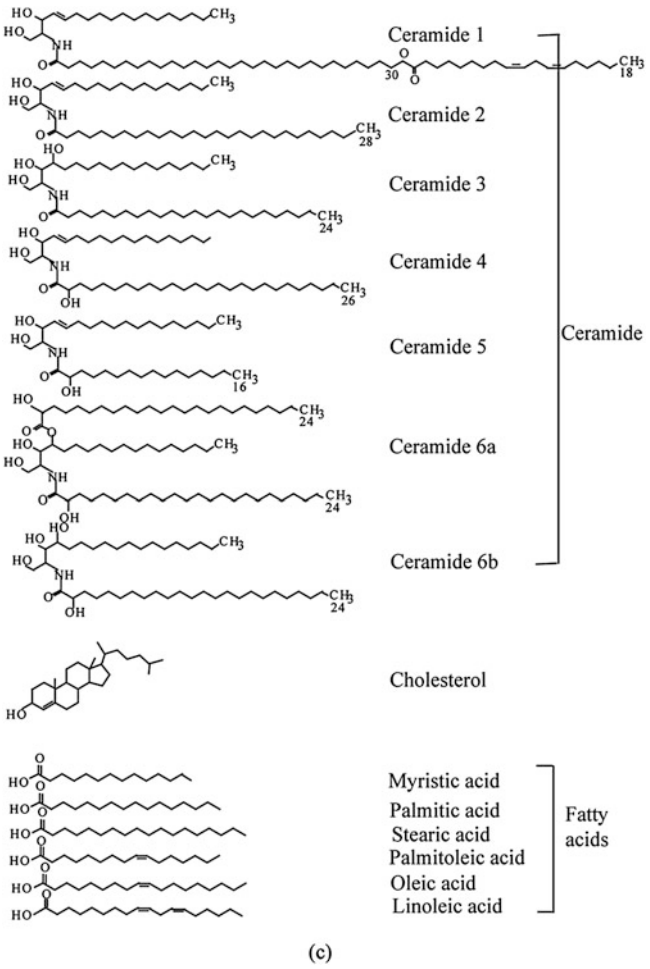

Fig. 2.4 Chemical structure of major lipid components of the stratum corneum (Förster 2002)

stratum corneum is between 10 and 30% (Elsner et al. 1994). If insufficient water remains in the stratum corneum, it leads to epidermal hyperplasia, mast cell degranulation, and cytokine secretion. These issues are considered harmful to the tribological requirement for healthy and desirable skin. Therefore, the main objectives of skin cream development are (1) to assist the stratum corneum in restoring lost moisture and the regular packing of the lipid lamellae, (2) normalizing cellular turnover, and (3) repairing the function of skin and creating an improved feel of skin.

Table 2.2 Selected surface properties of virgin rat and pig skin samples

	Virgin rat skin	Virgin pig skin
RMS (nm)[a]	148 ± 6	274 ± 10
Nanohardness (MPa)[a]	7 ± 1	19 ± 3
Elastic modulus (MPa)[a]	70 ± 7	91 ± 28
Stratum corneum thickness (μm)[b]	5.0 ± 0.8	12.3 ± 0.7
Epidermis thickness (μm)[b]	21.7 ± 2.2	51.9 ± 1.5
Number of hair follicles (per cm^2)[b]	289 ± 21	11 ± 1

[a]Bhushan et al. (2012)
[b]Monterio-Riviere (2007)

2.2 Pig and Rat Skin

Porcine (pig) skin is considered a good model for human skin, and is commonly used for studies of aesthetic repair, percutaneous absorption of cosmetics and drugs, other biomedical research (Pflucker and Hohenberg 1999; Braye et al. 2001; Yuan and Verma 2006) and tribological research (Bhushan et al. 2012). Domestic pig skin resembles human skin in general micromorphology, histochemistry, and epidermal cell kinetics. It has been reported to be the most suitable model for human skin because of its similar surface properties, such as body mass and skin-to-body surface-area ratio, sparse hair, thick epidermis, hair-follicle density, epidermal turnover kinetics, lipid composition and the biophysical properties of the lipids (Monterio-Riviere 2007; Stahl et al. 2009), and similar permeability, i.e., the fluxes through the skin and concentrations in the skin are of the same order of magnitude for both tissues (Bartek 1972; Schmook et al. 2001).

Murine (rat) skin has also been used as an animal model in studies of mechanical (Vogel and Denkel 1985; Belkoff and Haut 1991; Kendall et al. 2007; Bhushan et al. 2010) and tribological properties (Tang and Bhushan 2010; Tang et al. 2010). Further, rat skin has been used to study the percutaneous absorption of cosmetics and drugs (Yourick and Bronaugh 1997; Yourick et al. 2008).

Table 2.2 shows selected surface properties of virgin rat and pig skin. The stratum corneum and epidermis of pig skin are thicker than those of rat skin, and pig skin has fewer hair follicles than rat skin. Pig skin and rat skin have been compared for percutaneous absorption of cosmetics and drugs (Bartek et al. 1972; Schmook et al. 2001), epidermal barrier layer lipids and morphology (Monterio-Riviere 2007; Stahl et al. 2009).

2.3 Skin Cream

Skin care products are used to moisturize the skin surface. Skin cream can result in a smooth, soft skin surface and help the stratum corneum restore lost moisture and supplement the barrier lipids. Table 2.3 shows the function of various common skin

Table 2.3 Function of various common skin cream ingredients (Rawlings et al. 2004)

Type	Ingredients	Formula	Function
Humectants	Glycerin (glycerol)	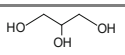	– Attracts and holds water in the skin, acting on the inside out (i.e., moisture from the dermis to the epidermis/stratum corneum) and on the outside in (i.e., moisture from the environment to the skin)
	Lactic acid		
	Sodium pyrrolidone carboxylic acid	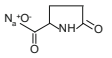	
	Ammonium lactate	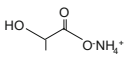	
	Potassium lactate	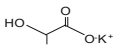	
	Sorbitol	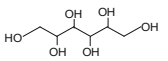	
	Urea	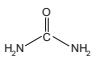	
Occlusives	Petrolatum	Mixture of hydrocarbons; C_nH_{2n+2}	– Forms a layer on the surface of the skin and moisturizes by retarding the evaporation of water – Increases the penetration of lipophilic steroids into the skin by hydrating the lipid-filled intercellular spaces in the stratum corneum
	Mineral oil	Mixture of liquid hydrocarbons from petroleum	
	Dimethicone	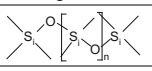	
	Caprylic/capric triglyceride	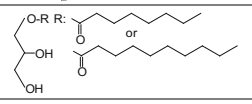	
Emollients	Glycol stearate	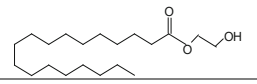	– Gives skin a soft and smooth feel by hydrating the stratum corneum and filling the spaces between desquamation corneocytes
	Glyceryl stearate	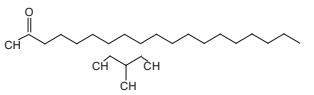	
	Lanolin	Mixture of mainly esters diesters, hydroxy esters, lanolin alcohols, lanolin acids, and lanolin hydrocarbons	
	Sunflower seed oil glycerides	Mixture of mono-, di-, and triglycerides derived from sunflower seed oil	

cream ingredients, and Table 2.4 shows the typical compositions of common skin creams (Rawlings et al. 2004). Humectants, occlusives, and emollients are the three basic components used in skin cream. Skin creams are primarily emulsions of oil in water or water in oil. These emulsions are formed by adding surfactants or emulsifiers that aid in mixing the humectants, occlusives, and emollients (Leyden and Rawlings 2002). Many other ingredients are added as well to meet the needs of the

Table 2.4 Typical compositions of common skin creams (Rawlings et al. 2004)

	Range of percentage content[a]	
Component	Hand and body products	Face care products
Water	50–88 (85)	50–85 (80)
Humectants (primarily glycerin)	1–44 (6)	2–10 (5)
Emollients/occlusives	1.5–35 (2)	2–15 (4)
Surfactant network	3–9 (6)	0–19 (6)
Silicone	0–7 (1)	0–10 (2)
Polymer/thickener	0–3 (0.3)	0–4 (0.3)
Preservatives	0.2–0.7 (0.5)	0.3–1.4 (0.4)
Fragrance	0–0.5 (0.2)	0–0.5 (0.2)

[a]Number in parentheses correspond to "typical" of oil in water cream

consumer. Humectants are a component of skin creams that can increase the moisture retention of stratum corneum and reduce the incidence of dry and flaky skin in vivo (Middleton and Roberts 1978). Humectants in skin cream attract and hold water in the skin, acting on the inside (i.e., moisture from the dermis to the epidermis/stratum corneum) and on the outside (i.e., moisture from the environment to the skin) (Rawlings et al. 2004). Glycerin, lactic acid, potassium lactate, urea, sodium PCA, and propylene glycol are the humectants in common skin creams (Leyden and Rawlings 2002). In general, polyols are the most effective humectants, especially the trihydroxylated molecule glycerol. Moisturizers containing glycerol provide enduring moisturization by binding and retaining water or by minimizing of water loss. Glycerol can also hinder crystal-phase transitions induced by humidity in stratum corneum lipids, and thus enhance the function of the skin as a barrier. In healthy skin, as corneocytes migrate to the skin surface they mature from a fragile to a resilient phenotype. When moisturizers are used, however, the corneocytes may still mature to the resilient phenotype. It has been demonstrated through in vivo studies that moisturizers containing glycerol promote the maturation of these corneocytes, probably by activating the residual transglutaminase activity retained within the stratum corneum (Rawlings et al. 2004).

As an illustration of a typical cream structure, Fig. 2.5 shows the gel structures of an oil-in-water-type cream (Rieger and Rhein 1997; Kónya et al. 2003). The oil-in-water-type cream stabilized with an emulsifier is at least a four-phase system: crystalline/hydrophilic gel phase, bulk water layer, lipophilic gel phase, and dispersed oil phase (Kónya et al. 2003). The crystalline/hydrophilic gel phase is composed of bilayers of a surfactant and fatty amphiphile. Water molecules are inserted between the bilayers, and thus the interlamellar water layer is formed. Bulk water is mainly fixed mechanically by the hydrophilic gel phase and is in equilibrium with the interlamellarly fixed water in the gel phase. The lipophilic gel phase is the excess of the fatty amphiphile, which is not part of the hydrophilic gel phase. It builds up a matrix with lipophilic characteristics. Generally, dispersed oil phase is immobilized mechanically from the lipophilic gel phase.

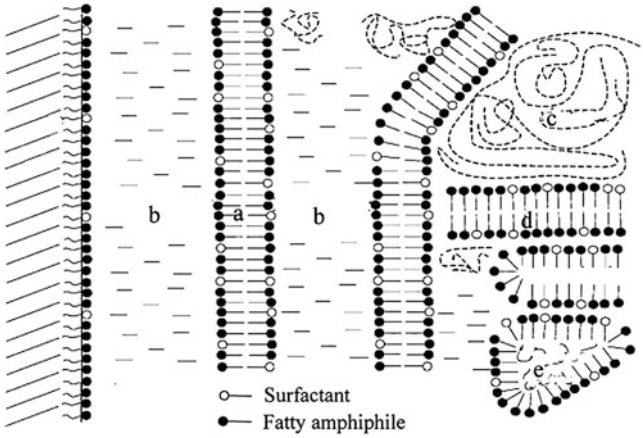

a: mixed crystal bilayer of surfactant and fatty amphiphile
b: interlamellarly fixed water layer
a+b: crystalline/hydrophilic gel phase
c: bulk water
d: lipophilic gel phase
e: dispersed oil phase

Fig. 2.5 Typical gel structures of oil-in-water-type cream (Kónya et al. 2003; Rieger and Rhein 1997)

2.4 Synthetic Skin for Cosmetics Science

In the medical and cosmetic industries, skin models are needed for permeation and toxicity studies, in treatment of wounds, and for skin replacement in burns (Netzlaff et al. 2005; Batheja et al. 2006). Given that human skin provides prevention of desiccation and protection against environmental hazards (e.g., bacteria, chemicals, and UV radiation), a synthetic skin is of interest. It should have a barrier function, permeability, and reaction to environmental hazards the same as human skin. Besides the use for medical applications, synthetic skin is needed as a human tissue substitute in cosmetic science to study the tribological properties of skin and hair during development and assessment of skin and hair care products and development and assessment of textiles' feel (Barry et al. 1992; Jermann et al. 2002; Bhushan et al. 2005; LaTorre and Bhushan 2005; Bhushan 2008, 2010; Gerhardt et al. 2009; Nonomura et al. 2009; Horiuchi et al. 2009; Bhushan and Tang 2011; Chen and Bhushan 2013). The selected formulation should have film-forming ability, should simulate properties of interest, and respond to cosmetic treatment similar to natural skin. However, they do not need to be as similar to skin as in medical applications.

Real human skin and animal skin present ethical issues in their use, are hard to obtain, expensive, and give highly variable results due to individual skin variability. For this reason, there is a great need for the development of synthetic skin. The first synthetic skin was invented by Burke et al. (1981) and was created to treat burn victims. Many other synthetic skin substitutes have been developed since then for medical use (Heimbach et al. 1988; Sheridan et al. 1994; Wainwright 1995; Gentzkow et al. 1996; Eaglstein and Falanga 1997; Choi et al. 1999a, b; Sheridan and Tompkins 1999; Chou et al. 2001; Jones et al. 2002; Kumar et al. 2004; Someya et al. 2004; Mansbridge 2006). Human skin equivalent for these studies is in vitro cultured skin that is essentially living skin that is grown in vitro, also referred to as 3-D living skin equivalents. Various types of skin equivalents are commercially available as Episkin™ (L'Oreal, France), SkinEthic™ (SkinEthic, Nice, France), and Epiderm™ (MatTek Corporation, Ashland, MA, USA). These are epidermis-only models, and attempts have been made to produce full skin models (Curren et al. 2005). Unfortunately, production of tissue-engineered materials is a complicated process.

For cosmetics research use, various synthetic and natural materials have been evaluated as skin substitutes such as poly(vinyl chloride), polyethylene, poly(tetrafluoroethylene) (Teflon™), poly(methyl methacrylate), polycarbonate, polyurethane, polyglycolic acid (Dexon™), polyglactin-910 (Vicryl™), polyamide (Nylon™), silicon, collagen, cellulose-acetate, catgut, and gelatin films (Jones et al. 2002; Lir et al. 2007; Bhushan 2008, 2010). A gelatin based synthetic film (with protein from an animal skin) developed initially at Procter & Gamble is commercially available as Vitro-Skin™ (IMS, Inc. Milford, Conn., USA). It is commonly used for evaluation of skin care products including suntan lotion and cleansing formulations (e.g., Turner et al. 2004; Wakefield and Stott 2006). Lir et al. (2007) proposed a formulation of synthetic skin which was molded on the replica of human skin to obtain appropriate topography.

To evaluate the nanotribological and nanomechanical properties of various relatively inexpensive synthetic skins for cosmetic science, tribological studies have been carried out by Bhushan and Tang (2011) and Chen and Bhushan (2013).

References

Barry, T. R., David, D., & Michael, R. (1992). An in vitro method for screening sunscreen formulations for sun protection factor using a full-thickness skin model. *Journal of the Society of Cosmetic Chemists, 43*, 307–312.

Bartek, M. J., LaBudde, J. A., & Maibach, H. I. (1972). Skin permeability in vivo: Comparison in rat, rabbit, pig and man. *Journal of Investigative Dermatology, 58*, 114–123.

Batheja, P., Song, Y., Michniak, B., & Kohn, J. (2006). A Bioengineered Human Skin Equivalent (HSE) for the Evaluation of Protectants. Accession No. ADA481863, Defense Technical Information Center, Fort Belvoir, VA.

Baumann, L. (2002). *Cosmetic Dermatology: Principles and Practice*. New York: McGraw-Hill.

Belkoff, S. M., & Haut, R. C. (1991). A structural model used to evaluate the changing microstructure of maturing rat skin. *Journal of Biomechanics, 24*, 711–720.

Bender, M. (1991). *Interfacial Phenomena in Biological Systems*. New York: Marcel Dekker.

Bhushan, B. (2008). Nanoscale characterization of human hair and hair conditioners. *Progress in Materials Science, 53*, 585–710.

Bhushan, B. (2010). *Biophysics of Human Hair—Structural, Nanomechanical and Nanotribological Studies*. Heidelberg, Germany: Springer.

Bhushan, B., Chen, S., & Ge, S. (2012). Friction and durability of virgin and damaged skin with and without skin cream treatment using atomic force microscopy. *Beilstein Journal of Nanotechnology, 3*, 731–746.

Bhushan, B., & Tang, W. (2011). Surface, tribological and mechanical characterization of synthetic skins for cosmetic science. *Journal of Applied Polymer Science, 120*, 2881–2890.

Bhushan, B., Tang, W., & Ge, S. (2010). Nanomechanical characterization of skin and skin cream. *Journal of Microscopy, 240*, 135–144.

Bhushan, B., Wei, G., & Haddad, P. (2005). Friction and wear studies of human hair and skin. *Wear, 259*, 1012–1021.

Braye, F. M., Stefani, A., Venet, E., Pieptu, D., Tissot, E., & Damour, O. (2001). Grafting of large pieces of human reconstructed skin in a porcine model. *British Journal of Plastic Surgery, 54*, 532–538.

Burke, J. F., Yannas, I. V., Quinby, W. C., Bondoc, C. C., & Jung, W. K. (1981). Successful use of a physiologically acceptable artificial skin in the treatment of extensive burn injury. *Annals of Surgery, 194*, 413–428.

Chen, S., & Bhushan, B. (2013). Naonomechanical and nanotribological characterization of two synthetic skins with and without skin cream treatment using atomic force microscopy. *Journal of Colloid and Interface Science, 398*, 247–254.

Choi, Y. S., Hong, S. R., Lee, Y. M., Song, K. W., Park, M. H., & Nam, Y. S. (1999a). Study on gelatin-containing artificial skin: I. Preparation and characteristics of novel gelatin-alginate sponge. *Biomaterials, 20*, 409–417.

Choi, Y. S., Hong, S. R., Lee, Y. M., Song, K. W., Park, M. H., & Nam, Y. S. (1999b). Studies on gelatin-containing artificial skin: II. Preparation and characterization of cross-linked gelatin-hyaluronate sponge. *Journal of Biomedical Materials Research, 48*, 631–639.

Chou, T., Chen, S., Lee, T., Chen, S., Cheng, T., Lee, C., et al. (2001). Reconstruction of burn scar of the upper extremities with artificial skin. *Plastic and Reconstructive Surgery, 108*, 378–384.

Curren, R. D., Mun, G., Gibson, D. P., & Aardema, M. J. (2005). Development of a novel micronucleus assay in the human 3-D skin model, EpiDerm™. *The Toxicologist, 84*, 453–464.

Dargahi, J., & Najarian, S. (2004). Human tactile Perception as a standard for artificial tactile sensing—A review. *The International Journal of Medical Robotics and Computer Assisted Surgery, 1*, 23–35.

Downing, D. T., Strauss, J. S., & Pochi, P. E. (1969). Variability of the chemical composition of skin surface lipids. *Journal of Investigative Dermatology, 53*, 322–327.

Eaglstein, W. H., & Falanga, V. (1997). Tissue engineering and the development of Apligraf®, a human skin equivalent. *Clinical Therapeutics, 19*, 894–905.

Elias, P. M., & Friend, D. S. (1975). The permeability barrier in mammalian epidermis. *The Journal of Cell Biology, 65*, 180–191.

Elsner, P., Berardesca, E., & Maibach, H. I. (Eds.). (1994). *Bioengineering of the Skin: Water and the Stratum Corneum*. Boca Raton, Florida: CRC Press.

Elsner, P., Berardesca, E., Wilhelm, K. P., & Maibach, H. I. (Eds.). (2002). *Bioengineering of the Skin: Skin Biomechanics*. Boca Raton, Florida: CRC Press.

Förster, T. (Ed.). (2002). *Cosmetic Lipids and the Skin Barrier*. New York: Marcel Dekker.

Francomano, M. T., Accoto, D., & Guglielmelli, E. (2013). Artificial sense of slip—A review. *IEEE Sensors Journal, 13*, 2489–2498.

Fuchs, E., & Raghavan, S. (2002). Getting under the skin of epidermal morphogenesis. *Nature Reviews Genetics, 3*, 199–209.

Gardner, E., Martin, J., & Jessell, T. (2000). The bodily senses. In E. Kandel, J. Schwartz, & T. Jessell (Eds.), *Principles of Neural Science* (pp. 430–450). York: McGraw-Hill New.

Gentzkow, G. D., Iwasaki, S. D., Hershon, K. S., Mengel, M., Prendergast, J. J., Ricotta, J. J., et al. (1996). Use of dermagraft, a cultured human dermis, to treat diabetic foot ulcers. *Diabetes Care, 19*, 350–354.

Gerhardt, L. C., Schiller, A., & Müller, B. (2009). Fabrication, characterisation and tribological investigation of artificial skin surface lipid films. *Tribology Letters, 34*, 81–93.

Harding, C. R., Watkinson, A., & Rawlings, A. V. (2000). Dry skin, moisturization, and corneodesmolysis. *International Journal of Cosmetic Science, 22*, 21–52.

Heimbach, D., Luterman, A., Burke, J., Cram, A., Herndon, D., Hunt, J., et al. (1988). Artificial dermis for major burns. A multi-center randomized clinical trial. *Annals of Surgery, 208*, 313–319.

Hollins, M., & Bensmaïa, S. J. (2007). The coding of roughness. *Canadian Journal of Experimental Psychology, 61*, 184.

Hollins, M., Bensmaïa, S. J., & Washburn, S. (2001). Vibrotactile adaptation impairs discrimination of fine, but not coarse, textures. *Somatosensory & Motor Research, 18*, 253–262.

Horiuchi, K., Kashimoto, A., & Tsuchiya, R. (2009). Relationship between tactile sensation and friction signals in cosmetic foundation. *Tribology Letters, 36*, 113–123.

Imokawa, G., Abe, A., Jin, K., Higaki, Y., Kawashima, M., & Hidano, A. (1991). Decreased level of ceramides in stratum corneum of atopic dermatitis: An etiologic factor in atopic dry skin. *Journal of Investigative Dermatology, 96*, 523–526.

Imokawa, G., Akasaki, S., Minematsu, Y., & Kawai, M. (1989). Importance of intercellular lipids in water-retention properties of the stratum-corneum—Induction and recovery study of surfactant dry skin. *Archives of Dermatological Research, 281*, 45–51.

Jermann, R., Toumiat, M., & Imfeld, D. (2002). Development of an in vitro efficacy test for self-tanning formulations. *International Journal of Cosmetic Science, 24*, 35–42.

Jones, I., Currie, L., & Martin, R. (2002). A guide to biological skin substitutes. *British Journal of Plastic Surgery, 55*, 185–193.

Katz, D. (1989). *The World of Touch* (L. E. Krueger & Lawrence Erlbaum Associates, Inc., Trans.). Hillsdale, New Jersey.

Kendall, M. A. F., Chong, Y. F., & Cock, A. (2007). The mechanical properties of the skin epidermis in relation to targeted gene and drug delivery. *Biomaterials, 28*, 4968–4977.

Kónya, M., Sorrenti, M., Ferrari, F., Rossi, S., & Csóka, I. (2003). Study of the microstructure of O/W creams with thermal and rheological methods. *Journal of Thermal Analysis and Calorimetry, 73*, 623–632.

Kumar, R. J., Kimble, R. M., Boots, R., & Pegg, S. P. (2004). Treatment of partial-thickness burns: A prospective, randomized trial using Transcyte™. *ANZ Journal of Surgery, 74*, 622–626.

LaTorre, C., & Bhushan, B. (2005). Nanotribological characterization of human hair and skin using atomic force microscopy. *Ultramicroscopy, 105*, 155–175.

Lawson, L. B., Freytag, L. C., & Clements, J. D. (2007). Use of nanocarriers for transdermal vaccine delivery. *Clinical Pharmacology and Therapeutics, 82*, 641–643.

Lederman, S. J., & Taylor, M. M. (1972). Fingertip force, surface geometry, and the perception of roughness by active touch. *Perception and Psychophysics, 12*, 401–408.

Leyden, J. J., & Rawlings, A. V. (Eds.). (2002). *Skin Moisturization*. New York: Marcel Dekker.

Lir, I., Haber, M., & Dodiuk-Kenig, H. (2007). Skin surface model material as a substrate for adhesion-to-skin testing. *Journal of Adhesion Science and Technology, 21*, 1497–1512.

Lodén, M., & Maibach, H. I. (Eds.). (2000). *Dry Skin and Moisturizers: Chemistry and Function*. Boca Raton, Florida: CRC Press.

Mansbridge, J. (2006). Commercial considerations in tissue engineering. *Journal of Anatomy, 209*, 527–532.

Middleton, J. D., & Roberts, M. E. (1978). Effects of a skin cream containing the sodium salts of pyrrolidone carboxylic acid on dry and flaky skin. *Journal of the Society of Cosmetic Chemists, 29*, 201–205.

Monterio-Riviere, N. A. (2007). 4 anatomical factors affecting barrier function. In H. Zhai, K. Wilhelm, & H. I. Maibach (Eds.), *Marzulli and Maibach's Dermatotoxicology* (7th ed., pp. 39–50). Boca Raton, Florida: CRC Press.

Netzlaff, F., Lehr, C. M., Wertz, P. W., & Schaefer, U. F. (2005). The human epidermis models EpiSkin®, SkinEthic® and Epiderm®: An evaluation of morphology and their suitability for testing phototoxicity, irritancy, corrosivity, and substance transport. *European Journal of Pharmaceutics and Biopharmaceutics, 60*, 167–178.

Nonomura, Y., Fujii, T., Arashi, Y., Miura, T., Maeno, T., Tashiro, K., et al. (2009). Tactile impression and friction of water on human skin. *Colloids and Surfaces B: Biointerfaces, 69*, 264–267.

Pflucker, F., & Hohenberg, H. (1999). The outermost stratum corneum layer is an effective barrier against dermal uptake of topically applied micronized titanium dioxide. *International Journal of Cosmetic Science, 21*, 399–411.

Pugliese, P. T. (Ed.). (1996). *Physiology of the Skin*. Illinois: Allured Pub Carol Stream.

Rawlings, A. V., Canestrari, D. A., & Dobkowski, B. (2004). Moisturizer Technology versus clinical performance. *Dermatologic Therapy, 17*, 49–56.

Rawlings, A. V., Mayo, A. M., Rogers, J., & Scott, J. R. (1993). Aging and the seasons influence stratum corneum lipid levels. *Journal of Dermatological Science, 101*, 483–490.

Rawlings, A. V., Scott, I. R., Harding, C. R., & Bowser, P. A. (1994). Stratum corneum moisturization at the molecular level. *Journal of Investigative Dermatology, 103*, 731–740.

Rieger, M. M., & Rhein, L. D. (1997). *Surfactants in Cosmetics* (2nd ed.). New York: CRC Press.

Schmook, F. P., Meingassner, J. G., & Billich, A. (2001). Comparison of human skin or epidermis models with human and animal skin in in-vitro percutaneous absorption. *International Journal of Pharmaceutics*, *215*, 51–56.

Shai, A., Maibach, H. I., & Baran, R. (2001). *Handbook of Cosmetic Skin Care*. London: Martin Dunitz.

Sheridan, R. L., Hegarty, M., Tompkins, R. G., & Burke, J. F. (1994). Artificial skin in massive burns-results to ten years. *European Journal of Plastic Surgery, 17*, 91–93.

Sheridan, R. L., & Tompkins, R. G. (1999). Skin substitutes in burns. *Burns, 25*, 97–103.

Someya, T., Sekitani, T., Iba, S., Kato, Y., Kawaguchi, H., & Sakurai, T. (2004). A large-area, flexible pressure sensor matrix with organic field-effect transistors for artificial skin applications. *Proceedings of the National Academy of Sciences of the United States of America, 101*, 9966–9970.

Stahl, J., Niedorf, F., & Kietzmann, M. (2009). Characterisation of epidermal lipid composition and skin morphology of animal skin ex vivo. *European Journal of Pharmaceutics and Biopharmaceutics, 72*, 310–316.

Sutton, R. L. (1962). *The Skin: A Handbook*. New York: Doubleday.

Tang, W., & Bhushan, B. (2010). Adhesion, friction and wear characterization of skin and skin cream using atomic force microscope. *Colloid Surface B, 76*, 1–15.

Turner, R. B., Biedermann, K. A., Morgan, J. M., Keswick, B., Ertel, K. D., & Barker, M. F. (2004). Efficacy of organic acids in hand cleansers for prevention of rhinovirus infections. *Antimicrobial Agents and Chemotherapy, 48*, 2595–2598.

Vogel, H. G., & Denkel, K. (1985). In vivo recovery of mechanical properties in rat skin after repeated strain. *Archives of Dermatological Research, 277*, 484–488.

Wainwright, D. J. (1995). Use of an acellular allograft dermal matrix (alloderm) in the management of full-thickness burns. *Burns, 21*, 243–248.

Wakefield, G., & Stott, J. (2006). Photostabilization of organic UV-absorbing and anti-oxidant cosmetic components in formulations containing micronized manganese-doped titanium oxide. *Journal of Cosmetic Science, 57*, 385–395.

Wilhelm, K. P., Elsner, P., Berardesca, E., & Maibach, H. I. (Eds.). (1997). *Bioengineering of the Skin: Skin Surface Imaging and Analysis*. Boca Raton, Florida: CRC Press.

Yourick, J. J., & Bronaugh, R. L. (1997). Percutaneous absorption and metabolism of coumarin in human and rat skin. *Journal of Applied Toxicology, 17*, 153–158.

Yourick, J. J., Jung, C. T., & Bronaugh, R. L. (2008). In vitro and in vivo percutaneous absorption of retinol from cosmetic formulations: Significance of the skin reservoir and prediction of systemic absorption. *Toxicology and Applied Pharmacology, 231*, 117–121.

Yuan, Y., & Verma, R. (2006). Measuring microelastic properties of stratum corneum. *Colloids Surfaces B: Biointerfaces, 48*, 6–12.

Chapter 3
Experimental Techniques

3.1 Animal Skins and Skin Creams

3.1.1 Animal Skin

Pig skin is commonly used as a model in aesthetic repair and percutaneous absorption of cosmetics and drugs (Pflucker and Hohenberg 1999; Braye et al. 2001; Yuan and Verma 2006). Rat skin has also been used as an animal model in the mechanical property studies of skin (Papir et al. 1975; Vogel and Denkel 1985; Belkoff and Haut 1991; Kendall et al. 2007) and percutaneous absorption of cosmetics and drugs (Yourick and Bronaugh 1997; Kraeling and Bronaugh 2005; Yourick et al. 2008). For tribological and mechanical property studies, Bhushan et al. (2010), Tang and Bhushan (2010), Tang et al. (2010a, b), and Bhushan and Tang (2011) used rat skin as the animal model. Bhushan et al. (2012) and Chen and Bhushan (2013) used pig skin as the animal model in their studies.

Male rats and pigs were sacrificed by overdosing them with carbon dioxide. The dorsal skin was immediately excised, subcutaneous tissues were scraped off with scissors, and the hair was shaved carefully. Then, the skin was gently cleaned with a 10% (v/v) soap solution (liquid dishwashing detergent) and rinsed with tap water for 30 s and leveled on the table to dry in an ambient condition (22 °C, RH 35–40%). After that, the skin was rinsed with a commercial facial cleanser treatment (Clean & Clear Shine Control facial cleanser). The facial cleanser was applied evenly down the skin surface with a cotton swab. Skin was lathered for 30 s and rinsed with tap water for 60 s. Then, the skin was leveled on the table and dabbed with Kimwipes^{TM} to remove excess water. After that, the skin was cut into 10 mm × 10 mm size samples. The thickness of the virgin skin sample was about 0.7 mm. For the AFM studies, the sample was mounted on AFM sample pucks with a rapid drying glue (Bhushan et al. 2010, 2012; Tang and Bhushan 2010;

B. Bhushan, *Biophysics of Skin and Its Treatments*, Biological and Medical Physics, Biomedical Engineering, DOI 10.1007/978-3-319-45708-6_3

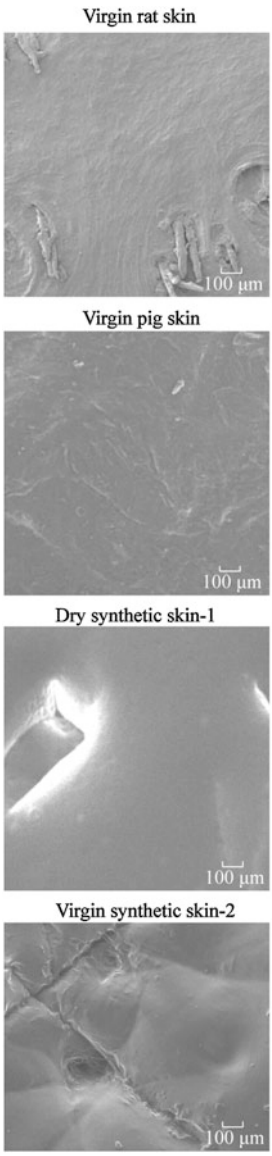

Fig. 3.1 SEM images of the surface of the virgin rat skin, virgin pig skin, dry synthetic skin-1, and virgin synthetic skin-2 (Chen and Bhushan 2013)

Tang et al. 2010a). For the surface potential test, the sample was mounted on the AFM sample puck with a rapid drying glue on insulating electrical tape (Tang et al. 2010a, b). Scanning electron microscope (SEM) images of the rat skin and pig skin are shown in Fig. 3.1.

3.1.2 Damaged Skin

A dry (damaged) skin can be realized by repeated skin wash with harsh soaps/detergents containing sodium lauryl sulfate (SLS) or by sodium dodecyl sulfate (SDS) surfactant (Fulmer and Kramer, 1986; Imokawa et al. 1989; Egawa et al. 2002) or by 20 min of treatment of the skin with acetone/ether (1/1), which causes removal of skin lipids and induces a chapped and scaly appearance. SEM studies of SDS-treated stratum corneum revealed selective depletion of the lipids from the intercellular spaces, accompanied by marked disruption of multiple lamellae structures. Lipids analysis showed a considerable and selective loss of intercellular lipids such as cholesterol, cholesterol ester, free fatty acid, and sphingolipids (Fulmer and Kramer 1986; Imokawa et al. 1989). Another approach is to use sticky cellophane tape to remove upper layers of skin, which also results in skin damage and scaly appearance after one day (Denda et al. 1992; Alikhan et al. 2010). Tape stripping has been reported to produce results similar to treatment with a surfactant of a 5% aqueous solution of SDS under an occlusive dressing for 4 h (Denda et al. 1992).

In a study by Bhushan et al. (2012), SDS was chosen to prepare damaged skin without any inflammatory reaction accompanied by a significant decrease in its water-retention function. To produce a controllably damaged skin sample, a 5% weight aqueous solution of SDS, prepared by adding 5 g SDS (Bio-Rad Laboratories, Hercules, CA) into 100 g demineralized distilled water was applied to the virgin skin surface by rubbing with a cotton swab for 30 s. The skin was allowed to dry for 10 min, and then the process was repeated once.

3.1.3 Various Skin Creams and Cream Treatment Procedure

3.1.3.1 Rat Skin—Virgin

Bhushan et al. (2010), Tang and Bhushan (2010), and Tang et al. (2010a, b) used up to six categories of skin samples in their tests: virgin skin and skin treated with pure lanolin, pure petroleum jelly, oil free skin cream (Clinique Moisture Surge Extended Thirst Relief), common skin cream (Vaseline Intensive Care Lotion), and aqueous glycerin (weight fraction = 1/4). Since lanolin, petroleum jelly, and glycerin are three typical ingredients used in skin cream and can be separately used as skin cream, these three ingredients were chosen as test skin creams to compare with two commercial skin creams (oil free skin cream and common skin cream). Table 3.1 shows the ingredients of the various skin creams.

Table 3.1 Compositions of various skin creams (based on manufacturer information)

Skin cream	Compositions
Pure lanolin	Lanolin
Pure petroleum jelly	Petroleum jelly
Oil free skin cream	Water, Cyclopentasiloxane, Butylene glycol, Glycerin, Betula alba, Silybum marianum, Camellia sinensis, Saccharomyces lysate, Sucrose, Aloe Barbadensis, Trehalose, Hydroxyethyl urea, Sorbitol, Oleth-10, Tromethamine, Caffeine, Hydrogenated lecithin, Sodium Hyaluronate, Tocopheryl acetate, Palmitoyl oligopeptide, Caprylyl glycol, Dimethicone, Glyceryl polymethacrylate, PEG-8, Ammonium acryloyldimethyltaurate/VP Copolymer, Magnesium ascorbyl phosphate, Carbomer, Hexylene glycol, Disodium EDTA, Phenoxyethanol, Hydrolyzed extensin
Common skin cream	Water, Glycerin, Stearic acid, Helianthus Annuus seed oil, Glycine soja, Lecithin, Tocopheryl acetate, Retinyl palmitate, Urea, Collagen amino acids, Sodium stearoyl lactylate, Sodium isostearoyl lactate, Mineral oil, Sodium PCA, Potassium lactate, Lactic acid, Petrolatum, Dimethicone, Avena sativa, Keratin, Glyceryl stearate, Cetyl alcohol, Methyl palmitate, Magnesium aluminum silicate, Fragrance, Carbomer, Stearamide amp, Triethanol amine, Corn Oil, Methylparaben, DMDM Hydantoin, Disodium EDTA, BHT, Propylene glycol, Titanium dioxide
Aqueous glycerin	Water and glycerin

Virgin skin was considered to be a baseline specimen. For the film thickness study on the nanoscale for common skin cream (Vaseline Intensive Care Lotion), 0.1, 0.2, 0.3, 0.4, and 0.5 mg of skin cream was applied on 1 cm^2 area and rubbed throughout the skin surface for 30 s with a cotton swab, resulting in approximately 80, 150, 240, 330, and 450 nm of cream film thickness, respectively (Tang and Bhushan 2010). For all other studies on the nanoscale, 0.2 mg of skin cream ($\sim$150 nm film thick) were applied on 1 cm^2 area. For the film thickness study on the macroscale for common cream treatment, 1, 1.5, 2, 2.5, and 3 mg of skin cream were applied on a 1 cm^2 area of skin surface, resulting in approximately 0.92, 1.4, 1.8, 2.3, and 2.8 μm of cream film thickness, respectively (Tang and Bhushan 2010). For all other macroscale studies, 1.5 mg of skin cream was applied on 1 cm^2 area with approximately 1.4 μm in thickness. The samples were measured immediately after cream application. For each type of cream treated skin, three skin samples were tested, and three different sample areas were chosen randomly and measured.

It is important to note that because of the heterogeneous nature of skin, certain factors will induce scatter in the measurement data. For example, lipid coverage of corneocyte surface cells is non-uniform and the water content is heterogeneously distributed over the skin (Caspers et al. 2003; Williams and Barry 2004). For cream treated skin, the cream layer is non-uniform on the skin surface, and it gets continuously absorbed by skin, resulting in a change of film thickness.

3.1.3.2 Rat Skin and Pig Skin—Virgin and Damaged

Bhushan et al. (2012) used four categories of skin samples in their tests: virgin skin, treated virgin skin, damaged skin, and treated damaged skin for both rat and pig skin. Virgin skin and damaged skin were treated with common skin cream, which was rubbed over the entire skin surface for 30 s with a cotton swab. For the nanoscale tests, 0.2 mg of a common skin cream (Vaseline Intensive Care Lotion) was applied to obtain a 150 nm film thickness. On the macroscale, 2 mg was applied forming a film of 1.8 μm thickness (Tang and Bhushan 2010). The same methodology was used both on rat and pig skin.

3.2 Synthetic Skin Samples

As discussed earlier, synthetic skin is of interest for cosmetic research as animal skin may be hard to obtain, expensive, and give highly variable results due to individual skin variability. Chen and Bhushan (2013) selected two synthetic skin formulations for their study, and, similar to pig and rat skin discussed earlier, both synthetic skins were treated with a common skin cream. Measurements were taken on samples with and without a common cream treatment to study their response and to compare with rat skin and pig skin. Synthetic skin samples were cut into 10 mm × 10 mm size for study.

3.2.1 Synthetic Skin-1

Synthetic skin labeled as synthetic skin-1 is Vitro-Skin™ (Bhushan and Tang 2011; Chen and Bhushan 2013). It is a synthetic (non-biological) product that effectively mimics the surface properties of human skin. It contains both optimized protein and lipid components and is designed to have topography, pH, critical surface tension and ionic strength similar to human skin (Jermann et al. 2002). It must be used following a specific hydration procedure. Vitro-Skin was cut into 6.2 cm × 9.0 cm rectangles and hydrated for 12 h in an IMS, Inc., hydration chamber containing a 15% glycerin solution in water.

Vitro-Skin™ has been successfully applied in a broad range of in vitro methods including evaluation of skin care products such as suntan lotion (Wakefield et al. 2004; Wakefield and Stott 2006; Beasley and Meyer 2010), cleansing formulations (Turner et al. 2004), the measurement of Sun Protection Factor (SPF) and Ultraviolet A (UVA) protection factors (Springsteen et al. 1999; Hanson et al. 2006; Garoli et al. 2009), assessment of the performance of sunless tanning formulations (Ferrero et al. 2002; Nesseem 2011), evaluation of the performance of adhesive bandages (Wokovich et al. 2008), and assessment of prototype and emollient

spreading (Chaudhuri et al. 2006; Cohen et al. 2009). Testing done on Vitro-Skin is generally more reproducible than that performed on human skin due to the consistent topography and wetting properties across each sheet.

Both hydrated (referred to as wet synthetic skin-1) and not hydrated (referred to as dry synthetic skin-1) samples were tested in a study by Chen and Bhushan (2013) in order to assess possible differences. A SEM image of the surface of the dry synthetic skin-1 is shown in Fig. 3.1. Synthetic skin-1 is hairless, but consists of a number of pits on the surface.

3.2.2 Synthetic Skin-2

A second synthetic skin was produced based on the method presented by Lir et al. (2007), and supplied by Souroushian and Lu (2009). Gelatin plasticized by glycerol, polysaccharides and a mixture of lipids were used that mimic the skin's lipid structure and to create a hydrophobic surface.

The fabrication procedure follows. First, a silicon replica technique was used to create a mold with the surface topography of real skin. A biocompatible silicone liquid (Flexico, a division of Davis Healthcare Services, UK), purchased from Cuderm Corporation, Dallas, Texas (Soroushian and Lu, 2009), was applied to the facial skin of a healthy, male 24-year-old volunteer for 20 min. Next, the silicone was peeled off the skin to obtain a mold with the surface topography of real skin. This provides a negative replica of the real skin. The replica was cut and glued to a Petri dish for casting of the synthetic skin.

Next, a casting blend was poured over the mold to create a positive replica (Lir et al. 2007). The casting blend was produced from gelatin from pig skin (bloom/gel strength = 175 Bloom[1]; Sigma Aldrich), glycerol (Sigma Aldrich), formaldehyde as 37% water solution (Sigma-Aldrich), Prolipid 141[2] (ISP Global Technologies, Wayne, NJ; Herbarie, Prosperity, SC), and Natrosol 250 HHX PHARM (Hercules), and was prepared as follows. A 1% gelatin solution was made by dissolving 5 g of gelatin in 495 ml of 55 °C deionized water. The pH was adjusted to 9.0 using 1 mol NaOH. 8 g of Natrosol®, and 0.2 g of glycerol were added to the solution and stirred for 2 min. Then 0.4 g of Prolipid were dissolved in 2 ml of hot ethyl alcohol at 60 °C for 5 min and then mixed with the gelatin solution. Next, 2 ml of formaldehyde solution was added and stirred for 1 min. The blend was cast on the mold and dried at room temperature for 20 h in a chemical hood, followed by vacuum drying to a constant weight (Soroushian and Lu 2009).

[1]Bloom is a test used to measure the strength of a gel or gelatin. The test determines the weight (in grams) needed by a probe (normally with a diameter of 12.7 mm) to deflect the surface of the gel 4 mm without breaking it. The result is expressed in Bloom (grades).

[2]Prolipid 141 is composed of glyceryl stearate, behenyl alcohol, palmitic acid, stearic acid, lecithin, lauryl alcohol, myristyl alcohol and cetyl alcohol.

A SEM image of the surface of the virgin synthetic skin-2 is shown in Fig. 3.1. There are trenches on the surface of synthetic skin-2.

3.3 Physical Characterization

Skin hydration changes contact angle with a water droplet, and has been measured for skin in various states. The viscosity of skin cream describes a fluid's internal resistance to flow, which affects friction. Viscosity of various creams was measured to relate to friction. Cream film thickness distribution is of importance, and has been mapped on cream treated surfaces. Tribological properties (surface roughness, adhesion, friction, wear resistance, and scratch resistance), mechanical properties (hardness, Young's modulus, and in situ tensile measurements), and electrical properties (surface potential) have been measured to understand their role on tactile perception. Friction, wear, and surface potential measurements were made on the nanoscale and macroscale to develop a fundamental understanding of the interfacial process, as well as to study scale effects. Experiments were performed at various humidities and temperatures.

3.3.1 Contact Angle Measurements

Tang and Bhushan (2010), Bhushan and Tang (2011), Bhushan et al. (2012) and Chen and Bhushan (2013) measured apparent contact angles for various samples. Measurements were made with a Rame-Hart automated goniometer model 290-F4, where 5 μL water droplets were deposited onto the sample surface and the contact angle was measured.

3.3.2 Dynamic Viscosity Measurements

Tang et al. (2010a) measured the dynamic viscosity of pure lanolin, pure petroleum jelly, oil free skin cream, and common skin cream using a strain-controlled rheometer (TA Instruments, New Castle, DE (ARES LS2)) with a torque transducer (0.02–200 g cm) and normal force transducer (2–2000 g). Parallel plate configuration with 50 mm diameter plates was used for the measurements. The gap was kept in the range of 0.8–0.9 mm for all tests. The range of shear rate was 0.1–30 s^{-1}. Because of the low viscosity, the dynamic viscosity of aqueous glycerin was measured with the Couette configuration (27 mm diameter cup and 25 mm diameter bob) instead of parallel plates (Tang et al. 2010a). The range of shear rate

was 15–300 s^{-1}. All measurements were carried out at about 25 °C and relative humidity (RH) 55%.

3.3.3 Nanoscale Surface Roughness, Friction, Adhesive Force, and Wear Resistance Measurements

Tang and Bhushan (2010), Tang et al. (2010a, b), Bhushan and Tang (2011), Bhushan et al. (2012), and Chen and Bhushan (2013) conducted experiments using a commercial AFM system (Dimension Nanoscope IIIa, Veeco, Santa Barbara, CA) in ambient conditions (22 °C, RH 55%). A force modulation etched square pyramidal Si tip of nominal 10 nm radius attached to the end of a Si cantilever beam (RFESP or rotated force-modulation etched silicon probe, spring constant of 3 N/m, Bruker) was used. The quantitative measurement of friction force was made using the method described by Palacio and Bhushan (2010) and Bhushan (2011). The friction force measurements were made over a scan length of 10 μm and at a scan rate of 1 Hz (resisting in a scanning velocity of 20 μm/s) at various normal load increments ranging from 25 to 250 nN. By plotting the friction force as a function of normal load, an average coefficient of friction was obtained from the slope of the fit line of the data. For each sample, a minimum of six measurements were made. The $\pm 1\sigma$ values were presented in the data points.

Tang et al. (2010a) measured the adhesive force from the horizontal intercept of the friction force versus normal load curve at a zero value of friction force, since the friction force F is governed by the relationship:

$$F = \mu(W + F_a) \tag{3.1}$$

where μ is the coefficient of friction, W is the applied normal load, and F_a is the adhesive force (horizontal intercept). This adhesive force value serves as an average over the course of the full scan profile and differs slightly from the adhesive force which is calculated from the force distance curve.

To study the wear resistance (durability) of the skin with and without cream treatment, the coefficient of friction and adhesive force as a function of the number of sliding cycles were measured by Tang and Bhushan (2010), Tang et al. (2010a), and Bhushan et al. (2012) over a scan length of 10 μm at a normal load of 250 nN, scanning rate of 1 Hz (resulting in a scanning velocity of 20 μm/s), and in ambient conditions (22 °C, RH 55%). A total of 3800 cycles were performed. Changes in the coefficient of friction and adhesive force were monitored during the durability tests as a measure of degradation. It was observed that both the coefficient of friction and adhesive force increase with an application of the skin cream. The stable values correspond to higher wear resistance.

As a result of the duration of the cream treatment on skin, the film thickness changes. The change in film thickness leads to a change in the friction and adhesion

of skin surface, which also affects the wear resistance. To study the effect of the duration of the cream treatment on skin for various skin creams, the film thickness as a function of time was measured in ambient conditions (22 °C, RH 55%) by Tang et al. (2010a). Film thickness was measured by the mapping technique described in the next subsection. A 3×3 force distance curve array (total 9 measurement points) was collected over a scan area of 1×1 μm with a 1 Hz scan rate for each test point.

Nanoscale velocity effect tests were carried out using an AFM and an ultrahigh velocity stage by Tang and Bhushan (2010). The low velocity effect tests were carried out by changing the scan frequency of the AFM from 0.1 to 50 Hz while the scan size was maintained at 10 μm, which allowed the velocity to vary from 2 to 1000 μm/s (Tang and Bhushan 2010; Bhushan et al. 2012). An ultrahigh velocity stage was incorporated with the AFM in order to achieve the high velocity (Tao and Bhushan 2007). On the ultrahigh velocity stage, the velocity varied from 1000 to 2×10^5 μm/s on a 1000 μm scan length. 1000 μm is the minimum scan length to achieve a velocity of 2×10^5 μm/s.

In the nanoscale normal load effect tests, the normal load was varied from 50 to 750 nN at a 10 μm scan length and a 20 μm/s scanning velocity by Tang and Bhushan (2010) and Bhushan et al. (2012).

3.3.4 *Film Thickness, Adhesive Forces, and Young's Modulus Mapping*

A RFESP silicon probe was used for film thickness and adhesion force measurements, and Young's modulus mapping by Tang and Bhushan (2010), Tang et al. (2010a), and Chen and Bhushan (2013). The typical radius of a square pyramidal Si tip is less than 10 nm, but blunt tips were preferred for this study so that when the tip compressed the surface, the surface tended to deform elastically instead of being indented (plastic deformation).

The cream film thickness and adhesive force were calculated from the force distance curve technique (Bhushan and Blackman 1991; LaTorre and Bhushan 2005; Chen and Bhushan 2006; Lodge and Bhushan 2006; Tang and Bhushan 2010; Bhushan 2010b). In this technique, the AFM tip is brought into contact with the sample by extending a piezoelectric tube (or simply piezo) vertically, then retracting it. The method is described in detail by Bhushan (2010a, b, 2011).

Figure 3.2 shows a typical force distance curve for a pure lanolin treated skin sample (Tang et al. 2010a). The measurement starts at a large separation (point A), where there is no deflection of the cantilever. As the piezo moves to the sample, a sudden mechanical instability occurs between point B and point C, and skin cream jumps into contact with the tip and wicks up around it to form a meniscus. The cantilever bends downward because of the attractive meniscus force acting on the tip. As the piezo further approaches the skin surface, the deflection of the cantilever

increases while the tip travels in the skin cream and eventually contacts the underlying skin surface at point D, and then cantilever starts to bend upward. Once the piezo reaches the end of its designated ramp size at point E, it is retracted to its starting position. The tip goes beyond zero deflection (point F) and enters the adhesion region. At point G, the elastic force of the cantilever becomes equivalent to the adhesive force, causing the cantilever to snap back to point H. The adhesive force F_a is the force needed to pull the tip away from the sample, and is the sum of van der Waals force and surface tensile force. It also can be calculated from the force distance curve by multiplying the vertical distance between *F* and *G* with the stiffness of the cantilever.

As the tip travels in the skin cream, it is deflected as well. The tip deflection occurs in the same direction as the piezo travels for the AFM used in this study. The film thickness is the sum of the travel distance of the piezo (described as h_1 in Fig. 3.2) and the deflection of cantilever (described as h_2 in Fig. 3.2).

In addition, the effective Young's modulus of the sample can be determined using Hertz analysis (Chen and Bhushan 2006; Bhushan 2010b)

$$F + F_a = \frac{3}{4}\sqrt{R}E\Delta z^{3/2} \tag{3.2}$$

where R is the tip radius, $F + F_a$ is the total force acting on the surface is calculated by multiplying the spring constant with the vertical distance between points G and E, Δz is the indentation depth on the skin surface calculated by subtracting the deflection of cantilever from the piezo travel distance between points D and E, and *E* is the effective Young's modulus of the sample. The total force acting on the surface and the resulting deformation (indentation depth) of the sample Δz can be extracted from the force distance curve.

By defining the zero tip-nominal sample separation as the position where the tip applies zero force when in contact with the sample (corresponding to point D in Fig. 3.2), the force distance curve (Fig. 3.2) can be converted to a force versus

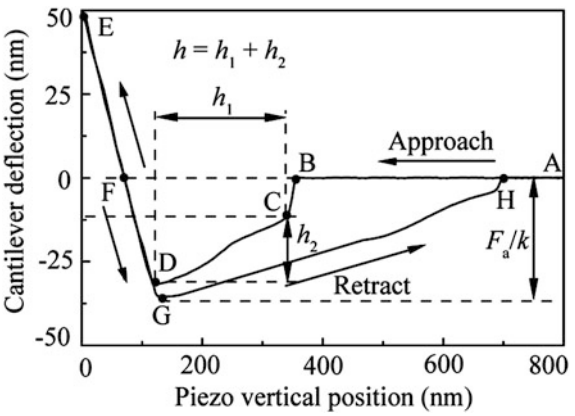

Fig. 3.2 A typical force distance curve for pure lanolin treated skin; points A-H represent the different stages as the AFM tip approaches, contacts, and retreats from skin surface. The film thickness is equal to $h_1 + h_2$ and adhesive force is equal to the vertical distance between F and G, multiplied by the cantilever stiffness (*k*) (Tang et al. 2010a)

tip-sample separation curve. Figure 3.3a shows the forces acting on the tip as a function of tip-nominal sample separation for pure lanolin, oil free cream, aqueous glycerin treated skin, and virgin skin. The lowest point on the approach curve, which corresponds to point D in Fig. 3.2, is assumed to be the point that the tip contacts the skin surface and applies zero force on the skin sample. Afterward, the tip applies force to the skin surface, and the skin surface deforms elastically under the force. As described earlier, the indentation depth of the surface and the total force (on approach curve) applied on the skin surface can be extracted from the force distance curve. Plotting the obtained indentation depth against the total force applied on the skin surface gives force versus indentation depth curves. The force versus indentation depth curves for pure lanolin, oil free cream, aqueous glycerin treated skin, and virgin skin are shown in Fig. 3.3b, and the effective Young's

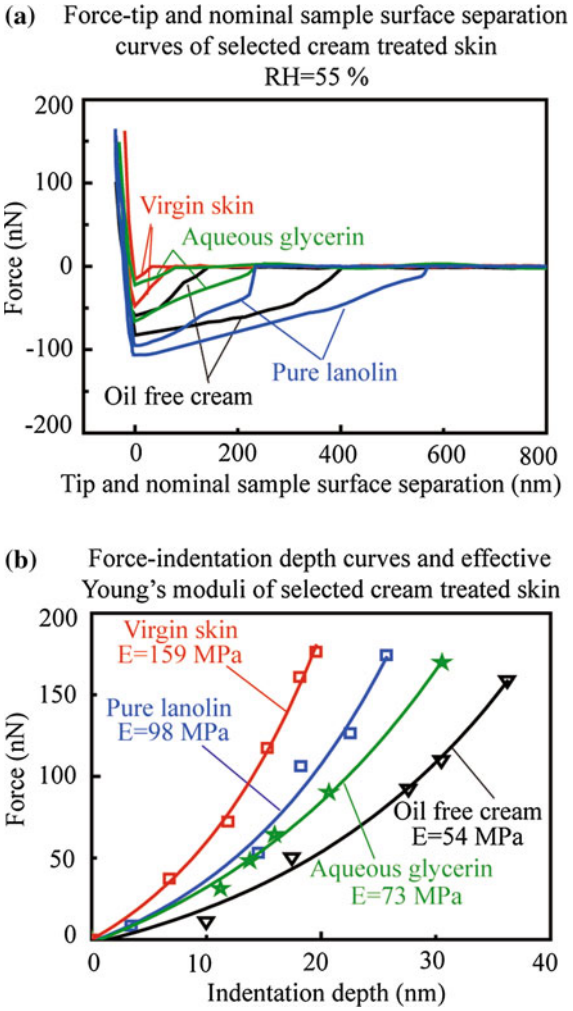

Fig. 3.3 **a** The force applied on the tip as a function of tip and nominal sample separation for selected cream treated skin samples, and **b** force-indentation depth and effective Young's modulus values extracted from the force distance curves. The *solid lines* show the best fit for the data points of the selected cream treated skin samples (Tang et al. 2010a)

modulus of various samples can be determined from these curves by fitting them to (3.2) (Tang et al. 2010a).

The force curves were collected at the same maximum cantilever deflection of 50 nm (relative trigger mode). A 64 × 64 force distance curve array (total 4096 measurement points) was collected over a scan area of 10 × 10 μm with a 4 Hz scan rate for all skin samples. For each force distance curve, there are 128 data points. A custom program coded in Matlab was used to calculate and display skin cream thickness, adhesive force, and effective Young's modulus mapping.

3.3.5 Macroscale Friction and Wear Resistance (Durability) Measurements

For bridging the gap between nanoscale and macroscale properties, macroscale measurements were also made by Tang and Bhushan (2010) and Bhushan et al. (2012). The tests were conducted using a ball-on-flat tribometer under reciprocating motion, with a measurement technique described in detail by Bhushan (2013a, b), and later in Chap. 9. A sapphire ball with a 1.5 mm radius and surface roughness of about 2 nm root mean square (RMS) was fixed in a stationary holder. The normal load and friction force were measured with the semiconductor strain gauges mounted on a crossed-I-beam structure. The tests were conducted in the ambient environment either at a normal load of 10 mN, over a stroke length of 2.5 mm, and at a velocity of 4 mm/s (Tang and Bhushan 2010), or at a normal load of 50 mN, over a stroke length of 10 mm, and at a velocity of 0.4 mm/s (Bhushan et al. 2012), unless otherwise noted. For the effect of velocity, the velocity was varied from 1 to 4 mm/s. For the effect of load, the normal load was varied from 10 to 50 mN. The wear resistance (durability) experiments were carried out by repeated cycling tests for 3000 cycles. For each test condition, a minimum of six measurements were made. The $\pm 1\sigma$ values were presented in the data points.

3.3.6 Nanomechanical Properties Measurements

3.3.6.1 Nanoscratch Measurements

Bhushan et al. (2010) performed nanoscale scratch measurements using a pyramidal diamond tip (tip radius $\sim$100 nm) in an AFM. The tip was mounted on a platinum-coated stainless steel rectangular cantilever of stiffness 10 N/m and was scanned orthogonally to the long axis of the cantilever to generate the scratch. Scratches were generated under normal loads of 3, 9, 15, 21, 27, and 33 μN for 15 cycles over a scan length (stroke length) of 30 μm and with an average velocity of 300 μm/s. Scanning along a line was achieved by disabling the slow scan axis

during scanning and increasing the applied normal load to the desired value. After 15 reciprocating cycles, the normal load was decreased to the value of 1.2 μN, and the slow scan axis was enabled until the next region for a subsequent scratch test was reached. After the scratch tests, a silicon cantilever RFESP with a nominal tip radius of 10 nm and nominal stiffness of 3 N/m was used to get the scratch AFM image in tapping mode.

3.3.6.2 Nanoindentation Experiments

Bhushan et al. (2010, 2012) carried out nanoindentation experiments out using a Nano Indenter II® (MTS Systems Corp., Knoxville, Tennessee) in the constant displacement rate loading mode with a three-sided pyramidal diamond (Berkovich) tip. The maximum indentation displacement was controlled to 1000 nm. The method for hardness (H) and elastic modulus (E) determination was based on established methods (for details, see Oliver and Pharr 1992; Bhushan and Li 2003). The Poisson's ratio of skin needed in the analysis was assumed to be 0.5; similar assumptions have been made by Sanders (1973) and Yuan and Verma (2006).

3.3.6.3 In Situ Tensile Measurements

Bhushan et al. (2010) carried out in situ tensile measurements of skin with and without cream treatment using a custom-built tensile stage that attaches to the AFM base and uses a linear stepper motor to load a skin sample in tension. Figure 3.4 shows a schematic of the stage used in place of the regular AFM sample holder (Seshadri and Bhushan 2008a; Bhushan et al. 2010). The skin sample was firmly clamped between two sliders to prevent slipping on load application. Stage motion was achieved by a left-right combination lead screw that kept the sample at approximately the same position with respect to the scanning tip. This helped in locating the same control area after each loading increment was applied. A 40 TPI pitch lead screw in combination with a 400 steps per revolution stepper motor (model PX245-01AA, using the controller NF-90, both from Velmex Inc.) gave a minimum displacement of 1.6 μm. For a sample length of 36 mm, this corresponded to a minimum strain rate of $8.9 \times 10^{-3\%}$ s^{-1}. The strain applied was obtained from the total number of steps through which the stepper motor was rotated. A strain rate of $8.9 \times 10^{-2\%}$ s^{-1} was used. The maximum travel was 21 mm. A beam-type strain gauge force sensor (model LCL-010, Omega Engineering Inc., Stamford, CT) with a resolution of 10 mN was used for measuring stress in the skin samples. The stiffness of the force sensor (18 kN m^{-1}) was very high compared with the sample stiffness. To minimize airborne vibrations during AFM imaging, the skin sample was supported with an aluminum block having a smooth radius of curvature of 25.4 mm.

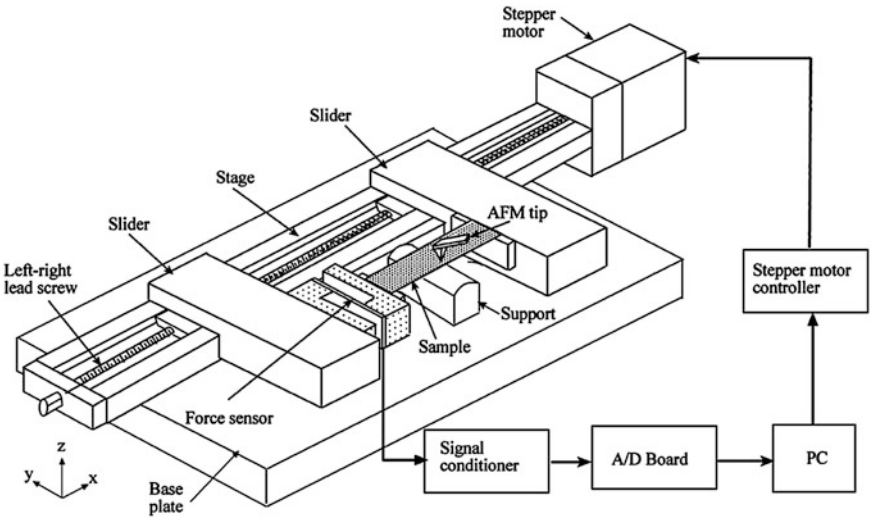

Fig. 3.4 Schematic diagram of the setup used to conduct the in situ tensile measurement of skin samples in AFM (Bhushan et al. 2010)

During the tensile test, the loading was stopped intermittently, and the sample was scanned with AFM for changes in morphology. The support block was removed during straining and carefully inserted again while imaging. For AFM scanning, a RFESP silicon tip was used in tapping mode. The scan size was 10 μm. For stress-strain curves, data from the load cell were used. With every load increment, there was a corresponding increase in the length of the skin sample and hence a shift in the location of the control area from its previous position. It was therefore necessary to accurately locate the scan area after every load increment before scanning. To locate the same scan area in skin, a mark was selected on the skin surface itself. The scan area was located each time by locating the tip of the cantilever on the selected mark of the skin surface. Then the final area was scanned.

3.3.7 Surface Potential Measurements

To charge the skin surfaces, Tang et al. (2010a, b) rubbed skin samples with the polystyrene as it is known that polystyrene creates a charge on skin surface when the two materials come in contact. A polystyrene plate (Tang et al. 2010b) and a polystyrene microsphere (Tang et al. 2010a, b) were chosen as the rubbing elements for rubbing on the macroscale and microscale, respectively.

For the experiments, the skin sample first was electrically isolated from the ground to prevent quick discharging (mounted on insulating electrical tape as stated

earlier). Then, a surface potential map of the skin sample was obtained for "before rubbing" data. Next, the sample was rubbed with the polystyrene under different conditions. Finally, the surface potential was mapped immediately for "after rubbing" data.

The macroscale rubbing process was carried out using a polystyrene plate (Fisher Scientific, 5×5 mm^2) fixed in a stationary holder to rub against the skin surface over a rubbing area of 5×5 mm^2 using a tribometer with a rotating motion. In the macroscale velocity effect test, the velocity varied from 10 to 30 mm/s at a normal load of 2 N and a rubbing time of 30 s. In the macroscale normal load effect test, the normal load varied from 2 to 4 N at a velocity of 16 mm/s and a rubbing time of 30 s. In the macroscale rubbing time effect test, the rubbing time varied from 20 to 40 s at a velocity of 16 mm/s and a normal load of 2 N.

The microscale rubbing process was carried out using a polystyrene microsphere (07314-5, Polysciences, Inc., Warrington, PA, U.S.A.) with a diameter of 45 μm glued to the end of a silicon rectangular cantilever with a stiffness of 3 N/m on a RFESP tip using epoxy glue (Fig. 3.5) (Tang et al. 2010b). This polystyrene microsphere was rubbed against the skin surface over a rubbing area of 60×60 μm^2 by an AFM. The microscale velocity effect test was carried out by changing the scan velocity of the AFM from 480 to 720 μm/s at a normal load of 2 μN and a rubbing time of 600 s. The microscale normal load effect test was carried out by changing the normal load from 1 to 2 μN at a velocity of 600 μm/s and a rubbing time of 600 s. The microscale rubbing time effect test was carried out by changing the rubbing time from 300 to 900 s at a velocity of 600 μm/s and a normal load of 2 μN.

The surface potential measurements were conducted using an AFM equipped with the Extender Electronics module (Multimode Nanoscope IIIa, Veeco, Santa Barbara, CA) (Tang et al. 2010a, b). The Extender allows for surface potential measurements to be taken. A Ti–Pt coated conducting tip (NSC18/Ti–Pt/50) with a cantilever spring constant of 3.5 N/m and 40 nm radius was used. The surface potential of the skin samples was measured using the Kelvin probe method. Measurements were conducted using a two pass method (Lodge and Bhushan 2007a, b; Seshadri and Bhushan 2008b; Bhushan 2010a, b, 2011; Tang et al. 2010a, b). In the first pass, surface topography was measured using the standard AFM tapping mode. In the second pass, the tip was scanned over the previously measured

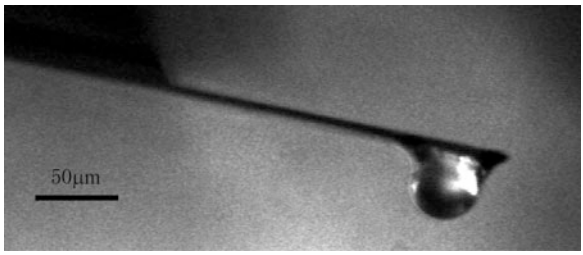

Fig. 3.5 Optical microscopy image of the side view of the probe obtained by gluing a 45 μm diameter polystyrene microsphere at the end of a commercial rectangular cantilever with a tip (Tang et al. 2010b)

topography at a specified distance above the surface. In all measurements, that distance was 50 nm. In the second pass, the piezo used in tapping mode was turned off. Instead, an oscillating voltage was applied directly to the conducting tip which generated an oscillating electrostatic force. To measure the surface potential, dc voltage was applied to the tip until the oscillating amplitude was zero. The surface potential at that point was equal to the dc voltage applied to the tip. All measurements were carried out in ambient conditions (22 °C, RH 35–40%), with the exception of some experiments to study the effect of relative humidity.

3.3.8 Humidity and Temperature Control

In order to study the effect of relative humidity, a humidity control system was used by Tang and Bhushan (2010), Tang et al. (2010a), and Bhushan et al. (2012). In the relative humidity effect measurements, the relative humidity was changed from 4 to 90% RH. A humidity sensor and humidity control software were used to monitor the humidity inside a Plexiglas test chamber enclosing the AFM system. RH 4% and RH 90% were obtained by inputting a positive pressure of air passed through a column filled with drier air and a cup filled with hot water, respectively. RH 55% was obtained in ambient conditions. The temperature was maintained at 22 °C. Skin samples were kept at each humidity condition for about 1 h prior to test.

In the temperature effect tests, a thermal stage was used and the temperature ranged from 22 to 45 °C while the humidity was maintained at 35–40% (Tang and Bhushan 2010). The skin sample was placed at each temperature for about 30 min prior to the test.

References

Alikhan, A., & Maibach, H. I. (2010). Biology of stratum corneum: Tape stripping and protein quantification in the human face: Regional and age-related differences. In M. A. Farage, K. W. Miller, & I. Howard (Eds.), *Textbook of Aging Skin* (pp. 401–408). New York: Springer.

Beasley, D. G., & Meyer, T. A. (2010). Characterization of the UVA protection provided by avobenzone, zinc oxide, and titanium dioxide in broad-spectrum sunscreen products. *American Journal of Clinical Dermatology, 11*, 413–421.

Belkoff, S. M., & Haut, R. C. (1991). A structural model used to evaluate the changing microstructure of maturing rat skin. *Journal of Biomechanics, 24*, 711–720.

Bhushan, B. (2010a). *Biophysics of Human Hair—Structural, Nanomechanical and Nanotribological Studies*. Heidelberg, Germany: Springer.

Bhushan, B. (Ed.). (2010b). *Springer Handbook of Nanotechnology* (3rd ed.). Heidelberg, Germany: Springer.

Bhushan, B. (2011). *Nanotribology and Nanomechanics I—Measurement Techniques and Nanomechanics, II—Nanotribology, Biomimetics, and Industrial Applications* (3rd ed.). Heidelberg, Germany: Springer.

Bhushan, B. (2013a). *Principles and Applications of Tribology* (2nd ed.). New York: Wiley.

Bhushan, B. (2013b). *Introduction to Tribology* (2nd ed.). New York: Wiley.
Bhushan, B., & Blackman, G. S. (1991). Atomic force microscopy of magnetic rigid disks and sliders and its applications to tribology. *ASME Journal of Tribology, 113*, 452–457.
Bhushan, B., Chen, S., & Ge, S. (2012). Friction and durability of virgin and damaged skin with and without skin cream treatment using atomic force microscopy. *Beilstein Journal of Nanotechnology, 3*, 731–746.
Bhushan, B., & Li, X. (2003). Nanomechanical characterisation of solid surfaces and thin films. *International Materials Reviews, 48*, 125–164.
Bhushan, B., & Tang, W. (2011). Surface, tribological and mechanical characterization of synthetic skins for cosmetic science. *Journal of Applied Polymer Science, 120*, 2881–2890.
Bhushan, B., Tang, W., & Ge, S. (2010). Nanomechanical Characterization of Skin and Skin Cream. *Journal of Microscopy, 240*, 135–144.
Braye, F. M., Stefani, A., Venet, E., Pieptu, D., Tissot, E., & Damour, O. (2001). Grafting of large pieces of human reconstructed skin in a porcine model. *British Journal of Plastic Surgery, 54*, 532–538.
Caspers, P. J., Lucassen, G. W., & Puppels, G. J. (2003). Combined in vivo confocal Raman spectroscopy and confocal microscopy of human skin. *Biophysical Journal, 85*, 572–580.
Chaudhuri, R. K., Lascu, Z., Puccetti, G., Deshipande, A. A., & Paknikar, S. K. (2006). Design of a photostabilizer having built-in antioxidant functionality and its utility in obtaining broad-spectrum sunscreen formulations. *Photochemistry and Photobiology, 82*, 823–828.
Chen, N., & Bhushan, B. (2006). AFM studies of conditioner thickness distribution and binding interactions on hair surface. *Journal of Microscopy, 221*, 203–215.
Chen, S., & Bhushan, B. (2013). Naonomechanical and nanotribological characterization of two synthetic skins with and without skin cream treatment using atomic force microscopy. *Journal of Colloid and Interface Science, 398*, 247–254.
Cohen, J. C., Hartman, D. G., Garofalo, M. J., Basehoar, A., Raynor, B., Ashbrenner, E., et al. (2009). Comparison of closed chamber and open chamber evaporimetry. *Skin Research and Technology, 15*, 51–54.
Denda, M., Hori, J., Koyama, J., Yoshida, S., Nanba, R., Takahashi, M., et al. (1992). Stratum-corneum sphingolipids and free amino-acids in experimentally-induced scaly skin. *Archives of Dermatological Research, 284*, 363–367.
Egawa, M., Oguri, M., Hirao, T., Takahashi, M., & Miyakawa, M. (2002). The evaluation of skin friction using a frictional feel analyzer. *Skin Research and Technology, 8*, 41–51.
Ferrero, L., Pissavini, M., Marguerie, S., & Zastrow, L. (2002). Sunscreen in vitro spectroscopy: application to UVA protection assessment and correlation with in vivo persistent pigment darkening. *International Journal of Cosmetic Science, 24*, 63–70.
Fulmer, A. W., & Kramer, G. J. (1986). Stratum-Corneum lipid abnormalities in surfactant-induced dry scaly skin. *Journal of Investigative Dermatology, 5*, 598–602.
Garoli, D., Pelizzo, M. G., Nicolosi, P., Peserico, A., Tonin, E., & Alaibac, M. (2009). Effectiveness of different substrate materials for in vitro sunscreen tests. *Journal of Dermatological Science, 56*, 89–98.
Hanson, K. M., Gratton, E., & Bardeen, C. J. (2006). Sunscreen enhancement of UV-induced reactive oxygen species in the skin. *Free Radical Biology and Medicine, 41*, 1205–1212.
Imokawa, G., Akasaki, S., Minematsu, Y., & Kawai, M. (1989). Importance of intercellular lipids in water-retention properties of the stratum-corneum—Induction and recovery study of surfactant dry skin. *Archives of Dermatological Research, 281*, 45–51.
Jermann, R., Toumiat, M., & Imfeld, D. (2002). Development of an in vitro efficacy test for self-tanning formulations. *International Journal of Cosmetic Science, 24*, 35–42.
Kendall, M. A. F., Chong, Y. F., & Cock, A. (2007). The mechanical properties of the skin epidermis in relation to targeted gene and drug delivery. *Biomaterials, 28*, 4968–4977.
Kraeling, M. K. K., & Bronaugh, R. L. (2005). In vitro percutaneous absorption of acrylamide and styrene from cosmetic vehicles through fuzzy rat and human skin. *Cutaneous and Ocular Toxicology, 24*, 65–79.

LaTorre, C., & Bhushan, B. (2005). Nanotribological characterization of human hair and skin using atomic force microscopy. *Ultramicroscopy, 105*, 155–175.

Lir, I., Haber, M., & Dodiuk-Kenig, H. (2007). Skin surface model material as a substrate for adhesion-to-skin testing. *Journal of Adhesion Science and Technology, 21*, 1497–1512.

Lodge, R. A., & Bhushan, B. (2006). Surface characterization of human hair using tapping mode atomic force microscopy and measurement of conditioner thickness distribution. *Journal of Vacuum Science and Technology A, 24*, 1258–1269.

Lodge, R. A., & Bhushan, B. (2007a). Surface potential measurement of human hair using Kelvin probe microscopy. *Journal of Vacuum Science and Technology A, 25*, 893–902.

Lodge, R. A., & Bhushan, B. (2007b). Effect of physical wear and triboelectric interaction on surface charge as measured by Kelvin probe microscopy. *Journal of Colloid and Interface Science, 310*, 321–330.

Nesseem, D. (2011). Formulation of sunscreens with enhancement sun protection factor response based on solid lipid nanoparticles. *International Journal of Cosmetic Science, 33*, 70–79.

Oliver, W. C., & Pharr, G. M. (1992). Improved technique for determining hardness and elastic modulus using load and displacement sensing indentation experiments. *Journal of Materials Research, 7*, 1564–1583.

Palacio, M., & Bhushan, B. (2010). Normal and lateral force calibration techniques for AFM cantilevers (invited). *Critical Reviews in Solid State and Materials Sciences, 35*, 73–104.

Papir, Y. S., Hsu, K. H., & Wildnauer, R. H. (1975). The mechanical properties of stratum corneum. I. The effect of water and ambient temperature on the tensile properties of newborn rat stratum corneum. *Biochimica et Biophysica Acta (BBA)-General Subjects, 399*, 170–180.

Pflucker, F., & Hohenberg, H. (1999). The outermost stratum corneum layer is an effective barrier against dermal uptake of topically applied micronized titanium dioxide. *International Journal of Cosmetic Science, 21*, 399–411.

Sanders, R. (1973). Torsional elasticity of human skin in vivo. *Pflügers Arch, 342*, 255–260.

Seshadri, I. P., & Bhushan, B. (2008a). In situ tensile deformation characterization of human hair with atomic force microscopy. *Acta Materialia, 56*, 774–781.

Seshadri, I. P., & Bhushan, B. (2008b). Effect of rubbing and load on nanoscale charging characteristics of human hair characterized by AFM based Kelvin probe. *Journal of Colloid and Interface Science, 325*, 580–587.

Soroushian, P., & Lu, J. (2009). Technova corporation. Lansing, Michigan, Personal Communication.

Springsteen, A., Yurek, R., Frazier, M., & Carr, K. F. (1999). In vitro measurement of sun protection factor of sunscreens by diffuse transmittance. *Analytica Chimica Acta, 380*, 155–164.

Tang, W., & Bhushan, B. (2010). Adhesion, friction and wear characterization of skin and skin cream using atomic force microscope. *Colloid Surface B, 76*, 1–15.

Tang, W., Bhushan, B., & Ge, S. (2010a). Friction, adhesion and durability and influence of humidity on adhesion and surface charging of skin and various skin creams using atomic force microscopy. *Journal of Microscopy, 239*, 99–116.

Tang, W., Bhushan, B., & Ge, S. (2010b). Triboelectrification studies of skin and skin cream using Kelvin probe microscopy. *Journal of Vacuum Science and Technology A, 28*, 1018–1028.

Tao, Z., & Bhushan, B. (2007). Velocity dependence and rest time effect on nanoscale friction of ultrathin films at high sliding velocities. *Journal of Vacuum Science and Technology A, 25*, 1267–1274.

Turner, R. B., Biedermann, K. A., Morgan, J. M., Keswick, B., Ertel, K. D., & Barker, M. F. (2004). Efficacy of organic acids in hand cleansers for prevention of rhinovirus infections. *Antimicrobial Agents and Chemotherapy, 48*, 2595–2598.

Vogel, H. G., & Denkel, K. (1985). In vivo recovery of mechanical properties in rat skin after repeated strain. *Archives of Dermatological Research, 277*, 484–488.

Wakefield, G., Lipscomb, S., Holland, E., & Knowland, J. (2004). The effects of manganese doping on UVA absorption and free radical generation of micronised titanium dioxide and its

consequences for the photostability of UVA absorbing organic sunscreen components. *Photochemical & Photobiological Sciences, 3*, 648–652.

Wakefield, G., & Stott, J. (2006). Photostabilization of organic UV-absorbing and anti-oxidant cosmetic components in formulations containing micronized manganese-doped titanium oxide. *Journal of Cosmetic Science, 57*, 385–395.

Williams, A. C., & Barry, B. W. (2004). Penetration enhancers. *Advanced Drug Delivery Reviews, 56*, 603–618.

Wokovich, A. M., Brown, S. A., McMaster, F. J., Doub, W. H., Cai, B., Sadrieh, N., et al. (2008). Evaluation of substrates for 90 degrees peel adhesion–A collaborative study. I. Medical tapes. *Journal of Biomedical Materials Research. Part B, Applied Biomaterials, 87*, 105–113.

Yourick, J. J., & Bronaugh, R. L. (1997). Percutaneous absorption and metabolism of coumarin in human and rat skin. *Journal of Applied Toxicology, 17*, 153–158.

Yourick, J. J., Jung, C. T., & Bronaugh, R. L. (2008). In vitro and in vivo percutaneous absorption of retinol from cosmetic formulations: Significance of the skin reservoir and prediction of systemic absorption. *Toxicology and Applied Pharmacology, 231*, 117–121.

Yuan, Y., & Verma, R. (2006). Measuring microelastic properties of stratum corneum. *Colloids Surfaces B: Biointerfaces, 48*, 6–12.

Part I
Rat Skin—Virgin

Chapter 4
Adhesion, Friction, and Wear of Rat Skin With and Without a Common Cream Treatment

This chapter presents adhesion, friction, and wear data of rat skin with and without a common cream treatment. Experiments were conducted both on the nanoscale and macroscale. First, the studies using a common cream treatment are presented, followed by those using a variety of creams.

4.1 A Common Cream Treatment

This section presents nanotribological data on rat skin with and without a common cream treatment (Vaseline Intensive Care Lotion) (Tang and Bhushan 2010). Except for the film thickness study, for all other tests on the nanoscale for skin with cream treatment, film thickness was approximately 150 nm, and for macroscale tests, it was approximately 1.4 μm.

4.1.1 Surface Roughness and Friction on the Nanoscale

Surface roughness and contact angle are important because their variations can cause differences in skin cream interactions with the skin surface, thus changing the tribological properties. Figure 4.1 shows images of surface roughness and friction force for skin with and without common cream treatment (Tang and Bhushan 2010). Above each image is a cross-sectional plot of the surface (taken at the accompanying arrows) corresponding to surface roughness and friction force, respectively.

Table 4.1 summarizes the surface roughness data on a 20 × 20 μm^2 scan size, contact angle data, and coefficient of friction for skin with and without common cream treatment. The data shows that after the application of skin cream, surface roughness decreases, skin becomes more hydrophilic, and friction force increases.

B. Bhushan, *Biophysics of Skin and Its Treatments*, Biological and Medical Physics, Biomedical Engineering, DOI 10.1007/978-3-319-45708-6_4

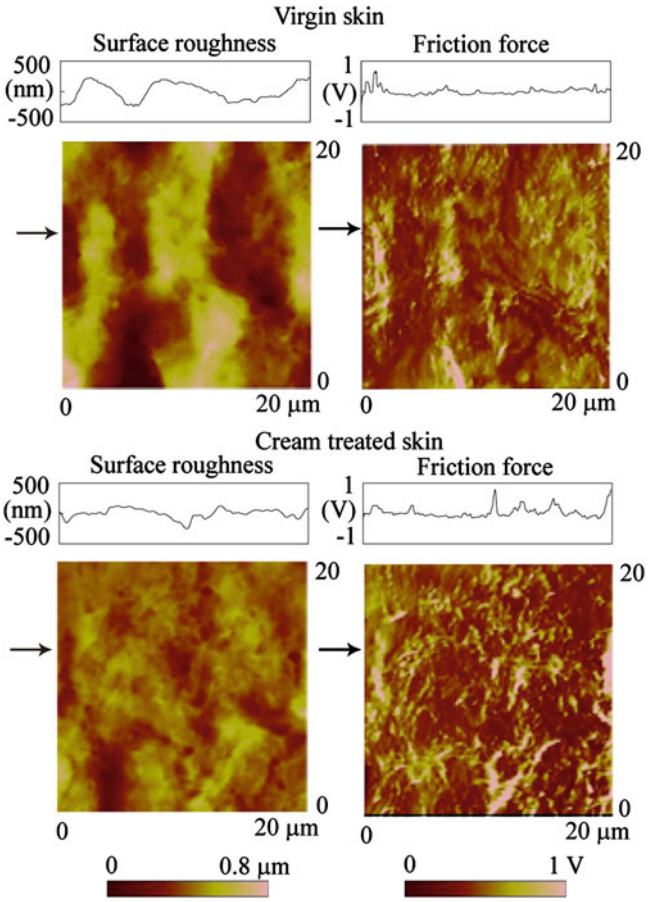

Fig. 4.1 Surface roughness and friction force AFM images for rat skin with and without a common cream treatment (Tang and Bhushan 2010)

Table 4.1 Surface roughness statistics on a 20 μm by 20 μm scan size, contact angle, and coefficient of friction and adhesive force on the nanoscale for rat skin with and without common cream treatment (adapted from Tang and Bhushan 2010)

Skin type	Surface roughness statistics		Contact angle (°)	Coefficient of friction	Adhesive force (nN)
	RMS (nm)	P-V distance (nm)			
Virgin skin	160 ± 28	983 ± 156	66 ± 6	0.08 ± 0.02	80 ± 10
Cream treated skin	119 ± 20	730 ± 125	40 ± 5	0.17 ± 0.03	100 ± 15

Skin cream treatment moisturizes and softens the surface and makes the surface smoother. Adsorption of the hydrophilic groups in the cream (Table 3.1) reduces the contact angle, making the skin surface hydrophilic. Moist and soft skin leads to greater ductility and a larger real area of contact, resulting in higher friction (Bhushan 2013a, b). Furthermore, as the tip slides in the skin cream film, meniscus and viscous contribution to friction of the tip with the surrounding liquid, becomes large, which also leads to an increase in the friction force. For background on friction mechanisms, see Appendix A.

4.1.2 *Effect of the Duration of Cream Treatment on Film Thickness and Effect of Cream Film Thickness, Velocity, and Normal Load on Adhesion and Friction on the Nanoscale*

To study the effect of the duration of cream treatment, the coated skin was allowed to sit in the ambient environment (22 °C, RH 55%) for some period of time. The film thickness, coefficient of friction, and adhesive force on the nanoscale as a function of aging time were measured. As shown in Fig. 4.2, the film thickness, coefficient of friction, and adhesive force decrease with time (Tang et al. 2010). Therefore, the tribological properties of skin should change with time.

Figure 4.3 shows the effect of cream film thickness on the coefficient of friction and adhesive force on the nanoscale (Tang and Bhushan 2010). The thickness of the lipid layer present on the virgin skin surface was measured to be about 10 nm, and the first data point on the graph corresponds to that of virgin skin. The result shows that cream treated skin has a larger coefficient of friction and adhesive force than virgin skin. (Also see Table 4.1.) The coefficient of friction and adhesive force increase as the cream film thickness increases. As the cream film increases, the

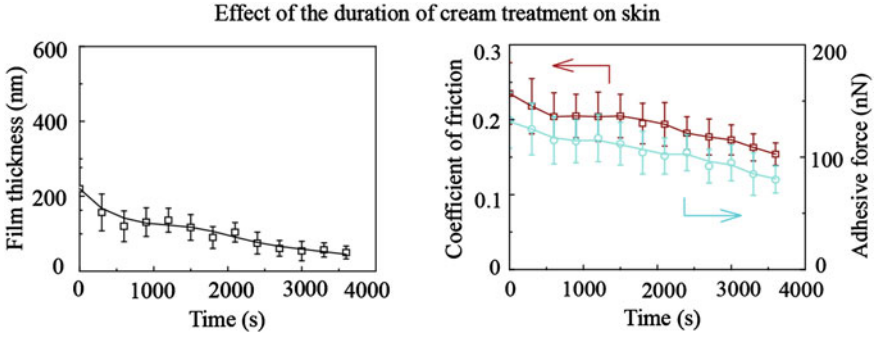

Fig. 4.2 Film thickness, coefficient of friction, and adhesive force on the nanoscale as a function of the duration of the cream treatment on the skin for rat skin with a common cream treatment (adapted from Tang et al. 2010a)

amount of liquid accumulating at the contact interface increases, resulting in a greater liquid height and greater resistance to the motion due to meniscus and viscous effects (Bhushan 2013a, b); see the schematic (right) in Fig. 4.3. This effect is believed to be responsible for the increase of the coefficient of friction and adhesive force.

Figure 4.4a shows the effect of sliding velocity (plotted on log scale) on the coefficient of friction and adhesive force on a logarithm scale for skin with and without common cream treatment (Tang and Bhushan 2010). The data on the left of

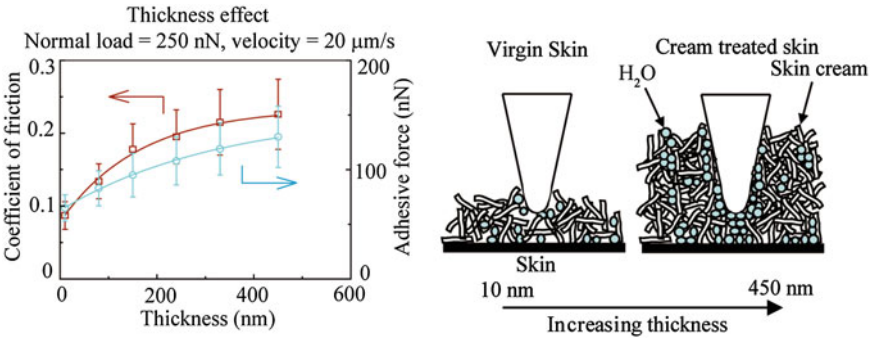

Fig. 4.3 Effect of cream film thickness on the coefficient of friction and adhesive force on the nanoscale for rat skin with and without a common cream treatment. Schematic of the increase in skin cream height around the tip (*right*) is also shown (adapted from Tang and Bhushan 2010)

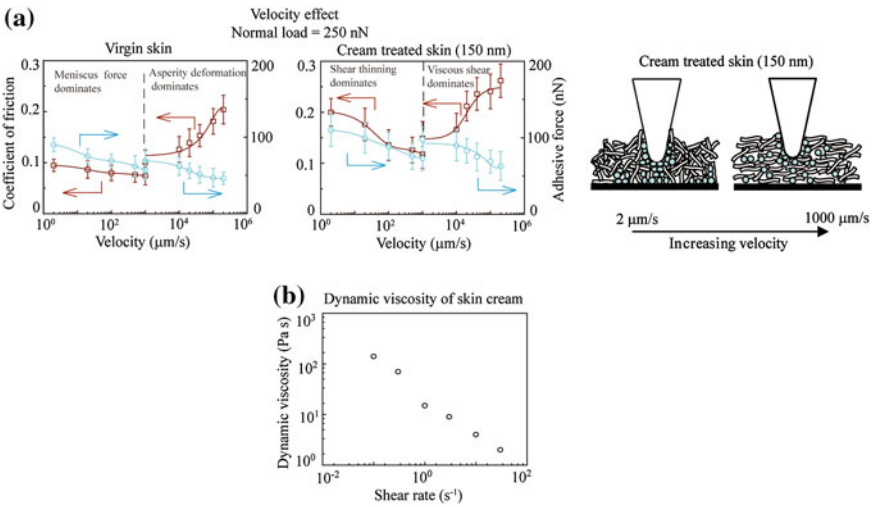

Fig. 4.4 **a** Effect of velocity on the coefficient of friction and adhesive force on the nanoscale for rat skin with and without a common cream treatment and schematic of the alignment of molecules with the increase of velocity (*right*), and **b** dynamic viscosity of common cream as a function of shear rate (Tang and Bhushan 2010)

the dotted line shows the results on a scan length of 10 μm with the velocity ranging from 2 to 1000 μm/s using the AFM. The data on the right of the dotted line shows the results on a scan length of 1000 μm with the velocity ranging from 1000 to 2×10^5 μm/s using an ultrahigh velocity stage. For skin with and without common cream treatment, when the velocity is below 1000 μm/s, the coefficient of friction and adhesive force decrease with an increase of velocity, and when the velocity is higher than 1000 μm/s, the coefficient of friction and adhesive force increase and decrease, respectively, with an increase of velocity. These can be explained as follows.

For virgin skin, a meniscus is formed by the condensed water and skin lipid (Bhushan 2013a, b). At a velocity lower than 1000 μm/s, since less energy is available for the deformation of the asperity, the friction is dominated by the meniscus force. The motion of the tip results in shearing and reformation of meniscus bridges. As the velocity increases, the meniscus bridges cannot be fully reformed, resulting in a drop of coefficient of friction and adhesive force (Liu and Bhushan 2003). At a velocity higher than 1000 μm/s, there is not sufficient time for the meniscus to form, and the meniscus force no longer plays a dominant role. The impacts between surface asperities result in more and more energy dissipation such that the friction is dominated by the deformation of the asperities, and the deformation-related friction increases monotonically with the sliding velocity, as initially proposed by Tambe and Bhushan (2005). In the case of cream treated skin, the skin cream is typically a shear-thinning fluid, i.e. the viscosity decreases with the increasing shear rate, as shown in Fig. 4.4b (Tang and Bhushan 2010; Tang et al. 2010). At a velocity lower than 1000 μm/s, the alignment of molecules (shear thinning) is responsible for the drop in the coefficient of friction with an increase of velocity. At a velocity higher than 1000 μm/s, the friction is believed to be dominated by viscous shearing, and friction increases with increasing velocity (Tambe and Bhushan 2005; Tao and Bhushan 2007).

Figure 4.5a shows the effect of normal load on the coefficient of friction and adhesive force for skin with and without common cream treatment (Tang and Bhushan 2010). The results indicate that for virgin skin and cream treated skin, the critical normal loads are 250 and 500 nN, respectively. When the normal load is lower than the critical value, the coefficient of friction is independent of the normal load, and when the normal load is higher than the critical value, the coefficient of friction increases as the normal load increases. An increase in the critical normal load for which the liquid film collapse suggests that the cream film exhibits a larger load carrying capacity than that of virgin skin, such that the cream film serves as a protective covering to the skin surface.

An increase in the critical load of the cream treated skin also suggests that its deformation characterization is improved as a result of the cream treatment. Skin and skin cream are expected to be viscoelastic materials. In order to study the deformation behavior, creep properties in the indentation mode were measured. The indent depth as a function of normal load at a time of 120 s for various normal loads is plotted in Fig. 4.5b. The data shows that the indent depth increased sharply when

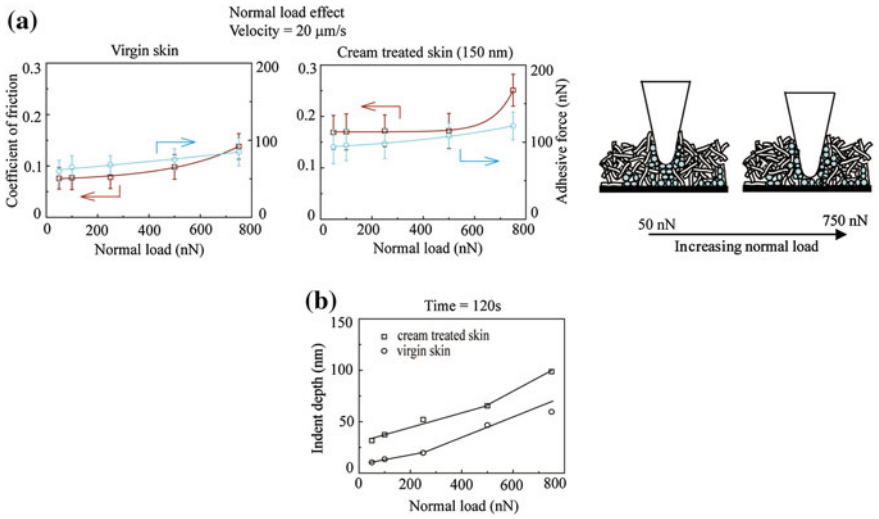

Fig. 4.5 **a** Effect of normal load on the coefficient of friction and adhesive force on the nanoscale for rat skin with and without a common cream treatment. Schematic of the increase of indent depth of the AFM tip into the cream with the increase of normal load (*right*) is also shown, and **b** the indent depth as a function of normal load at a time of 120 s is also shown (adapted from Tang and Bhushan 2010)

normal loads are higher than 250 and 500 nN for virgin skin and cream treated skin, respectively. Thus, the increase of coefficient of friction is correlated to the deformation.

4.1.3 Effect of Relative Humidity and Temperature on Adhesion and Friction on the Nanoscale

Figure 4.6 shows the effect of relative humidity on the coefficient of friction and adhesive force of skin with and without common cream treatment (Tang and Bhushan 2010). For virgin skin and cream treated skin, the coefficient of friction and adhesive force increase as the relative humidity increases. It is because the absorbed water molecules increase the film thickness of virgin skin and cream treated skin; see the schematic (right) in Fig. 4.6. As discussed earlier, the increase in film thickness leads to the increase of the coefficient of friction and adhesive force. It is also observed that the effect of humidity on cream treated skin is more obvious than on virgin skin. As shown in Table 3.1, glycerin, lactic acid, potassium lactate, urea, sodium PCA, and propylene glycol are the humectants in common skin cream (Leyden and Rawlings 2002). When the cream gel network layer covers the skin surface, the hydrophilic groups, such as hydroxyl group, amines group, and carboxyl group in the humectants, tend to form hydrogen bonds with water

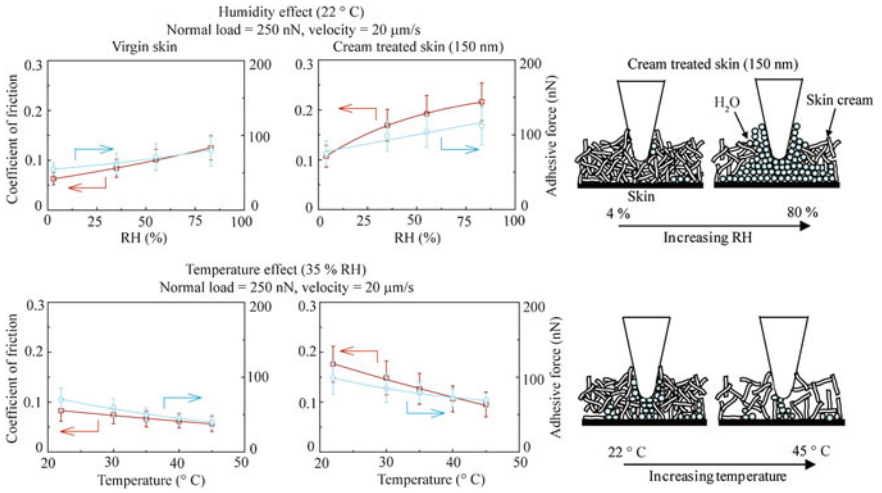

Fig. 4.6 Effect of relative humidity and temperature on the coefficient of friction and adhesive force on the nanoscale for rat skin with and without a common cream treatment. The schematics show the adsorption of water molecules with the increase of relative humidity, and the desorption of water molecules and the reduced viscosity with the increase of temperature (*right*) (Tang and Bhushan 2010)

molecules, such that the humectants help the skin surface to attract water molecules from the environment, especially at high humidity. The outer layer of virgin skin is covered with a thin, hydrophobic lipid layer that contains triglycerides, diglycerides, fatty acids, wax esters, squalene, cholesterol, and cholesterol esters (Downing et al. 1969). Due to this hydrophobic lipid layer, water is hardly absorbed and penetrated into a virgin skin surface. Thus, humidity has less effect on friction and adhesion for virgin skin.

Figure 4.6 also shows the effect of temperature on the coefficient of friction and adhesive force. It shows that the increasing temperature causes a decrease in the coefficient of friction and adhesive force for both virgin skin and cream treated skin. The schematic (right) in Fig. 4.6 shows that at a high temperature, desorption of water leads to a decrease in the coefficient of friction and adhesive force for virgin skin and cream treated skin. For cream treated skin, the reduction of viscosity at a high temperature also contributes to the decrease of coefficient of friction and adhesive force.

4.1.4 Wear Resistance on the Nanoscale

Figure 4.7a shows the coefficient of friction and adhesive force as a function of the sliding cycles for skin with and without common cream treatment (Tang and Bhushan 2010). It shows that the coefficient of friction and adhesive force of virgin

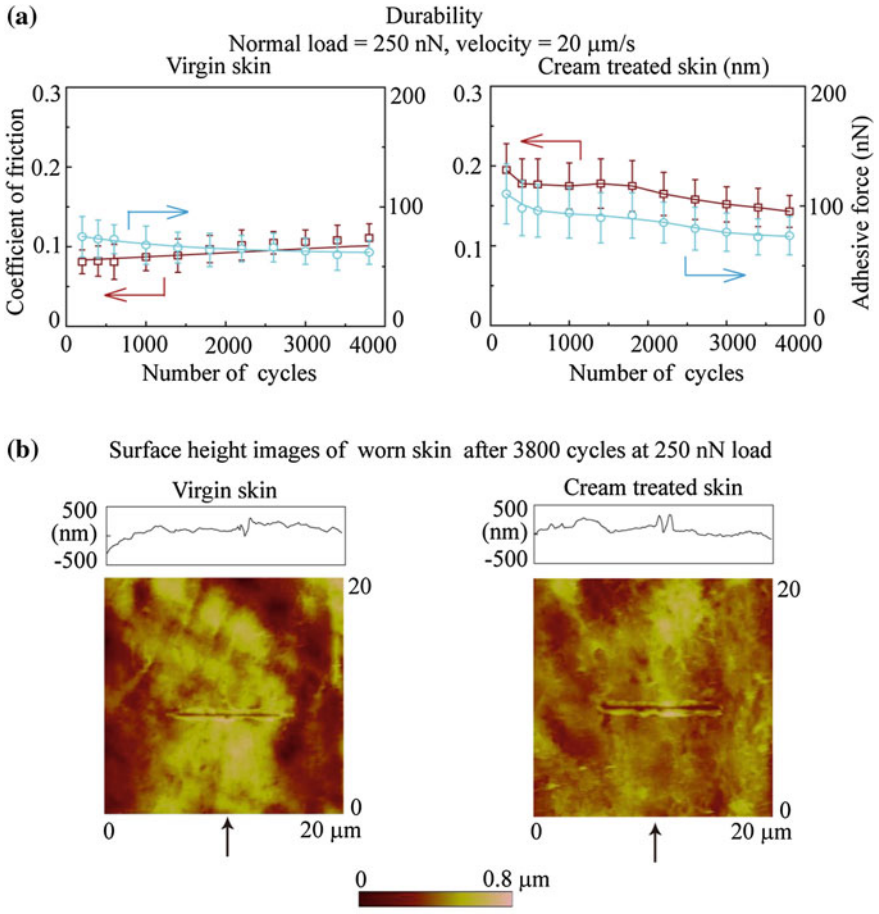

Fig. 4.7 **a** The coefficient of friction and adhesive force on the nanoscale as a function of the number of cycles for rat skin with and without a common cream treatment, and **b** AFM images for after 3800 cycles at 250 nN normal load (Tang and Bhushan 2010)

skin remain constant during the initial few cycles and then increase and decrease, respectively. This is related to the removal of the thin lipid film on the virgin skin surface. In the case of cream treated skin, the coefficient of friction and adhesive force decrease dramatically and then remain constant as the sliding cycles increase up to approximately 1800 cycles, after which the coefficient of friction and adhesive force decrease again. This is believed to be caused by the change of cream film thickness.

Common skin cream is formulated by adding surfactants or emulsifiers which aid in mixing the humectants, occlusives, and emollients (Leyden and Rawlings 2002). It is a high water content moisturizer, usually with 50–88% water (see Table 2.3). Studies show that most bulk water in skin cream will evaporate from the

skin surface within 15 min after application (Rietschel 1978; Wepierre et al. 1982). When cream is first applied to the skin surface, the cream cannot be absorbed immediately by skin, and the cream liquid accumulates at the contact interface, resulting in a greater liquid height and greater resistance to motion. However, after several scans, because of the absorption of the skin cream and the evaporation of the water content, the cream film thickness decreases, which is responsible for the decrease in the coefficient of friction and adhesive force. When the interaction between skin cream, skin surface, and environment reaches an equilibrium, the skin cream covers the skin surface as a stable gel network (surfactant, fatty amphiphile, and water) such that the coefficient of friction and adhesive force remain constant. However, there is a protection period for skin cream. Beyond this period, the skin cream film will be removed, and the protection of the cream will reduce, at which point the coefficient of friction and adhesive force will decrease again.

Figure 4.7b shows the AFM images of skin with and without common cream treatment after approximately 3800 cycles at approximately 250 nN normal load. The sliding interaction has caused degradation and wear (scratch) marks on the skin surface. This is the type of wear one can potentially see if the skin surface is in contact with hard and sharp materials in daily life.

4.1.5 *Effect of Cream Film Thickness, Velocity and Normal Load on Friction as Well as Wear Resistance on the Macroscale*

Figure 4.8 shows the effect of cream thickness on the coefficient of friction on the macroscale (Tang and Bhushan 2010). The data at near zero thickness ($\sim$10 nm) corresponds to that of virgin skin. The results show that cream treated skin has a larger coefficient of friction than virgin skin, and when the thickness is lower than 1.8 μm, the coefficient of friction remains almost constant. This thickness regime corresponds to boundary lubrication, and the surface interaction between the skin cream film and the asperities dominates the contact. When the thickness is higher than 1.8 μm, the coefficient of friction decreases. After the application of skin cream, the skin is moistened and softened by the skin cream, leading to a greater ductility and a larger real area of contact, which results in stronger adhesion and higher coefficient of friction. This corresponds to mixed lubrication or hydrodynamic lubrication, and skin cream serves as a lubricating film, which is more easily sheared, so the coefficient of friction further decreases with further increases in cream thickness. It is important to note that the magnitude of the coefficient of friction is higher on the macroscale than on the nanoscale for virgin skin and cream treated skin. This is related to the increase of tip size. Nanoscale test data are taken by using a sharp AFM tip with a 10 nm radius that contacts with nanoasperities, while the macroscale test data are taken by using a spherical tip with a 1.5 mm radius that contacts a larger number of asperities that are believed to be responsible

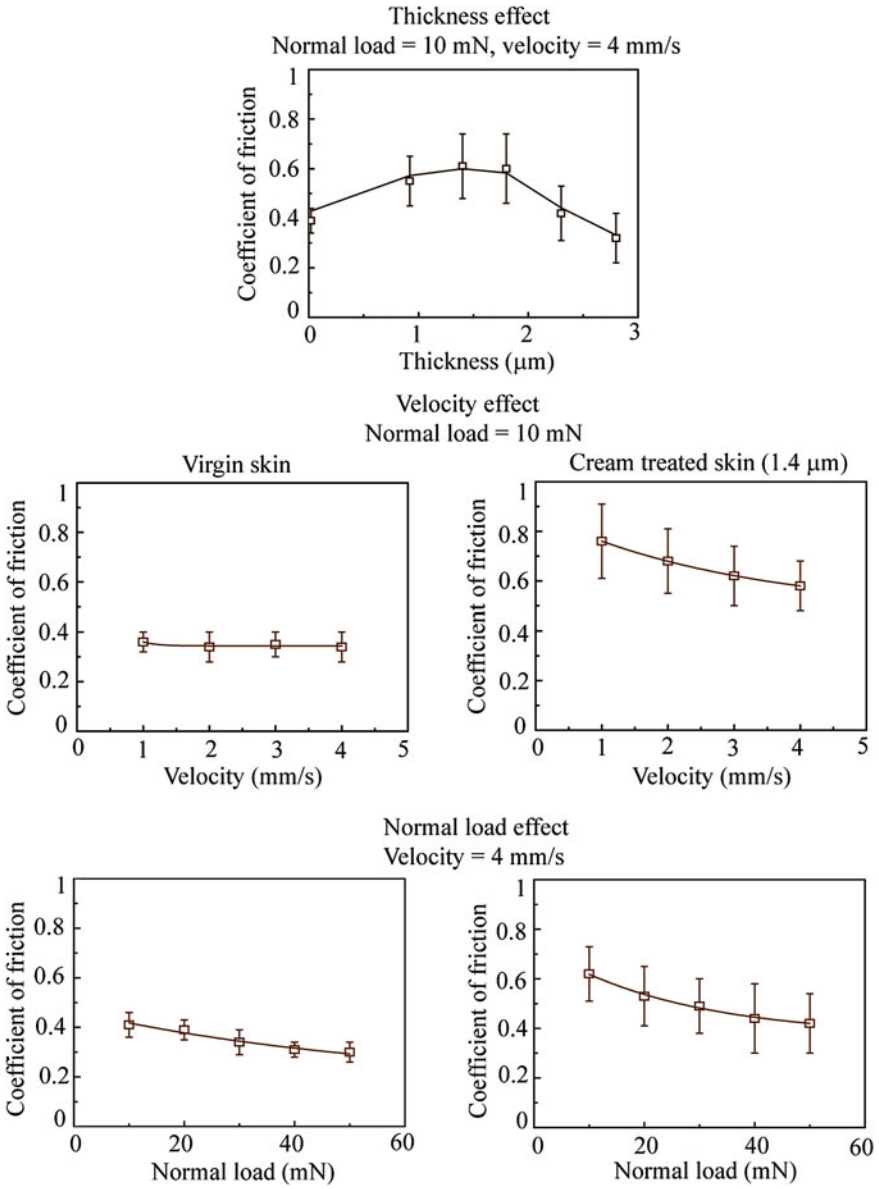

Fig. 4.8 Cream film thickness, velocity, and normal load effect on the coefficient of friction on the macroscale for rat skin with and without a common cream treatment (Tang and Bhushan 2010)

for the larger contact area. The combination of higher normal loads with a larger contact area is believed to be responsible for the increase of coefficient of friction on the macroscale.

Figure 4.8 also shows the effect of velocity and normal load on the coefficient of friction for skin with and without common cream treatment. The data indicates that the velocity has no effect on the coefficient of friction for virgin skin, but a higher velocity leads to a lower coefficient of friction for cream treated skin. As discussed earlier, skin cream is a shear-thinning fluid, i.e. the viscosity decreases with the increasing shear rate, which may be responsible for the decrease in the coefficient of friction. The effect of load data indicates that the coefficient of friction decreases as the normal load increases. This is because asperity deformation of skin is primarily elastic, and as the normal load increases, elastic deformation at the asperities is large, such that the individual asperities on the contacting surface are totally deformed, and the contact region approximates to the contact of a large single asperity (Bhushan 2013a, b). In this case, $\mu \propto W^{-1/3}$, and the coefficient of friction decreases with the increase of normal load (Appendix A).

Figure 4.9 shows the wear resistance of skin with and without a common cream treatment on the macroscale (Tang and Bhushan 2010). The data indicates that the coefficient of friction of virgin skin remains almost constant as a function of sliding cycles. For cream treated skin, the coefficient of friction increases dramatically when the sliding cycle increases up to approximately 400, after which it decreases slightly and then remains constant. It is because there are two phases in the application process of skin cream: absorption and protection. In the absorption phase, skin surface is moistened and softened by skin cream. Skin has a greater ductility and a larger real area of contact, which results in a larger coefficient of friction. After skin cream is fully absorbed, the evaporation of water on the skin surface may lead to a slight decrease in the coefficient of friction, and after that it reaches the protection phase and the coefficient of friction remains constant.

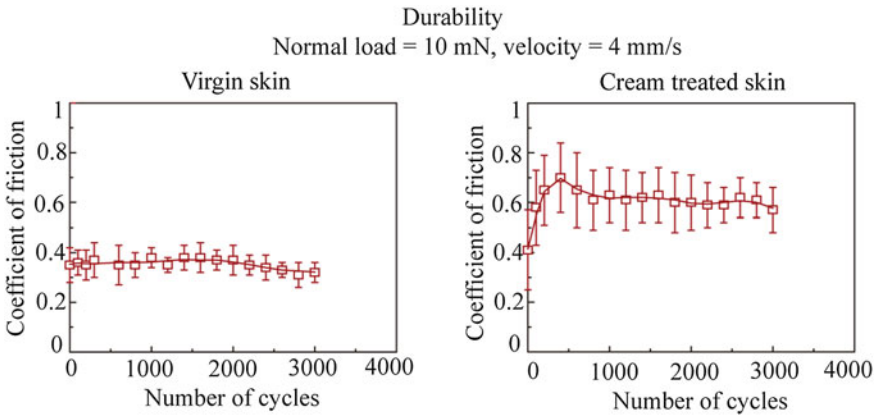

Fig. 4.9 The coefficient of friction on the macroscale as a function of the number of cycles for rat skin with and without a common cream treatment on the nanoscale (adapted from Tang and Bhushan 2010)

4.1.6 Summary

In this section, the effect the duration of cream treatment on film thickness and the effect of cream film thickness, velocity, normal load, relative humidity, and temperature on the coefficient of friction and adhesive force for skin with and without common cream treatment were studied on the nano- and macroscale. Wear resistance of skin with and without common cream treatment was also studied by repeated cycling tests. The major conclusions are as follows:

- Skin cream treatment reduces surface roughness and increases hydrophilicity and the coefficient of friction of skin.
- The duration of the cream treatment leads to lower film thickness, which should lead to lower coefficient of friction and adhesion with time.
- Cream film treated skin exhibits a larger load carrying capacity than untreated skin, and serves as a protective covering to the skin surface.
- For a thicker film, a larger meniscus at the contact interface results in larger meniscus and viscous forces leading to a larger coefficient of friction and adhesive force.
- Menisci shear and alignment of molecules affect coefficient of friction and adhesive force under low velocity. Viscoelastic shear affects these under high velocity.
- An increase in humidity increases adsorbed water molecules leading to a high coefficient of friction and adhesive force.
- Desorption of water molecules and reduced viscosity with an increase in temperature is responsible for a decrease in the coefficient of friction.
- On the macroscale, the magnitude of coefficient of friction is higher than on the nanoscale.
- The data show that skin cream treatment provides some protection from wear on nanoscale and macroscale for virgin and cream treated skin.

To sum up, this study demonstrates that skin cream can smooth the skin surface and increase the hydrophilic properties of skin. The coefficient of friction and adhesive force of virgin skin and cream treated skin depend on the duration of the cream treatment, cream film thickness, velocity, normal load, relative humidity, and temperature. The wear resistance studies show that the treatment of skin cream provides some protection from wear. A scale effect on the coefficient of friction is observed.

4.2 Various Cream Treatments

This section presents nanotribological data on skin with and without treatment with various creams (Tang et al. 2010a). For all tests on the nanoscale, for skin with cream treatment, film thickness was approximately 150 nm.

4.2.1 Duration of Cream Treatment, Adhesion, Friction, Dynamic Viscosity and Wear Resistance on the Nanoscale

As stated earlier, the duration of the cream treatment on skin leads to a decrease in film thickness. Figure 4.10 shows the film thickness as a function of time for skin treated with pure lanolin, pure petroleum jelly, oil free cream, common cream, and aqueous glycerin (Tang et al. 2010a). In all cases, the film thickness decreases and the rate of decrease is dependent upon the cream.

Figure 4.11 shows the coefficient of friction and adhesive force as a function of the sliding cycles for skin with and without treatment with various creams (Tang et al. 2010a). Both the coefficient of friction and adhesive force increase with an application of skin cream. The reasons for the increase in the friction and adhesion of cream treated skin is the presence of the cream film have been presented earlier. The result also shows that among the five kinds of skin cream, pure lanolin and pure petroleum jelly have the highest coefficient of friction and adhesive force, and aqueous glycerin has the lowest coefficient of friction and adhesive force.

Since dynamic viscosity describes a fluid's internal resistance to flow, it can help to better understand the different frictional behavior of various skin creams. The dynamic viscosities of various skin creams are shown in Fig. 4.12a (Tang et al. 2010a). The results show that aqueous glycerin has essentially a constant and low viscosity, indicating a slippery texture, while the other creams show a decreased viscosity with the increasing shear rate (i.e., shear thinning behavior). Compared to other skin creams, the pure lanolin and pure petroleum jelly have a high viscosity, indicating their sticky and greasy texture. The relationship between the coefficient of friction and dynamic viscosity of various skin creams are shown in Fig. 4.12b. The coefficient of friction increases with increasing dynamic viscosity, indicating that high viscosity results in the high coefficient of friction because of viscous effects.

Data in Fig. 4.11 show that the trends for coefficient of friction and adhesive force as a function of the number of cycles for pure lanolin and pure petroleum jelly are similar. For both creams, the coefficient of friction and adhesive force initially decrease slightly, and then remain at a higher and stable value with an increase of sliding cycles, implying a high wear resistance. The natural aging results presented in Fig. 4.10 show that for pure lanolin and pure petroleum jelly, the cream film remains at a high and constant value, indicating that when they are applied on the skin surface they form a thick and stable protective covering on the skin surface and block the evaporation of water from the skin, thus protecting the stratum corneum for a long time (Kligman 1978; Lodén and Maibach 2000).

In the case of oil-free cream and common cream treated skin, the coefficient of friction and adhesive force decrease dramatically. Then, as the sliding cycles increase up to approximately 2000, they remain constant, after which the coefficient of friction and adhesive force decrease again. In natural aging, the film thickness decreases dramatically within the first 600 s and then remains almost constant as the time increases up to approximately 2100 s, after which the film thickness

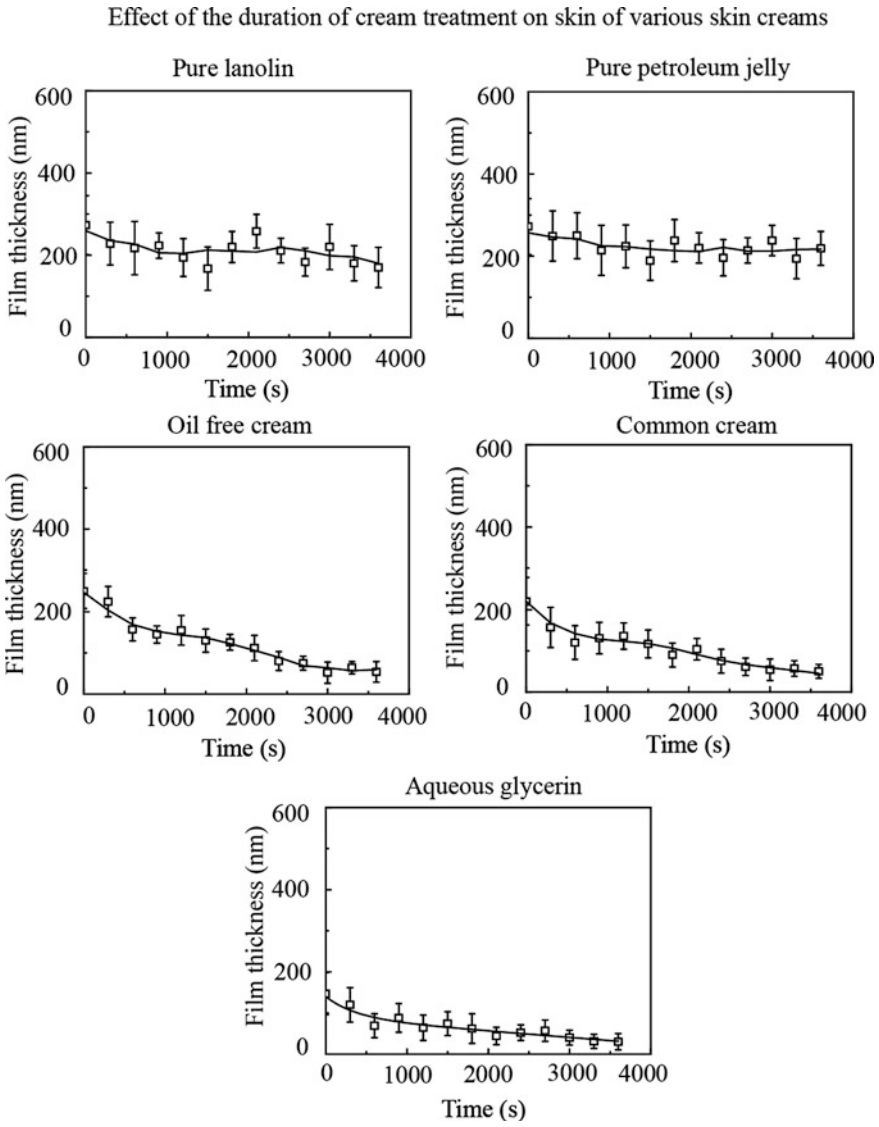

Fig. 4.10 Film thickness as a function of the duration of the cream treatment for rat skin treated with various creams (adapted from Tang et al. 2010a)

decreases again. For aqueous glycerin treated skin, the coefficient of friction and adhesive force decrease with the sliding cycles. In natural aging, the film thickness decreases with the time. The changes in the coefficient of friction and adhesive force with sliding cycles are believed to be caused by the change of cream film thickness, as a result of aging (Tang et al. 2010a). When skin cream is first applied to the skin surface, the cream cannot be absorbed fully, and the cream liquid accumulates at the

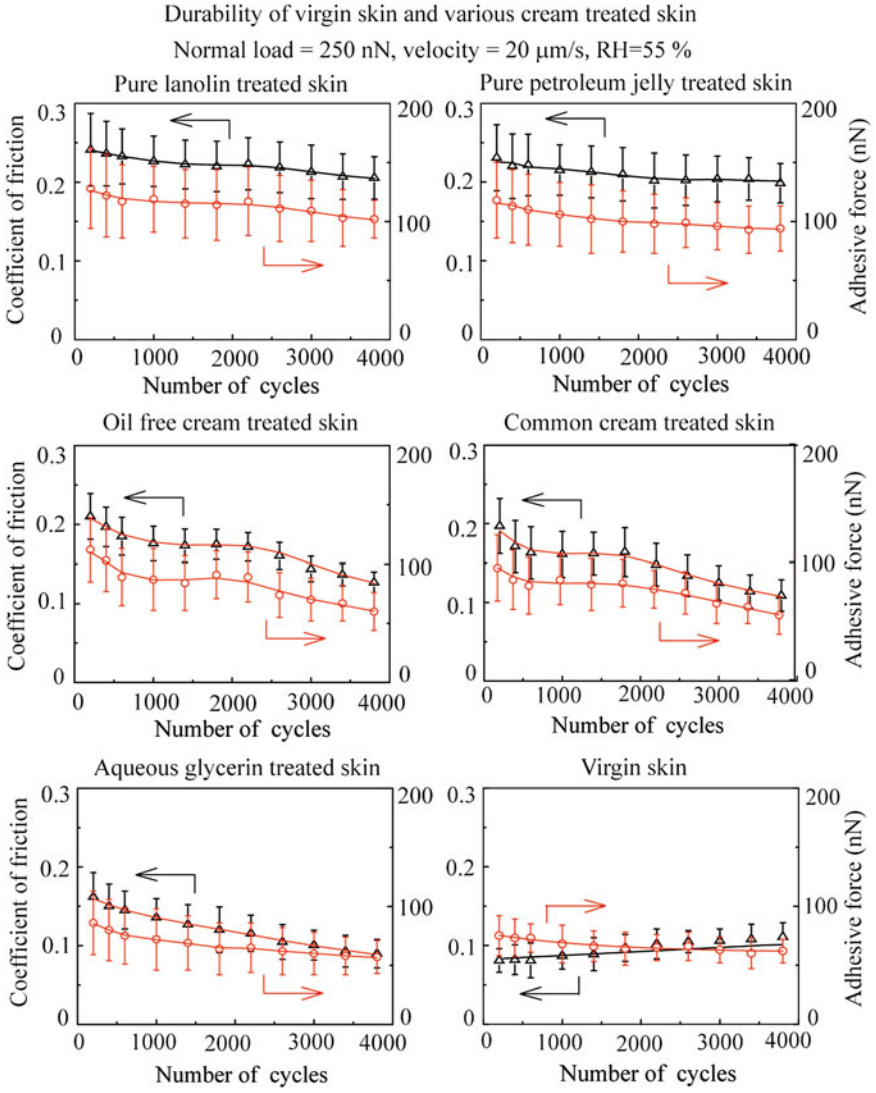

Fig. 4.11 The coefficient of friction and adhesive force on the nanoscale as a function of number of cycles of sliding for rat skin with and without various cream treatments (Tang et al. 2010a)

contact interface, resulting in a greater liquid height and greater resistance to motion. However, after several scans, because of the absorption of skin cream and evaporation of water content, the cream film thickness decreases, which is responsible for the decrease in the coefficient of friction and adhesive force. When the interaction between skin cream, skin surface, and environment reaches an equilibrium, the skin cream covers the skin surface as a stable gel network (surfactant, fatty amphiphile, and water) such that the coefficient of friction and

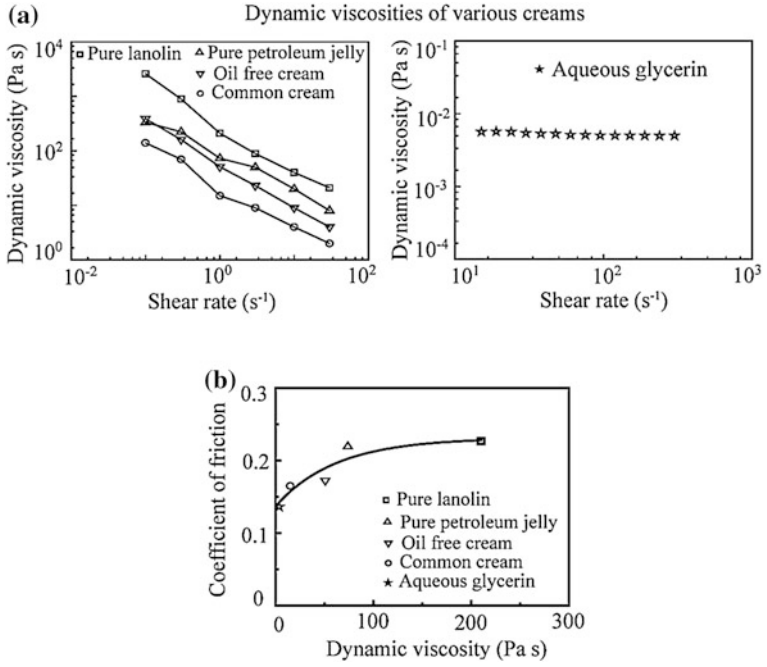

Fig. 4.12 **a** Dynamic viscosity as a function of shear rate for various creams, and **b** dynamic viscosity as a function of the coefficient of friction of rat skin treated with various creams. In (**b**), the dynamic viscosity is the data under the 1 s^{-1} shear rate and the coefficient of friction is the data for 1000 scan cycles (Tang et al. 2010)

adhesive force remain constant. However, there is a protection period for skin cream. Beyond this period, the skin cream film will be removed, and the durability of the cream will reduce, at which point the coefficient of friction and adhesive force will decrease again.

In the case of aqueous glycerin, unlike the common cream, glycerin cannot build up a stable gel phase network on skin surface, and the film thickness continuously decreases in the process of the absorption of glycerin and evaporation of water content. Therefore, the coefficient of friction and adhesive force keep decreasing with an increase of sliding cycles, which indicates low durability.

4.2.2 Effect of Relative Humidity on Film Thickness, Adhesive Forces and Effective Young's Modulus Mappings on the Nanoscale

Figure 4.13 shows typical film thickness, adhesive forces, and effective Young's modulus maps of skin with and without common cream treatment (Tang et al. 2010a). It shows that the cream film unevenly distributes on skin surface, and the

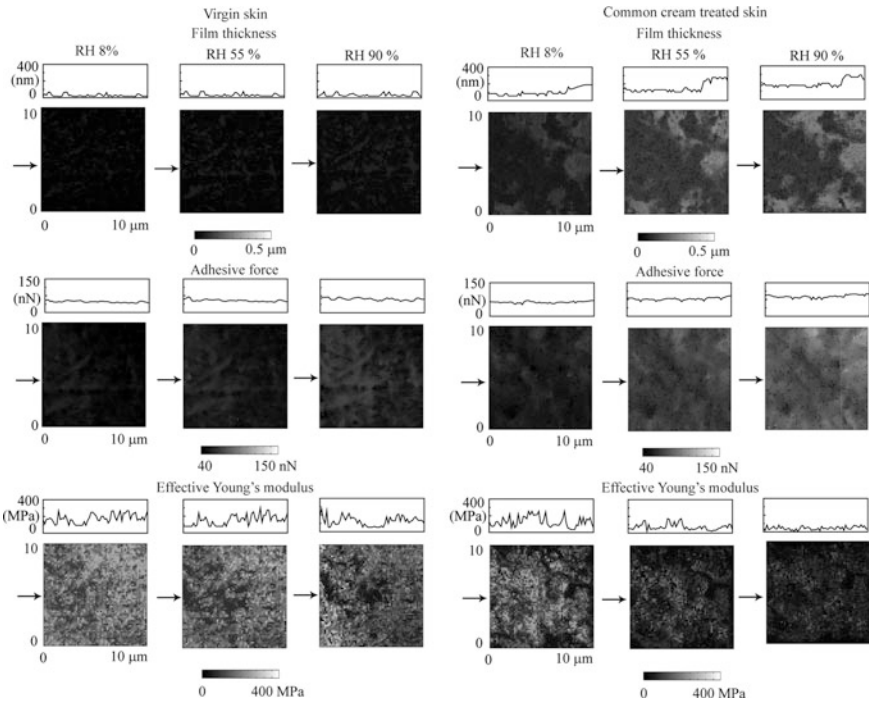

Fig. 4.13 Typical film thickness, adhesive forces, and Young's modulus maps on the nanoscale for rat skin with and without a common cream treatment at different humidities. Shown above each image is a cross-section taken at the position denoted by the corresponding arrows (adapted from Tang et al. 2010a)

region with a large adhesive force (bright region) in adhesive force maps corresponded to the region with a thicker cream film (bright region) in film thickness maps. It means that the adhesive force increases as the film thickness increases. The effect of cream film thickness on adhesive force has been discussed earlier.

Table 4.2 summarizes the film thickness, adhesive forces, and Young's modulus of skin with and without treatment with various creams at different humidities. Compared to other cream treated skin samples, the pure lanolin and pure petroleum jelly treated skin have a thicker film and higher adhesive force (Tang et al. 2010a). Virgin skin surface has an effective Young's modulus of about 157 MPa at RH 55%, which is consistent with other nanoindentation measurement results (Yuan and Verma 2006). Cream treated skin tends to have a larger film thickness and adhesive force and a smaller effective Young's modulus than that of virgin skin, indicating that all skin creams moisten and soften skin surface. However, the change in magnitude of various samples at different humidities is different.

The relative changes in film thickness, adhesive forces, and Young's modulus of various cream treated skin and virgin skin in reference to RH 55% are shown in Fig. 4.14 (Tang et al. 2010a). It shows that for all skin samples, low humidity

Table 4.2 Summary of skin cream film thickness, adhesive force, effective Young's modulus of rat skin with and without various cream treatments at different humidities (Tang et al. 2010)

Sample	Film thickness (nm)			Adhesive force (nN)			Young's modulus (MPa)		
	Humidity (RH)			Humidity (RH)			Humidity (RH)		
	8%	55%	90%	8%	55%	90%	8%	55%	90%
Pure lanolin treated	202 ± 49	234 ± 62	247 ± 59	101 ± 13	110 ± 15	117 ± 16	106 ± 67	98 ± 69	83 ± 55
Pure petroleum jelly treated	197 ± 48	220 ± 69	228 ± 71	99 ± 17	105 ± 19	109 ± 20	109 ± 69	105 ± 58	95 ± 51
Oil free cream treated	112 ± 31	178 ± 44	210 ± 54	66 ± 12	82 ± 15	96 ± 16	121 ± 77	65 ± 55	27 ± 33
Common cream treated	108 ± 30	157 ± 45	185 ± 52	67 ± 10	78 ± 12	89 ± 13	116 ± 61	72 ± 36	40 ± 27
Aqueous glycerin treated	52 ± 19	86 ± 25	98 ± 27	51 ± 10	65 ± 11	71 ± 11	148 ± 42	78 ± 30	51 ± 19
Virgin skin	28 ± 12	32 ± 16	36 ± 18	48 ± 7	52 ± 8	58 ± 9	176 ± 38	157 ± 41	130 ± 45

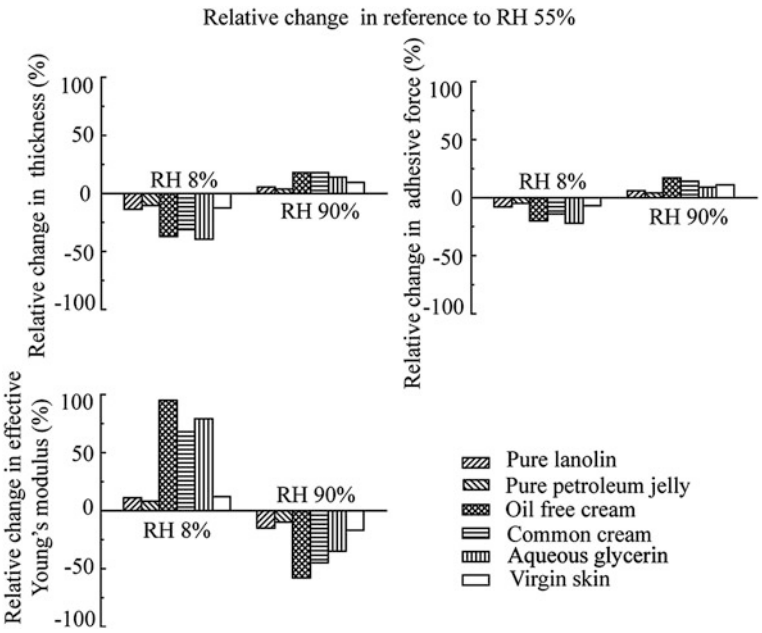

Fig. 4.14 Relative changes in film thickness, adhesive forces, and Young's modulus of rat skin with and without a common cream treatment in reference to RH 55% (Tang et al. 2010)

decreases the adhesive force and film thickness and increases the effective Young's modulus. High humidity increases the adhesive force and film thickness and decreases the effective Young's modulus. The results also show that at different humidities, the relative changes in the film thickness, adhesive force, and effective Young's modulus of pure lanolin and pure petroleum jelly treated skin and virgin skin are less than the oil free cream, common cream, and aqueous glycerin treated skin. This indicates that pure lanolin and pure petroleum jelly are less sensitive to changes in humidity. This is believed to be caused by the different hygroscopic capacities of their composition. Pure petroleum jelly is a mixture of non-polar hydrocarbons (Greenberg and Lester 1954). Due to the hydrocarbon molecules present in pure petroleum jelly, water is hardly absorbed (or desorbed) and penetrated into skin surface, and humidity has little effect on it. Pure lanolin is a very complex mixture of esters, diesters, and hydroxy esters of high molecule weight lanolin alcohols and lanolin acids (Lodén and Maibach 2000). The outer layer of the skin surface is covered with a thin layer of sebum, which contains triglycerides, diglycerides, fatty acids, wax esters, squalene, cholesterol, and cholesterol esters (Downing et al. 1969). Lanolin and sebum are both products of the sebaceous gland. Although their composition is different, the function is similar. Both of them are hydrophobic lipid layers and act to protect and waterproof skin, keeping it from becoming dry, brittle, and cracked by dehydration.

Oil free cream, common cream, and aqueous glycerin treated skin show higher relative changes in film thickness, adhesive forces, and effective Young's modulus at different humidities. As commercial skin creams, oil free cream and common cream have many humectants, which help to attract and hold water in the skin. As shown in Table 2.2, glycerin, lactic acid, potassium lactate, urea, sodium PCA, and propylene glycol are the humectants in common skin cream, and glycerin, hydroxyethyl urea, sorbitol, sodium hyaluronate, and PEG-8 (polyethylene glycol-8) are the humectants in oil free cream (Leyden and Rawlings 2002).

When the cream gel network layer covers the skin surface, the hydrophilic groups, such as the hydroxyl group, amines group, and carboxyl group in humectants, tend to form hydrogen bonds with molecules of water, such that the humectants help the skin surface to attract water molecules in the environment, especially in high humidity. However, these humectants fail to attract water at low humidity. The gel network of the skin cream film loses water content and collapses after staying in a dry environment.

4.2.3 Summary

In this section, Tang et al. (2010) studied adhesion, friction, and wear resistance of skin with and without various cream treatment on the nanoscale. The influence of relative humidity on cream film thickness, adhesive force and effective Young's modulus were also investigated. The major conclusions are as follows:

- Cream film is unevenly distributed on the skin surface.
- Skin cream treatment increases the coefficient of friction and adhesive force.
- Higher viscosity results in higher friction (stickiness) and higher wear resistance (durability). Pure lanolin and pure petroleum jelly have high wear resistance and sticky/greasy tactile perception compared with other skin creams.
- Adsorption of water molecules increases the film thickness and adhesive force and softens the skin surface.
- Lanolin and petroleum jelly are less sensitive to changes in humidity compared to other cream treatments.

References

Bhushan, B. (2013a). *Principles and Applications of Tribology* (2nd ed.). New York: Wiley.
Bhushan, B. (2013b). *Introduction to Tribology* (2nd ed.). New York: Wiley.
Downing, D. T., Strauss, J. S., & Pochi, P. E. (1969). Variability of the chemical composition of skin surface lipids. *Journal of Investigative Dermatology, 53*, 322–327.
Greenberg, L. A., & Lester, D. (1954). *Handbook of Cosmetic Materials*. New York: Interscience Publishers.

Kligman, A. M. (1978). Regression method for assessing the efficacy of moisturizers. *Cosmetics and Toiletries, 93*, 27–35.

Leyden, J. J., & Rawlings, A. V. (Eds.). (2002). *Skin Moisturization*. New York: Marcel Dekker.

Liu, H., & Bhushan, B. (2003). Nanotribological characterization of molecularly thick lubricant films for applications to MEMS/NEMS by AFM. *Ultramicroscopy, 97*, 321–340.

Lodén, M., & Maibach, H. I. (Eds.). (2000). *Dry Skin and Moisturizers: Chemistry and Function*. Boca Raton, Florida: CRC Press.

Rietschel, R. L. (1978). A method to evaluate skin moisturizers in vivo. *Journal of Investigative Dermatology, 70*, 152–155.

Tambe, N. S., & Bhushan, B. (2005). Friction model for the velocity dependence of nanoscale friction. *Nanotechnology, 16*, 2309–2324.

Tang, W., & Bhushan, B. (2010). Adhesion, friction and wear characterization of skin and skin cream using atomic force microscope. *Colloid Surface B, 76*, 1–15.

Tang, W., Bhushan, B., & Ge, S. (2010). Friction, adhesion and durability and influence of humidity on adhesion and surface charging of skin and various ski creams using atomic force microscopy. *Journal of Microscopy, 239*, 99–116.

Tao, Z., & Bhushan, B. (2007). Velocity dependence and rest time effect on nanoscale friction of ultrathin films at high sliding velocities. *Journal of Vacuum Science and Technology A, 25*, 1267–1274.

Wepierre, J., Adrangui, M., & Marty, J. P. (1982). Factors in the occlusivity of aqueous emulsions. *Journal of the Society of Cosmetic Chemists, 33*, 157–167.

Yuan, Y., & Verma, R. (2006). Measuring microelastic properties of stratum corneum. *Colloids Surfaces B: Biointerfaces, 48*, 6–12.

Chapter 5
Nanomechanical Properties of Rat Skin With and Without a Common Cream Treatment

In this chapter, nanomechanical properties of rat skin with and without a common cream treatment are presented (Bhushan et al. 2010). For all tests, for skin with cream treatment, film thickness was approximately 150 nm.

5.1 Nanoscratch

Figure 5.1a shows AFM topographical images and 2D profiles at the indicated plane of scratch marks generated at various normal loads for 15 cycles for skin with and without common cream treatment (Bhushan et al. 2010). Virgin skin could be scratched at a normal load of 3 μN and 15 cycles. The average scratch depth increases almost linearly with an increase in the normal load for virgin skin. Because of the plowing of the scratch tip, some pileup of worn corneocytes is formed at the side of the scratch wear track of virgin skin. The worn corneocytes pileup increases with normal load. For cream treated skin, from the 2D profiles of the AFM image it seems that the scratch depth and the pile up of the worn corneocytes is larger than virgin skin. However, it should be noted that because of the presence of the cream film (thickness $\sim$135 nm), when the scratch tip plows the skin surface, it is expected that it first plows the skin cream, and if the normal load is high enough, then the tip can reach the skin surface.

A plot of the average scratch depth as a function of the normal load is shown in Fig. 5.1b. In order to eliminate the effect of the cream film, the real scratch depth of cream treated skin was obtained by subtracting the average cream film thickness (135 $\pm$ 40 nm) from the scratch depth obtained from the 2D profiles of the AFM image. The data shows the scratch depth increases very little until a critical normal load of 15 μN is reached, above which the scratch depth increases rapidly. When the normal load is lower than 15 μN, the scratch depth of cream treated skin is lower than virgin skin; when it is higher than 15 μN, the scratch depth of cream treated skin is higher than virgin skin. These results suggest that cream treated skin exhibits scratch

B. Bhushan, *Biophysics of Skin and Its Treatments*, Biological and Medical Physics, Biomedical Engineering, DOI 10.1007/978-3-319-45708-6_5

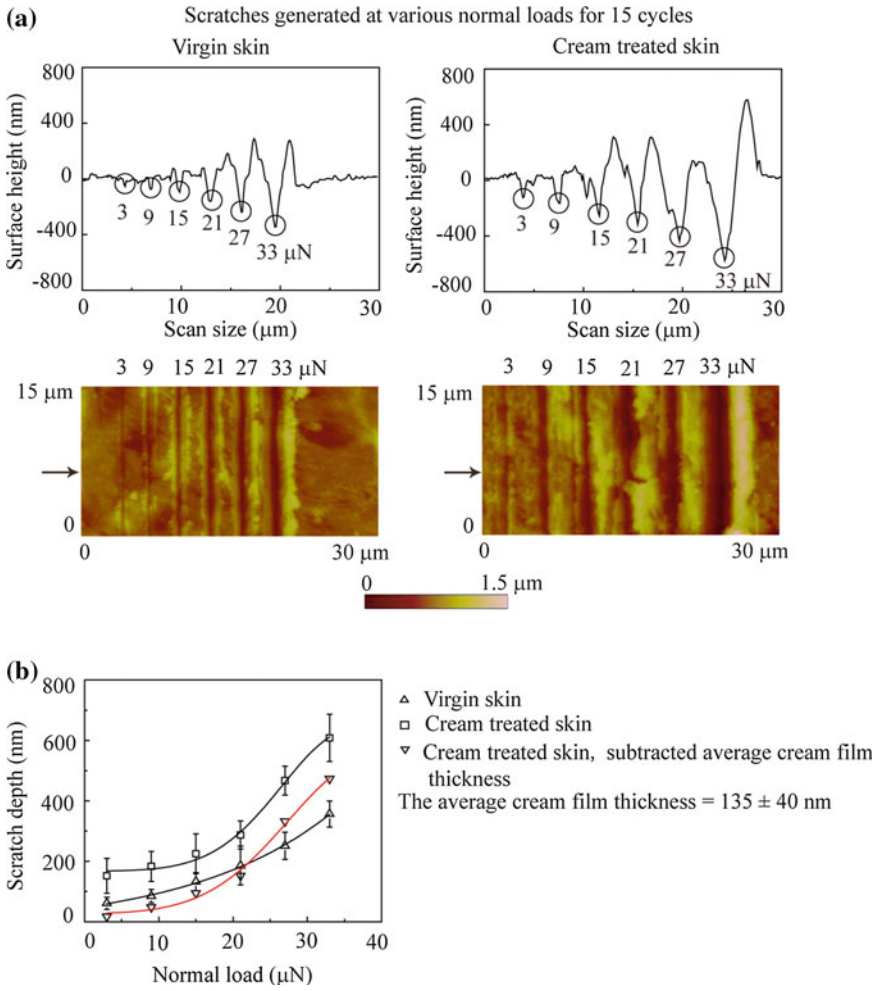

Fig. 5.1 **a** AFM topographical images of scratch marks generated at various normal loads for 15 cycles for rat skin with and without a common cream treatment. Shown above each image is a cross-section taken at the position denoted by the corresponding *arrows*, and **b** scratch depth as a function of normal load for virgin skin and cream treated skin (Bhushan et al. 2010)

resistance up to a normal load of 15 μN. When the load is below 15 μN, the skin cream film acts as a lubricant. Compared with virgin skin, it takes more sliding cycles to penetrate the cream film and damage skin surface. Therefore, the scratch depth of cream treated skin is lower than that of virgin skin below 15 μN load. When the load is above 15 μN, the tip goes through the entire cream film thickness, and the film does not provide protection anymore. Since skin cream softens and moistens skin surface and leads to a decrease in the hardness of the skin surface, as shown in Table 5.1, the tip can easily penetrate into the underlayer of skin. The scratch depth of cream treated skin is higher than that of virgin skin above 15 μN load (Bhushan et al. 2010).

Table 5.1 Hardness and elastic modulus of rat skin with and without common cream treatment, obtained using a nanoindenter (Bhushan et al. 2010)

	Virgin skin	Cream treated skin
Hardness (MPa)	2.0 ± 0.5	1.4 ± 0.4
Elastic modulus (MPa)	90 ± 31	49 ± 16

5.2 Nanoindentation

Figure 5.2 shows the representative load versus displacement plots for skin with and without common cream treatment (Bhushan et al. 2010). At 1000 nm indent depth, the load for virgin skin is about 35 μN, and load for cream treated skin is about 22 μN. Table 5.1 shows the summary of hardness and elastic modulus, which

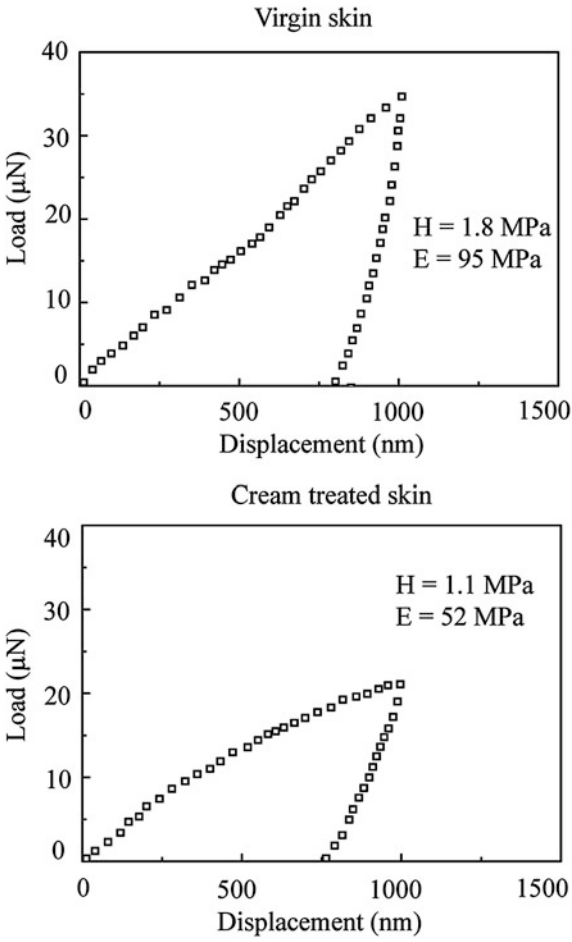

Fig. 5.2 Representative load–displacement plots of nanoindentations made at 1000 nm peak indentation displacement on rat skin with and without a common cream treatment (Bhushan et al. 2010)

were calculated from the indentation curves. The hardness and elastic modulus of cream treated skin is lower than virgin skin, indicating that the skin cream moistens and softens the skin surface. Note that since the skin consists of various layers, it does not exhibit isotropic mechanical properties from epidermis to dermis (Kendall et al. 2007). However, one can select a specific load and indentation depth to compare the nanomechanical properties of virgin skin and cream treated skin samples.

5.3 In Situ Tensile Measurements

Figure 5.3a shows the stress-strain curves for skin with and without common cream treatment (Bhushan et al. 2010). The stress-strain curves show a characteristic shape. During low strain range (0–42 and 0–50% for virgin skin and cream treated skin, respectively), the curve is concave. The stress-strain curve can be fitted to an exponential function. For the straight section, the elastic modulus can be calculated by dividing an increase of stress by the increase of strain. In the last part of the curve, in the strain range of 57–60% for virgin skin and 60–62% for cream treated skin, the yield occurs ending in a sudden necking of the skin sample; see the image in Fig. 5.3a. At this point, the ultimate tensile strength and ultimate strain can be measured. The results are shown in Table 5.2 (Bhushan et al. 2010).

According to various tensile test studies (Lanir and Fung 1974b; Vogel and Hilgner 1977; Dombi et al. 1993; Elsner et al. 2002), at the beginning of loading, a small stress will lead to a large strain since the collagen fibers are relaxed, and stress-strain curves thus show a characteristic concave shape. As the stress increases, the bundles of initially crimped or coiled collagen fibers in the dermis align along the axis of loading, and the stress-strain curves show a straight shape.

From both the stress-strain curves and the mechanical properties, it is observed that there is a slight decrease in the tensile properties of cream treated skin. The elastic modulus is a little lower than virgin skin, and ultimate strain is a little higher than virgin skin. This suggests that skin cream can improve the tensile properties of skin. The slight change may be because most of the ingredients in skin cream can only reach and act on the stratum corneum of skin and cannot affect the deep layer of skin (dermis layer), which is the main tension-carrying layer of skin.

Figure 5.3b shows AFM topographical images and 2D profiles of a control area with increasing strain for virgin skin and cream treated skin. Table 5.3 presents the surface roughness statistics (RMS and peak-valley distance or P-V distance) of skin with and without common cream treatment obtained from the AFM topographical images with increasing strain. The images show that the surface roughness of virgin skin and cream treated skin increase with an increase of strain, and the change of the roughness of virgin skin is larger than that of cream treated skin. For virgin skin, damage on the skin surface occurs in the form of patches at around 10% strain, and the amount increases as the strain increases. Skin is heterogeneous tissue. As mentioned before, the stratum corneum consists of layered anucleated corneocytes

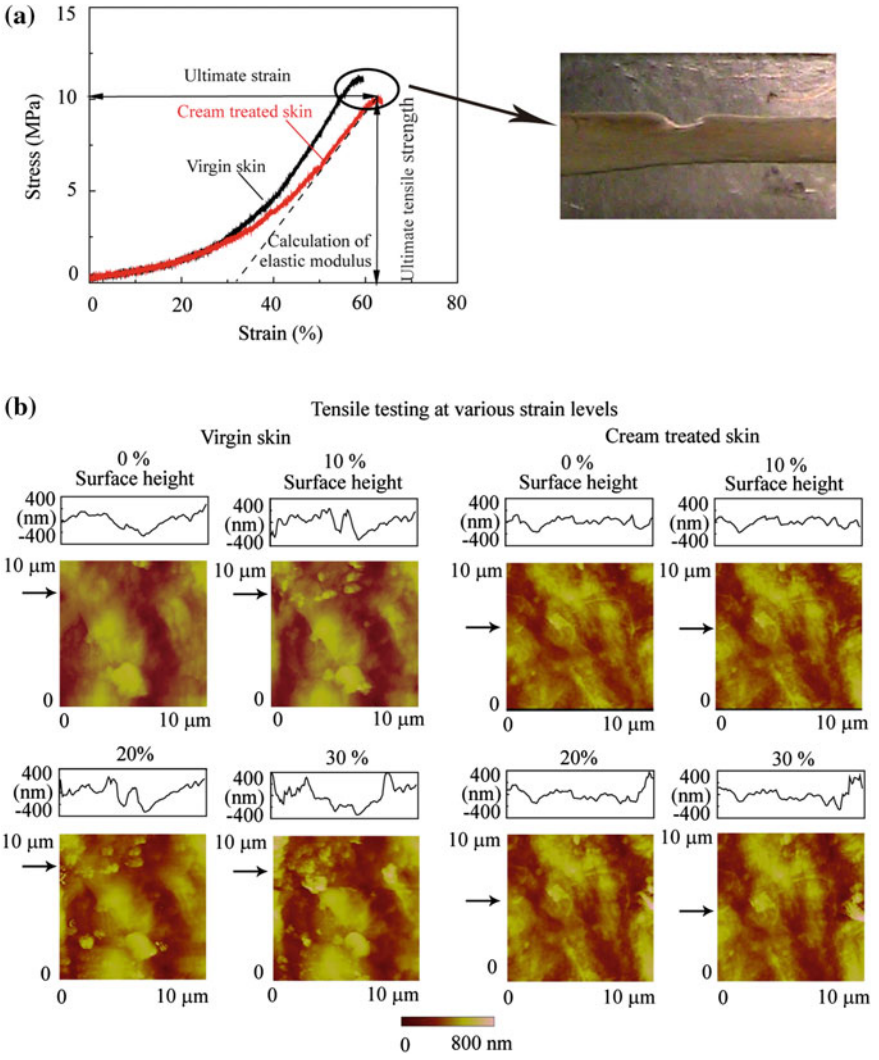

Fig. 5.3 **a** Stress-strain curves of rat skin with and without a common cream treatment and the image showing the necking of the skin sample under the ultimate strain, and **b** AFM topographical images of a control area showing progress of damage with increasing strain. Shown above each image is a cross-section taken at the position denoted by the corresponding *arrows* (Bhushan et al. 2010)

that are embedded in lipid lamellar regions. Because of the progressive degradation and desquamation of corneodesmosomes, the cohesive strength of corneocytes decreases from the inner side toward the outer side of stratum corneum, resulting in graded mechanical properties through the thickness of the stratum corneum (Weigand and Gaylor 1973; Chapman et al. 1991; Kenneth et al. 2006; Wu et al. 2006).

Table 5.2 Elastic modulus, ultimate tensile strength, and ultimate strain of rat skin with and without common cream treatment, obtained using in situ tensile tester (Bhushan et al. 2010)

	Virgin skin	Cream treated skin
Elastic modulus (MPa)	31 ± 11	22 ± 7
Ultimate tensile strength (MPa)	11 ± 2	10 ± 2
Ultimate strain (%)	59 ± 3	62 ± 5

Table 5.3 Surface roughness statistics of rat skin with and without common cream treatment, obtained from the AFM topographical images with the increasing strain in percent (Bhushan et al. 2010)

Skin type	RMS (nm)				P-V distance (nm)			
	0%	10%	20%	30%	0%	10%	20%	30%
Virgin skin	129	139	147	168	952	984	1029	1184
Cream treated skin	63	67	71	76	604	618	661	765

Skin hydration also strongly affects the mechanical properties of skin. It has been demonstrated that there is an increasing water gradient from the outer towards the inner stratum corneum (Rawlings and Matts 2005). The outer layer of the stratum corneum is low in water content and is rigid. The inner layer of the stratum corneum is high in water content and is more extensible. Stretching skin sets up the interlayer shear force of corneocytes due to the difference in cohesive strength and extensibility. As the strain increases, the corneocytes, which have less cohesive strength and extensibility, may desquamate; hence, the change in height and slope observed in the AFM images and the corresponding cross-sectional profiles. In the case of cream treated skin, there are a few patches present on skin surface at around 20% strain, which suggests the skin cream moistens and softens the skin surface, increasing the extensibility of the stratum corneum and reducing the generation of patches as the strain increases.

Though there are some patches showing in the AFM images with increasing strain, morphological changes are not significant. This may be because the main load-carrying capacity of skin is provided by the dermis and not the epidermis.

5.4 Summary

In this study, the nanoscratch, nanoindentation, and in situ tensile properties of skin with and without cream treatment were studied. The major conclusions from this study are as follows:

- Treated skin exhibits better scratch resistance up to a normal load of 15 μN. Once the normal load exceeds the value of 15 μN, the protection of the cream film fails.
- The hardness and elastic modulus of treated skin is lower than virgin skin, indicating that the cream can moisten and soften the skin surface.

- The stress-strain curves show a characteristic shape, which is related to the deformation of the collagen fibers in the dermis.
- Cream moistens and softens the skin surface, which increases the extensibility of the stratum corneum and reduces the damage shown by the generation of patches as the strain increases.

References

Bhushan, B., Tang, W., & Ge, S. (2010). Nanomechanical characterization of skin and skin cream. *Journal of Microscopy, 240*, 135–144.

Chapman, S. J., Walsh, A., Jackson, S. M., & Friedmann, P. S. (1991). Lipids, proteins and corneocyte adhesion. *Archives of Dermatological Research, 283*, 167–173.

Dombi, G. W., Haut, R. C., & Sullivan, W. G. (1993). Correlation of high-speed tensile strength with collagen content in control and lathyritic rat skin. *Journal of Surgical Research, 54*, 21–28.

Elsner, P., Berardesca, E., Wilhelm, K. P., & Maibach, H. I. (Eds.). (2002). *Bioengineering of the Skin: Skin Biomechanics*. Boca Raton, Florida: CRC Press.

Kendall, M. A. F., Chong, Y. F., & Cock, A. (2007). The mechanical properties of the skin epidermis in relation to targeted gene and drug delivery. *Biomaterials, 28*, 4968–4977.

Kenneth, S. W., Morgan, M. S., & Ananthapadmanabhan, K. P. (2006). Graded delamination behavior of human stratum corneum. *Biomaterials, 27*, 5861–5870.

Lanir, Y., & Fung, Y. C. (1974). Two-dimensional mechanical properties of rabbit skin-II. experimental results. *Journal of Biomechanics, 7*, 171–182.

Rawlings, A. V., & Matts, P. J. (2005). Stratum corneum moisturization at the molecular level: An update in relation to the dry skin cycle. *The Journal of Investigative Dermatology, 124*, 1099–1110.

Vogel, H. G., & Hilgner, W. (1977). Analysis of the low part of stress-strain curves in rat skin. *Archives of Dermatological Research, 258*, 141–150.

Weigand, D. A., & Gaylor, J. R. (1973). Removal of Stratum corneum in vivo: An improvement on the cellophane tape stripping technique. *Journal of Investigative Dermatology, 60*, 84–87.

Wu, K. S., van Osdol, W. W., & Dauskardt, R. H. (2006). Mechanical properties of human stratum corneum: Effects of temperature, hydration, and chemical treatment. *Biomaterials, 27*, 785–795.

Chapter 6
Triboelectrification of Rat Skin With and Without a Common Cream Treatment

This chapter presents surface charging (triboelectrification) of rat skin with and without a common cream treatment (Tang et al. 2010a, b). For all tests, the skin with a cream treatment, the film thickness was approximately 150 nm. In tests using the macroscale and microscale rubbing methods, the skin samples were rubbed with a polystyrene plate and a polystyrene microsphere, respectively.

6.1 Understanding of Triboelectric Charge Generation Between Skin and Polystyrene

Figure 6.1a, b shows a schematic of the electrostatic charge deposition on skin and the polystyrene surfaces used in the macroscale rubbing and microscale rubbing method, respectively (Tang et al. 2010b). Two observations are made in this schematic. First, before rubbing, the skin surface is negatively charged at neutral pH. This is because the epithelial cells in skin carry a negative charge on their surface due to the presence of negatively charged residues of proteins in the outer membrane (Burnette and Ongipipattanakul 1987; Piemi et al. 1999). The surfaces of the polystyrene plate and polystyrene microsphere are assumed to be uncharged before rubbing against the skin. Second, during rubbing, a positive charge is developed on the skin surface, and a negative charge is developed on the polystyrene plate or polystyrene microsphere.

In the triboelectric series (Diaz and Felix-Navarro 2004), skin is at the positive end of the scale and polystyrene is listed lower on the scale. This means that when skin is rubbed against polystyrene, a positive charge will be developed on the skin and an equal negative charge will be developed on the polystyrene. It is also important to note that the surface area of each of the contacting bodies affects charge development on each of them. Where one body has a larger surface area, it will tend to develop a positive chare, and the body with a smaller surface area will

B. Bhushan, *Biophysics of Skin and Its Treatments*, Biological and Medical Physics, Biomedical Engineering, DOI 10.1007/978-3-319-45708-6_6

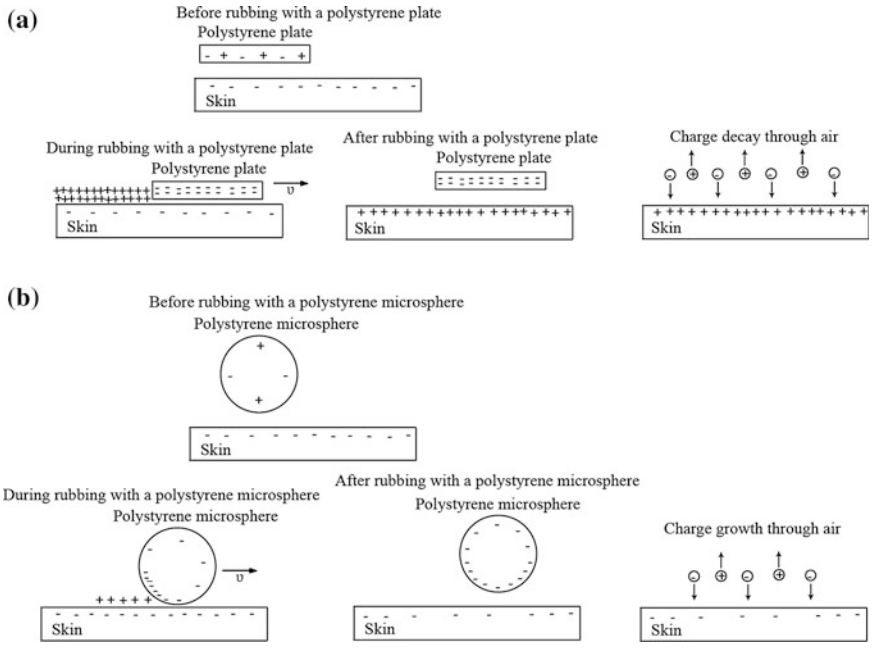

Fig. 6.1 Schematic of the deposition of electrostatic charge on rat skin and polystyrene surface using **a** macroscale rubbing method, and **b** microscale rubbing method (adapted from Tang et al. 2010b)

develop a negative charge (Henry 1953; Reynolds et al. 1957). In the tests described herein, the surface area of the skin sample was larger than the surface area of either the polystyrene plate or polystyrene microsphere. Therefore, a positive charge was developed on the skin and an equal negative charge on the polystyrene.

6.2 Effect of Velocity, Load, and Rubbing Time in Macroscale and Microscale Rubbing

6.2.1 Surface Potential Maps

Figure 6.2 shows the results of the macroscale rubbing tests for virgin and cream treated skin at two velocities (Tang et al. 2010b). In these tests, virgin and cream treated skin were mapped by AFM for surface height, absolute surface potential, and relative surface potential before and after rubbing with a polystyrene plate at a load of 2 N for 30 s at velocities of 10 and 30 mm/s. Figure 6.3 shows the results of the microscale rubbing tests for virgin and cream treated skin after rubbing at a load of 2 μN for 600 s at velocities of 480 and 720 μm/s (Tang et al. 2010b). Scanning by the AFM for both the macroscale rubbing test and the microscale

rubbing test was completed from left to right and from top to bottom for each image. In both Figs. 6.2 and 6.3, the first column is the surface height of the sample, the second column is the absolute surface potential, and the final column is the relative surface potential. The last column shows the same surface potential data as the second column, but the average absolute surface potential is subtracted out, and the scale is reduced to show more contrast. Shown above each image is a cross-sectional profile taken at the position denoted by the corresponding arrows.

Figure 6.2 (left) shows that, after rubbing virgin skin with a polystyrene plate, the cross-sectional profile of absolute surface potential exhibits a significant change from the before-rubbing condition (Tang et al. 2010b). In ambient conditions, a charged insulated body will lose its charge slowly when surrounded by air. The reason for this is that normally air contains few charged particles or ions, which are produced primarily by some ionization device, or electrical or radioactive radiation (Jonassen 1998). By being attracted to the charged body, these air ions might neutralize its charge and cause a decrease in the charge. Since the skin sample was attached to insulating electrical tape, its charge decayed mainly through air. As

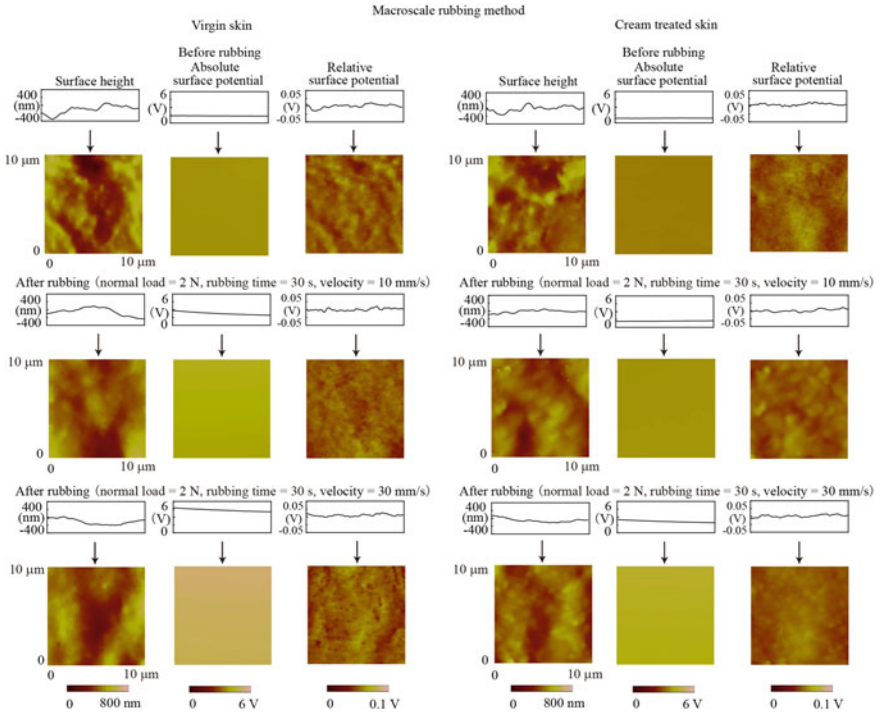

Fig. 6.2 AFM images of surface height, absolute surface potential and relative surface potential for virgin rat skin (*left*) and common cream treated skin (*right*) before and after rubbing with a polystyrene plate at two different velocities. Shown above each image is a vertical cross-section taken at the position denoted by the corresponding arrows. Scanning was done from *left* to *right* and from *top* to *bottom* for each experiment (Tang et al. 2010b)

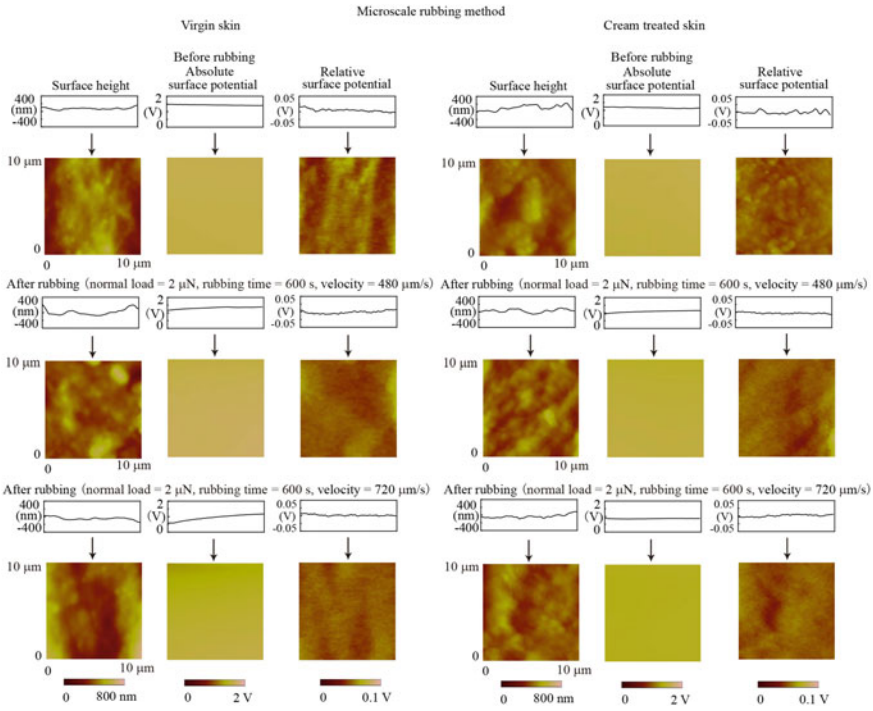

Fig. 6.3 AFM images of surface height, absolute surface potential and relative surface potential for virgin rat skin (*left*) and common cream treated skin (*right*) before and after rubbing with a polystyrene microsphere at two different velocities. Shown above each image is a vertical cross-section taken at the position denoted by the corresponding *arrows*. Scanning was done from *left* to *right* and from *top* to *bottom* for each experiment (Tang et al. 2010b)

shown in Fig. 6.1a, after rubbing with the polystyrene plate, the positively charged skin is surrounded by ionized air with positive and negative ions. The positive ions will not affect the charge on the skin surface, but the negative ions will cause the charge to decrease with time.

Figure 6.3 (left) shows that after rubbing virgin skin with a polystyrene microsphere, the cross-sectional profile of absolute surface potential shows a growth trend in absolute surface potential over the before-rubbing condition (Tang et al. 2010b). This growth trend is illustrated as a lower absolute surface potential at the top of the image than at the bottom. As shown in Fig. 6.1b, after rubbing with polystyrene microsphere, the negative charge on the skin surface is partly neutralized by the generated positive charge, which will be discussed in detail in the next subsection. The equilibrium of the surface charge is broken, and negative ions tend to deposit on the skin surface such that the surface potential shows growth with time.

Figures 6.2 (right) and 6.3 (right) show that, after rubbing cream treated skin with a polystyrene plate and polystyrene microsphere, respectively, the cross-sectional profile of the absolute surface potential indicates a more constant

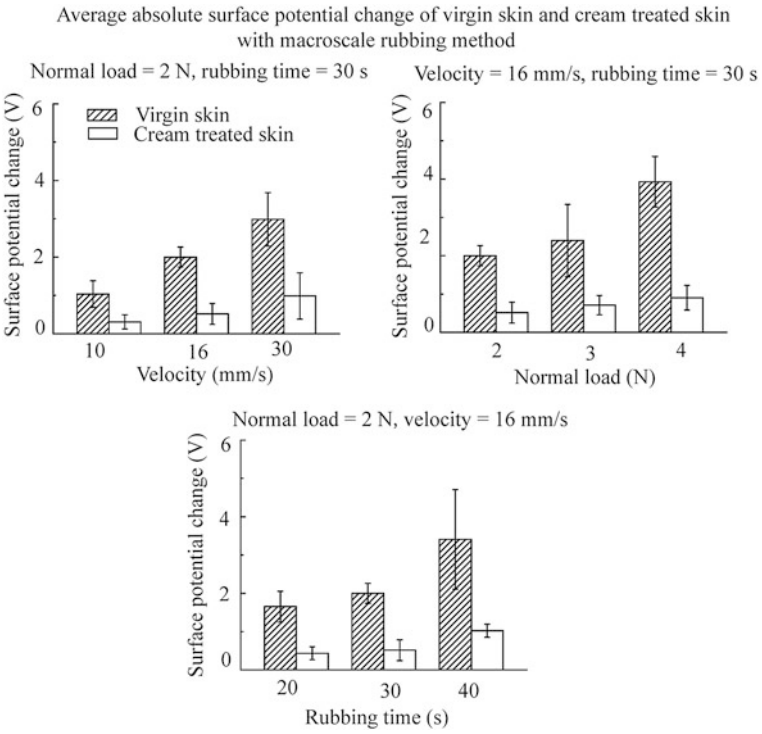

Fig. 6.4 Bar chart showing the average absolute surface potential change and its dependence on velocity, normal load, and rubbing time for rat skin with and without a common cream treatment after rubbing with a polystyrene plate (Tang et al. 2010b)

absolute surface potential during the tests (Tang et al. 2010b). This suggests that cream treated skin dissipates charge more quickly than virgin skin. Thus, by the time the measurement is taken, a generally constant surface potential is achieved.

6.2.2 *Effect of Skin Cream Treatment*

Figure 6.4 displays a quantitative bar chart showing the average absolute surface potential change by varying velocity, normal load, and rubbing time in the macroscale rubbing tests for virgin and cream treated skin (Tang et al. 2010b). Figure 6.5 shows the same data for the microscale rubbing tests (Tang et al. 2010b). Baseline data was taken before rubbing in order to report a change in the absolute surface potential due to rubbing. These figures show that for virgin skin, the change in absolute surface potential is more obvious than that for cream treated skin, indicating that cream treatment reduces the amount of charge present on the skin surface.

The tendency of virgin skin to become charged during rubbing is partially due to the high electrical resistance of its stratum corneum. The stratum corneum is a good

insulator with high electrical resistance, on the order of hundreds of kilo-ohms. Due to the high electrical resistance, it is susceptible to charging and retains that charge during triboelectric contact. The small change in the absolute surface potential of cream treated skin suggests that cream treatment reduces the generation of static charge. This reduction might be related to the reduction of surface resistivity and the reduction of the work function gap between the cream treated skin surface and the polystyrene surface.

When cream is applied to the skin surface, the bulk water in the cream will moisten the skin surface. Meanwhile, the hydrophilic groups, such as the hydroxyl group, amines group, and carboxyl group in the humectant, tend to form hydrogen bonds with molecules of water, such that the humectant in the skin cream also helps skin surface attract water molecules in the environment. The bulk water in skin cream and attracted water from the environment will introduce ions that may be formed by the auto-dissociation of water to skin. Further, impurities may be solvated and mobilized by water molecules. In addition, skin cream itself also can introduce ions to skin surface. All ions act as charge carriers that generate a current decreasing the surface resistivity, which reduces the amount of charge present on the skin surface from being rubbed with polystyrene. Additionally, the cream

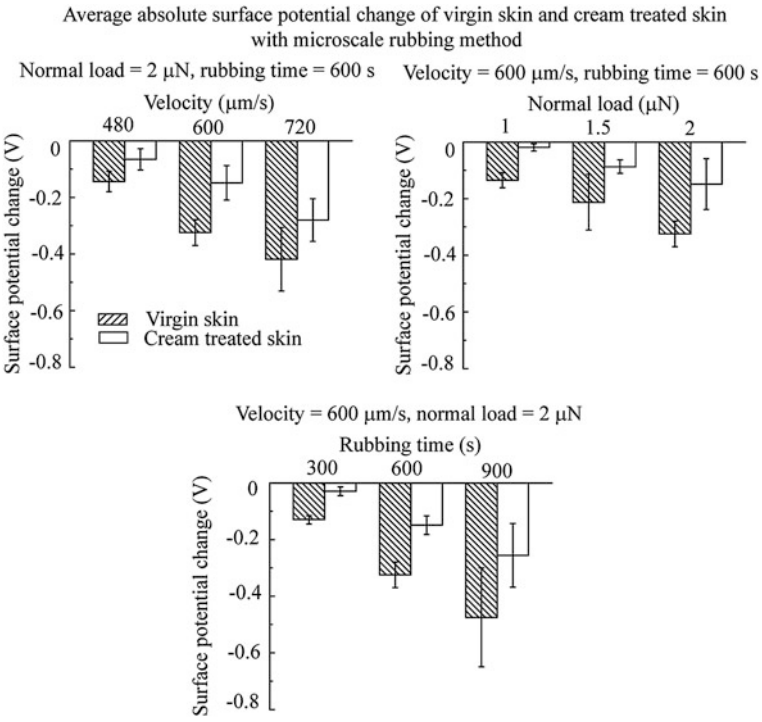

Fig. 6.5 Bar chart showing the average absolute surface potential change and its dependence on velocity, normal load, and rubbing time for rat skin with and without a common cream treatment after rubbing with a polystyrene microsphere (Tang et al. 2010b)

treatment may cause a considerable increase in the work function of skin surface, such that the gap between the work function of the contacting surfaces will decrease (Tang et al. 2010b). The decrease of contact potential difference will result in the reduction of transferred charge.

6.2.3 Comparison of Macroscale and Microscale Rubbing Data

By comparing the data in Figs. 6.4 and 6.5, it can be shown that the magnitude of the change in absolute surface potential resulting from the macroscale rubbing method is larger than that resulting from the microscale rubbing method for both virgin and cream treated skin (Tang et al. 2010b). This is related to the higher normal load, velocity, and rubbing area in macroscale rubbing tests.

The data also shows that with the macroscale rubbing method, the average absolute surface potential increases with an increase in velocity, normal load, and rubbing time. However, with the microscale rubbing method, the average absolute surface potential decreases with the increase of velocity, normal load, and rubbing time. This difference can be explained using the schematic shown in Fig. 6.1. As described earlier, skin is negatively charged at a neutral pH, and when skin is rubbed against polystyrene, a positive charge will develop on the skin. When skin is rubbed with a polystyrene plate, the large normal load, velocity, and rubbing area lead to a large generation of a positive charge on skin surface. This positive charge will neutralize the existing negative charge on the skin. Because the amount of positive charge is still larger than the original negative charge, the average absolute surface potential of skin shows an increasing trend. Finally, the skin surface ultimately is positively charged. This is not the case with the microscale rubbing method. When skin is rubbed with a polystyrene microsphere, the small normal load, velocity, and rubbing area lead to the generation of a small positive charge on the skin surface. This small positive charge is not sufficient to neutralize the original negative charge. With the increased generation of a positive charge, there is a larger decrease of the negative charge on skin surface. Therefore, the average absolute surface potential shows a decreasing trend. Thus, the skin surface remains negatively charged.

6.2.4 Effect of Velocity, Normal Load, and Rubbing Time on Absolute Surface Potential

Figures 6.4 and 6.5 show the average absolute surface potential change and its dependence on velocity, normal load, and rubbing time for skin with and without common cream treatment with the macroscale and microscale rubbing methods, respectively (Tang et al. 2010b). The change in absolute surface potential is smaller

for the cream treated skin compared to that of virgin skin in all operating conditions. For both virgin skin and cream treated skin, the change in absolute surface potential increases with an increase of velocity, normal load, and rubbing time (Tang et al. 2010b).

The dependence of surface potential on velocity is related to the thermal gradient across the interface. According to Henry (1953), when two samples of identical material but asymmetric size are rubbed together, the sample with the smaller contact area will have a larger increase in temperature relative to the sample with the larger contact area. This will generate a temperature gradient across the interface, which will result in a larger number of mobile particles migrating from the hot side to the cold side of the boundary. After contact, the colder sample is positively charged, and the hotter sample is negatively charged. Based on the temperature gradient theory, the magnitude of the generated charge is proportional to the temperature difference produced between the two samples. An increase in velocity will induce an increase in surface temperature, which will result in an increase in the electron migration rate. Thus, the surface potential increases with an increase in velocity.

In triboelectrification, the real contact area is an important factor that determines charge generation. Many studies suggest that the generated charge is proportional to the contact area when two materials are rubbed together (Montgomery et al. 1961; Wåhlin and Bäckström 1974; Lowell and Truscott 1986; Ohara et al. 1990). An increase in normal load will lead to an increase in the deformation of a single asperity and the number of contacting asperities, resulting in the increase of the real contact area (Bhushan 2013a, b). The larger the real contact area, the more electrons that are available to be transferred, such that the surface potential increases with an increase in normal load.

Skin is a viscoelastic material, meaning that the deformation of skin will increase with time under a constant normal load. The dependence of surface potential on rubbing time is believed to be caused by the gradual increase in the contact area. In addition, surface wear may be another reason for the increase in surface potential as rubbing time increases. Because of the duration of the cream treatment, the film thickness of the cream will decrease with time (see data presented earlier). Further, the cream film is removed from the skin surface after a number of sliding cycles. These will all lead to an increase in surface resistivity and an increase in the work function gap between the cream treated skin surface and the polystyrene surface, resulting in an increase in surface potential as rubbing time increases.

6.3 Effect of Relative Humidity on Surface Potential in Microscale Rubbing

Figure 6.6 shows surface potential maps of skin with and without common cream treatment after rubbing with a polystyrene microsphere at three different humidities of 8, 55, and 90% (Tang et al. 2010a). Compared to the cream treated skin sample,

there is more contrast in the relative surface potential images of virgin skin at low humidity, indicating the existence of trapped charge areas. These trapped charge areas are seen as bright areas on virgin skin in the relative surface potential image at RH 8%. However, the trapped charge areas are not seen at RH 90% for virgin skin. This observation indicates that in high humidity, water molecules in air play a significant role in the dissipation of surface charges. It is also noted that the trapped charges are less pronounced in the cream treated samples.

Figure 6.7 shows the relative change in average absolute surface potential of skin with and without a common cream treatment after the microscale rubbing method at two different humidities of 8 and 90% in reference to 55% (Tang et al. 2010a). It shows that for both skin samples, low humidity increases the surface potential and high humidity decreases the surface potential. The data indicates that cream treated skin is better able to reduce the buildup of surface charge at low humidity. It should be noted that although the virgin skin surface is covered naturally by a hydrophobic lipid layer, the layer is too thin to protect skin from dehydrating in low humidity, as cream treatment does. Therefore, virgin skin tends to build up more surface charge than cream treated skin and has the highest surface potential.

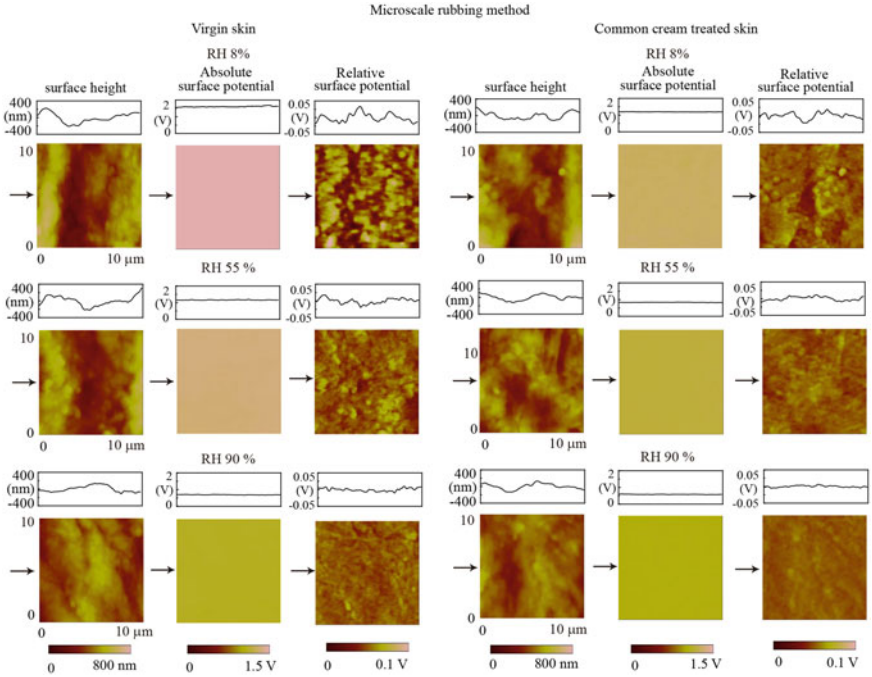

Fig. 6.6 AFM images of surface height, absolute surface potential, and relative surface potential for rat skin with and without a common cream treatment after rubbing with polystyrene microsphere at different humidities. Shown above each image is a cross-section taken at the position denoted by the corresponding *arrows* (adapted from Tang et al. 2010a)

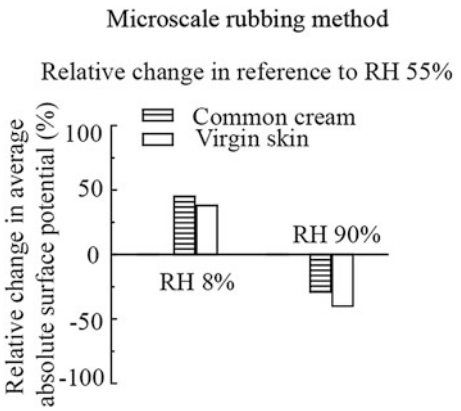

Fig. 6.7 Bar chart showing relative changes in surface potential of rat skin with and without a common cream treatment in reference to RH 55% after rubbing with a polystyrene microsphere (adapted from Tang et al. 2010a)

6.4 Summary

Triboelectrification of skin with and without a common cream treatment using the Kelvin probe method was carried out. The skin surface was charged by rubbing with a polystyrene plate on the macroscale and a polystyrene microsphere on the microscale. The effect of velocity, normal load, rubbing time, and relative humidity on the surface potential was investigated. The major conclusions are as follows:

- Cream treatment reduces the electrostatic charge buildup on the skin surface.
- Charge on skin can dissipate rapidly. The cream treatment can increase this rate of dissipation.
- An increase in velocity, normal load, or rubbing time increases the electrostatic charging on skin surface.
- Low humidity increases the surface potential and high humidity decreases it.
- Humidity facilitates charge dissipation.

References

Bhushan, B. (2013a). *Principles and Applications of Tribology* (2nd ed.). New York: Wiley.

Bhushan, B. (2013b). *Introduction to Tribology* (2nd ed.). New York: Wiley.

Burnette, R. R., & Ongipipattanakul, B. (1987). Characterization of the permselective properties of excised human skin during iontophoresis. *Journal of Pharmaceutical Sciences, 76*, 765–773.

Diaz, A. F., & Felix-Navarro, R. M. (2004). A Semi-quantitative tribo-electric series for polymeric materials: The influence of chemical structure and properties. *Journal of Electrostatics, 62*, 277–290.

Henry, P. S. H. (1953). The role of asymmetric rubbing in the generation of static electricity. *British Journal of Applied Physics, 4*, S31–S36.

Jonassen, N. (1998). *Electrostatics*. New York: Chapman & Hall.

Lowell, J., & Truscott, W. S. (1986). Triboelectrification of identical insulators: I. An experimental investigation. *Journal of Physics. D. Applied Physics, 19*, 1273–1280.

Montgomery, D. J., Smith, A. E., & Wintermute, E. H. (1961). Static electrification of filaments: effect of filament diameter. *Textile Research Journal, 31*, 25–31.

Ohara, K., Tonouchi, T., & Uchiyama, S. (1990). Frictional electrification of thin films deposited by the Langmuir-Blodgett method. *Journal of Physics. D. Applied Physics, 23*, 1092–1096.

Piemi, M. P. Y., Korner, D., Benita, S., & Marty, J. P. (1999). Positively and negatively charged submicron emulsions for enhanced topical delivery of antifungal drugs. *Journal of Controlled Release, 58*, 177–187.

Reynolds, S. E., Brook, M., & Gourley, M. F. (1957). Thunderstorm charge separation. *Journal of Meteorology, 14*, 426–436.

Tang, W., Bhushan, B., & Ge, S. (2010a). Friction, adhesion and durability and influence of humidity on adhesion and surface charging of skin and various skin creams using atomic force microscopy. *Journal of Microscopy, 239*, 99–116.

Tang, W., Bhushan, B., & Ge, S. (2010b). Triboelectrification studies of skin and skin cream using kelvin probe microscopy. *Journal of Vacuum Science and Technology A, 28*, 1018–1028.

Wåhlin, A., & Bäckströml, G. (1974). Sliding electrification of teflon by metals. *Journal of Applied Physics, 45*, 2058–2064.

Part II
Rat Skin and Pig Skin—Virgin and Damaged

Chapter 7
Friction, Wear, and Nanomechanical Properties of Virgin and Damaged Rat Skin and Pig Skin With and Without a Common Cream Treatment

The surface roughness, contact angle, and nano- and macroscale friction data of rat skin are presented first, followed by that of pig skin. Finally, nanoindentation data are presented (Bhushan et al. 2012). For all tests on the nanoscale on skin with cream treatment, film thickness was approximately 150 nm, and for macroscale tests, it was approximately 1.4 μm.

7.1 Surface Roughness, Contact Angle, Friction, and Wear Properties With and Without a Common Cream Treatment—Rat Skin

7.1.1 Surface Roughness, Contact Angle, and Nanoscale Friction

Figure 7.1 shows the surface roughness maps and corresponding height profiles of the cross section indicated by the arrows on a 20 μm × 20 μm scan size for virgin skin, damaged skin, cream-treated virgin skin, and cream-treated damaged skin (Bhushan et al. 2012). The height profiles appear smoother for virgin skin compared with damaged skin, and for cream-treated skin compared with untreated skin. The RMS roughness data, which serve as quantified expressions of the surface characteristics, are shown in Fig. 7.2a (Bhushan et al. 2012). The damaged skin has a higher roughness than virgin skin. After treatment with skin cream, the roughness of virgin skin and damaged skin decreased. A reasonable explanation is that the skin cream can fill the gap between the cells of stratum corneum.

The contact angle data for virgin skin and damaged skin are shown in Fig. 7.2b (Bhushan et al. 2012). The contact angle of virgin skin is lower than damaged skin due to physical and chemical changes to the skin surface. An increasing surface roughness may be partially responsible for an increase in the contact angle of the

B. Bhushan, *Biophysics of Skin and Its Treatments*, Biological and Medical Physics, Biomedical Engineering, DOI 10.1007/978-3-319-45708-6_7

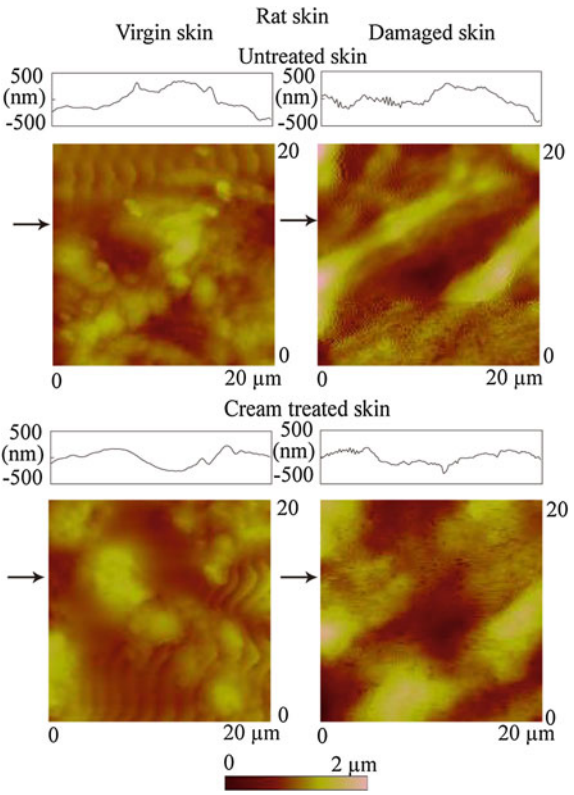

Fig. 7.1 AFM roughness maps and roughness profiles taken at *arrows* indicated for virgin rat skin, damaged skin, treated virgin skin, and treated damaged skin (Bhushan et al. 2012)

damaged skin. After treatment with skin cream, the contact angles of virgin and damaged skin decreased. The hydrophilic groups in skin cream, such as hydroxyl group, amines group, and carboxyl group in the humectants, increase the surface hydrophilicity and lead to a lower contact angle.

Friction force as a function of normal load curves for virgin rat and pig skin (to be discussed later) are shown in Fig. 7.3 (Bhushan et al. 2012). An average value of coefficient of friction was obtained from the slope of the fitted line of the data. The intercept on the horizontal axis of normal load is the adhesive force, which is dominated by the meniscus contribution. The coefficient of friction of various skin samples are presented in Fig. 7.2c (Bhushan et al. 2012). The coefficient of friction of damaged skin is higher than that of virgin skin, and increases for both virgin and damaged skin after treatment. Schematics show various rat skin interfaces. Damage to skin results in greater surface roughness and shrinking of the stratum corneum cells due to water loss. This increases the number of asperities on the surface (Bhushan 2013a, b). The natural lipids present also deplete. Cream treatment for both skin types increases friction. Liquid films (lipid and condensed water vapor) present on the skin surface reduce the interfacial shear strength leading to lower friction. However, a thicker film forms meniscus bridges at asperity contacts

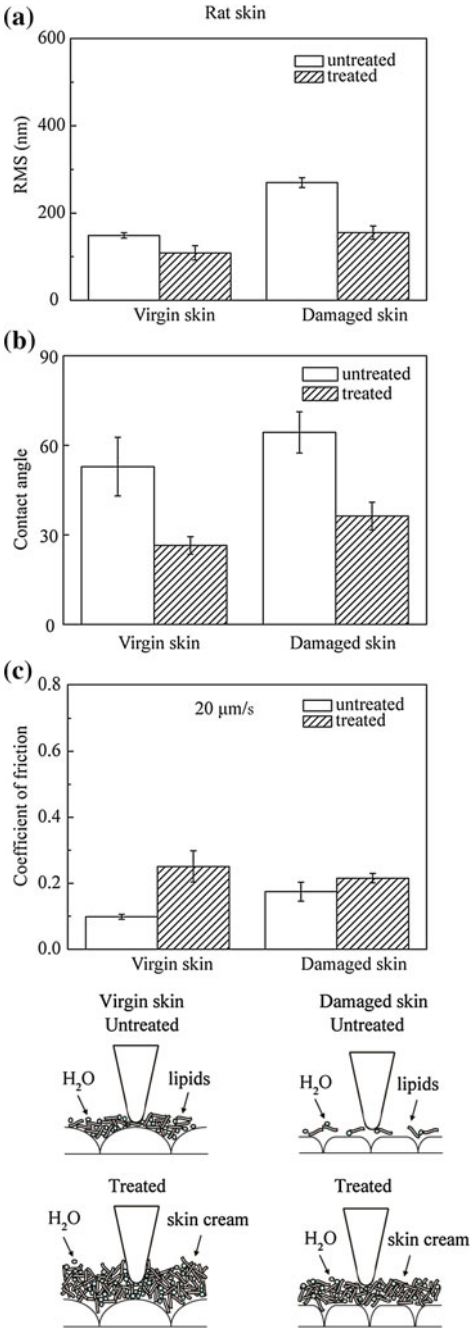

Fig. 7.2 **a** RMS roughness, **b** contact angle, and **c** coefficient of friction on the nanoscale and schematic cartoons of the tip–skin-cream interaction of virgin rat skin, damaged skin, treated virgin skin, and treated damaged skin (Bhushan et al. 2012)

leading to higher friction (Bhushan 2013a, b). Cream treatment moistens and softens the skin, which leads to a greater ductility and larger real area of contact. Larger contact area and formation of meniscus bridges are responsible for higher friction in cream-treated skin (Tang and Bhushan 2010; Bhushan et al. 2012).

7.1.2 *Effect of Velocity, Normal Load, Relative Humidity, and Number of Cycles on Nanoscale Friction*

Figure 7.4a shows the coefficient of friction as a function of velocity for various skin samples (Bhushan et al. 2012). The data shows that friction decreases with an increase of velocity for all skin samples. At low velocity, friction is dominated by meniscus forces as proposed by Tang and Bhushan (2010). The sliding of the tip results in shearing and reformation of meniscus bridges. As velocity increases, the meniscus bridges cannot be fully reformed, resulting in a drop in adhesive force and the coefficient of friction. In the case of cream-treated skin, skin cream is typically a shear-thinning fluid, and the viscosity decreases with the increasing shear rate leading to a decrease in the coefficient of friction (Liu and Bhushan 2003; Tang and Bhushan 2010).

Figure 7.4b shows the coefficient of friction as a function of normal load (Bhushan et al. 2012). The data shows that the friction for untreated skin samples first decreases then levels off, whereas, for the treated skin samples, it first decreased then increases above a certain load. As the tip moves towards the sample, a sudden mechanical instability occurs, and the tip jumps into contact with the film and a meniscus bridge is formed. However, the tip does not slide in a steady manner on the surface at a low normal load, and it may eliminate the meniscus bridges and bounce, leading to a high deflection of the tip resulting in high friction data at the

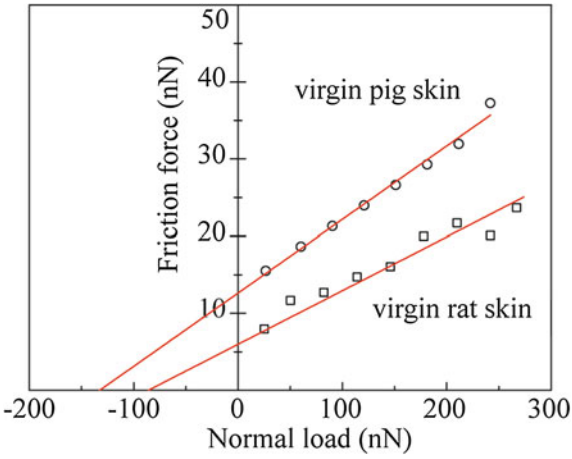

Fig. 7.3 Friction force as a function of normal load curves for virgin rat and pig skin (Bhushan et al. 2012)

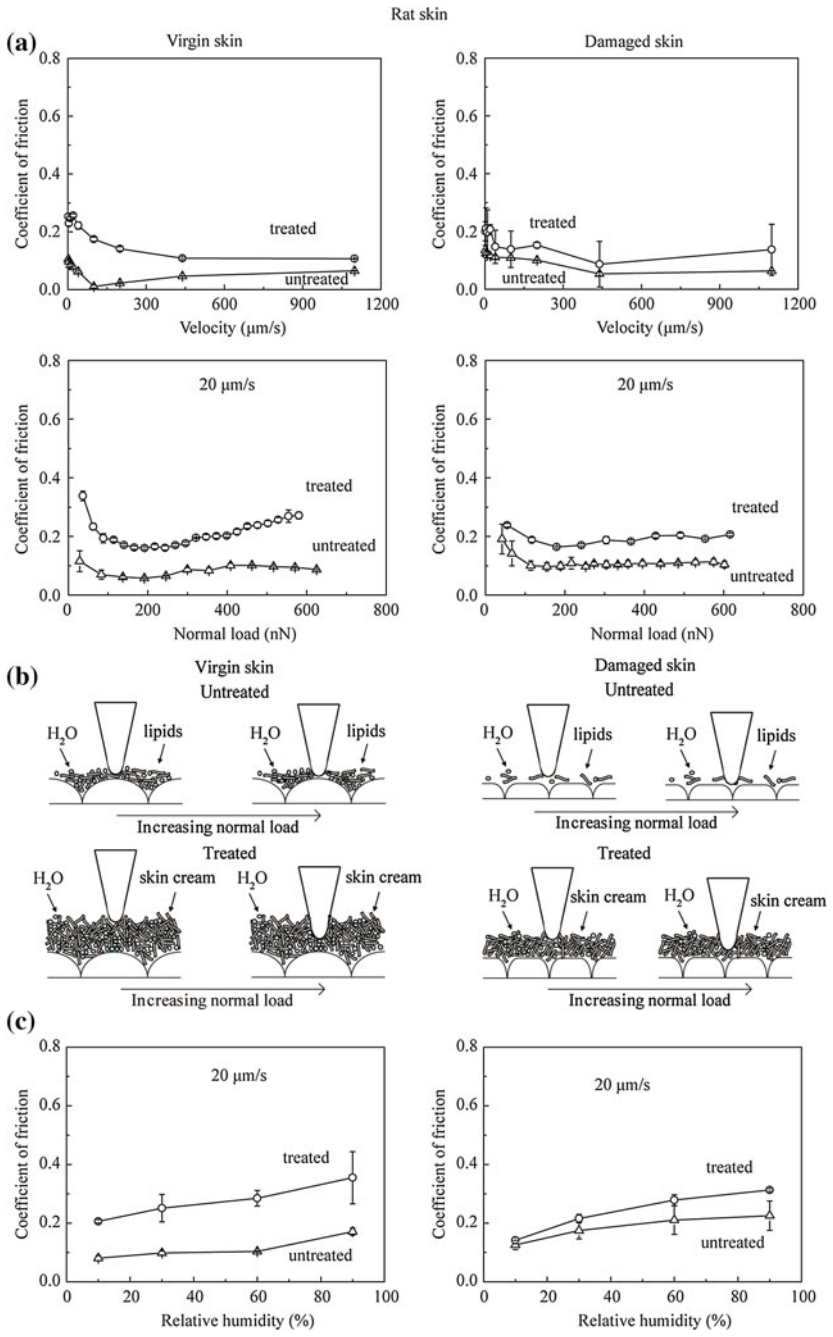

Fig. 7.4 Effect of **a** velocity, **b** normal load and schematic cartoons of tip-skin interaction, and **c** effect of relative humidity on the coefficient of friction on the nanoscale for virgin rat skin, damaged skin, treated virgin skin, and treated damaged skin (Bhushan et al. 2012)

beginning of the test. At higher loads, the tip penetrates into the film and slides in a steady manner, and the meniscus force dominates the friction. The coefficient of friction of treated skin samples increases above a certain load. It is believed that at larger loads, the tip penetrates into the thick film and the formation of large meniscus bridges provides additional resistance responsible for the increasing friction (Chen and Bhushan 2006; Lodge and Bhushan 2006).

Figure 7.4c shows the coefficient of friction as function of relative humidity (Bhushan et al. 2012). As the relative humidity increases, the coefficient of friction for all untreated and treated skin samples increases. As discussed earlier, the hydrophilic groups in the humectants of skin cream tend to form hydrogen bonds with water molecules, such that the humectants help the skin surface to attract water molecules in the environment. This increases the adhesive force leading to increasing coefficient of friction, especially at high humidity (Tang and Bhushan 2010). Due to the hydrophobic lipid layer of virgin skin and the reduced hydrophobic lipid layer of damaged skin, water hardly absorbs into or penetrates the skin surface, and humidity has less effect on it.

For wear resistance (durability) studies, the friction experiments were performed by cycling the tip over the samples. Figure 7.5 shows the effect of the number of cycles on various skin samples (Bhushan et al. 2012). For untreated virgin and damaged skin, the coefficient of friction in the initial cycles is related to the removal of the thin lipid film on the skin surface, and then remains constant because the interaction between the skin cream, skin surface, and environment reaches equilibrium. For cream-treated skin, the coefficient of friction decreases with an increase in the number of cycles. This is believed to be caused by the change of cream film thickness. When cream is first applied to the skin surface, the cream cannot be absorbed immediately by the skin. The cream accumulates at the contact interface, resulting in a larger liquid height and greater viscous drag to motion. However, after several scans, because of the absorption of the cream into the skin and the

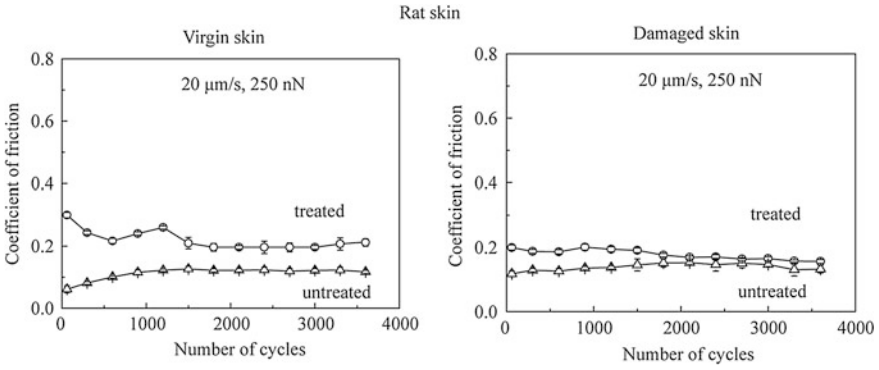

Fig. 7.5 The coefficient of friction on the nanoscale as a function of the number of cycles of rubbing for virgin rat skin, damaged skin, treated virgin skin, and treated damaged skin (Bhushan et al. 2012)

evaporation of the water content, the cream film thickness decreases. This decrease is responsible for the decrease in adhesive force and the coefficient of friction. The skin cream finally covers the skin surface as a stable gel network (surfactant, fatty amphiphile, and water) and friction remains constant (Tang and Bhushan 2010).

7.1.3 *Macroscale Friction and the Effect of Velocity, Normal Load, and Number of Cycles*

Figure 7.6 shows the macroscale data for coefficient of friction for various skin samples (Bhushan et al. 2012). The coefficient of friction of damaged skin is comparable to virgin skin. For damaged skin, as discussed earlier, the levels of fragile corneocytes generally increase, so the stratum corneum of damaged skin is torn rapidly at high loads in macroscale experiments. This torn stratum corneum then forms a lubricant layer between the tip and the skin surface, which is more

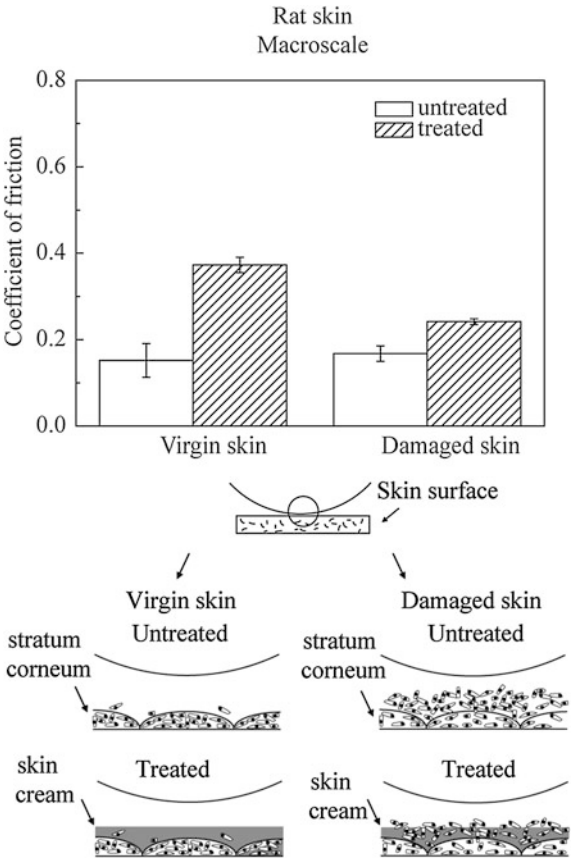

Fig. 7.6 Coefficient of friction on the macroscale and schematic cartoons of the tip-skin interaction for virgin rat skin, damaged skin, treated virgin skin, and treated damaged skin (Bhushan et al. 2012)

easily sheared, and may compensate the loss of the lipid layer. After the application of skin cream, the skin surface properties change. The skin is moistened and softened by the skin cream, which leads to a greater ductility and a larger real area of contact resulting in stronger adhesion. Thus, the coefficient of friction of cream treated skin is higher than that of virgin skin (Tang and Bhushan 2010).

The effect of velocity, normal load, and number of cycles on macroscale friction is shown in Fig. 7.7 (Bhushan et al. 2012). The coefficient of friction decreases as the

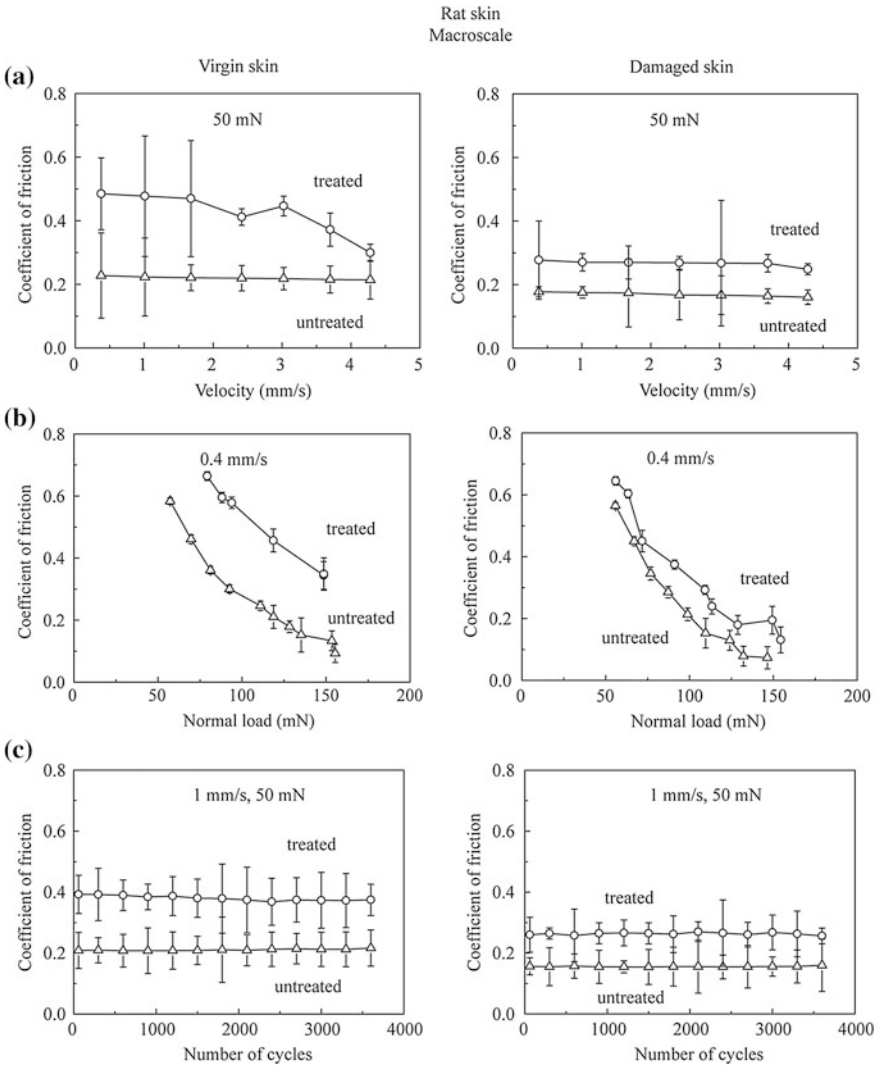

Fig. 7.7 Effect of **a** velocity, **b** normal load, and **c** number of cycles of rubbing on the coefficient of friction on the macroscale for virgin rat skin, damaged skin, treated virgin skin, and treated damaged skin (Bhushan et al. 2012)

velocity increases, as shown in Fig. 7.7a (Bhushan et al. 2012). The treated skin samples show a greater change than untreated skin samples. The reduction is similar to that on the nanoscale, since skin cream is a shear-thinning fluid as mentioned earlier.

Figure 7.7b shows the coefficient of friction decreases as the normal load increases (Bhushan et al. 2012). Increased surface roughening and a large quantity of wear debris are believed to be responsible for the decrease of friction with an increase of normal load (Bhushan 1996). Asperity deformation of skin is primarily elastic, and as the normal load increases, elastic deformation at the asperities is large, such that the individual asperities on the contacting surface are totally deformed, and the contact region approximates to the contact of a large single asperity (Bhushan 2013a, b). In this case, $\mu \propto W^{-1/3}$, and the coefficient of friction μ decreases with the increase of normal load as $W^{-1/3}$ (Tang and Bhushan 2010). The coefficient of friction remains almost constant on the macroscale for the four skin samples with the number of cycles (Fig. 7.7c), which suggests little damage during the cycling test (Bhushan et al. 2012).

7.2 Surface Roughness, Contact Angle, and Friction Properties with a Common Cream Treatment—Pig Skin

7.2.1 Surface Roughness, Contact Angle, and Nanoscale Friction

Figure 7.8 shows surface roughness maps on a 20 μm × 20 μm scan size for virgin, cream-treated virgin, damaged, and cream-treated damaged skin (Bhushan et al. 2012). Damaged skin has a higher surface roughness than virgin skin (Fig. 7.9a), with the same trend as for rat skin. However, the difference between virgin and damaged pig skin is more distinct than that for rat skin (Bhushan et al. 2012). After treatment, the roughness of both virgin and damaged skin decreased. The contact angle of damaged skin is higher and decreases after treatment with skin cream (Fig. 7.9b), as observed earlier for rat skin (Bhushan et al. 2012).

The coefficient of friction of various skin samples is shown in Fig. 7.9c (Bhushan et al. 2012). The coefficient of friction of damaged skin is higher than virgin skin. After treatment, the coefficient of friction of virgin and damaged skin increases. The coefficient of friction of pig skin is higher than that of rat skin because of the different from top to bottomdiscussed earlier (Table 2.1).

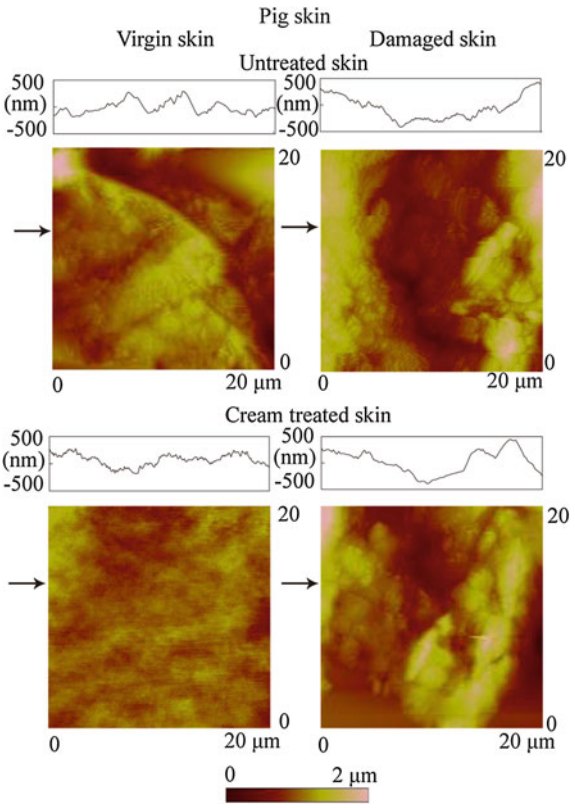

Fig. 7.8 AFM roughness maps and roughness profiles taken at *arrows* indicated for virgin pig skin, damaged skin, treated virgin skin, and treated damaged skin (Bhushan et al. 2012)

7.2.2 *Effect of Velocity, Normal Load, Relative Humidity, and Number of Cycles on Nanoscale Friction*

Figure 7.10 shows the effect of velocity, normal load and relative humidity on the coefficient of friction of various pig skin samples (Bhushan et al. 2012). The coefficient of friction slightly decreases initially with an increase of velocity; the decrease is significant with an increase in normal load. It increases as the relative humidity increases. The trends are the same as those for rat skin.

The effect of the number of cycles on various skin samples is shown in Fig. 7.11 (Bhushan et al. 2012). The coefficient of friction of treated pig skin samples shows a greater decrease than untreated pig skin samples. The reason is the same as discussed for rat skin.

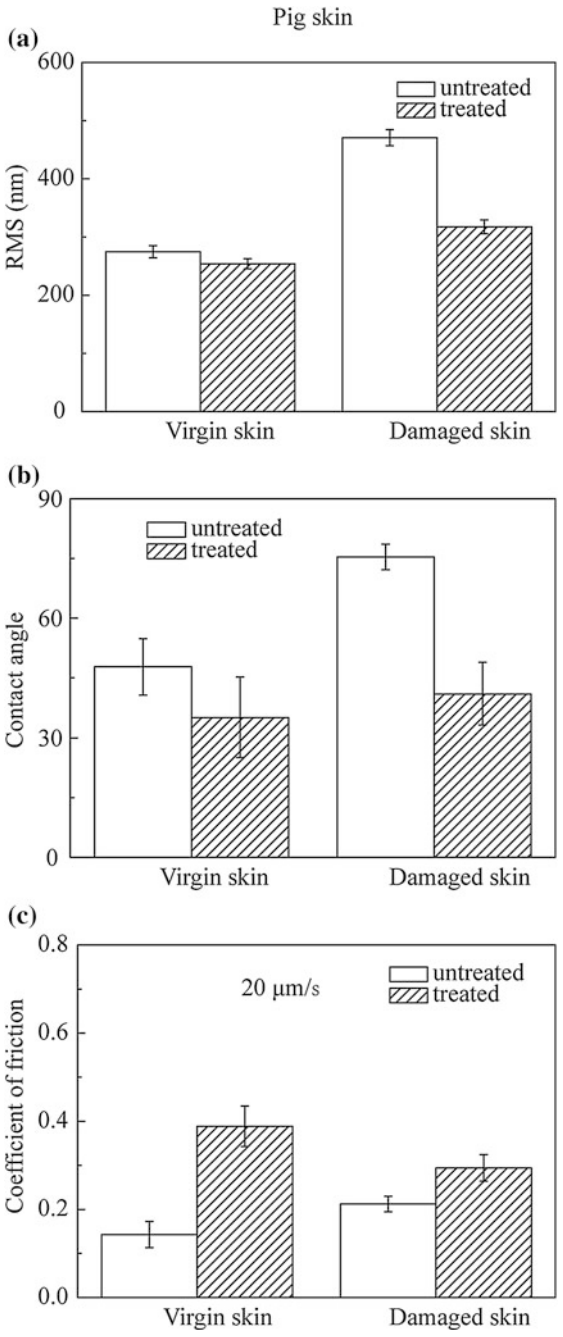

Fig. 7.9 **a** RMS roughness, **b** contact angle, and **c** coefficient of friction on the nanoscale of virgin pig skin, damaged skin, treated virgin skin, and treated damaged skin (Bhushan et al. 2012)

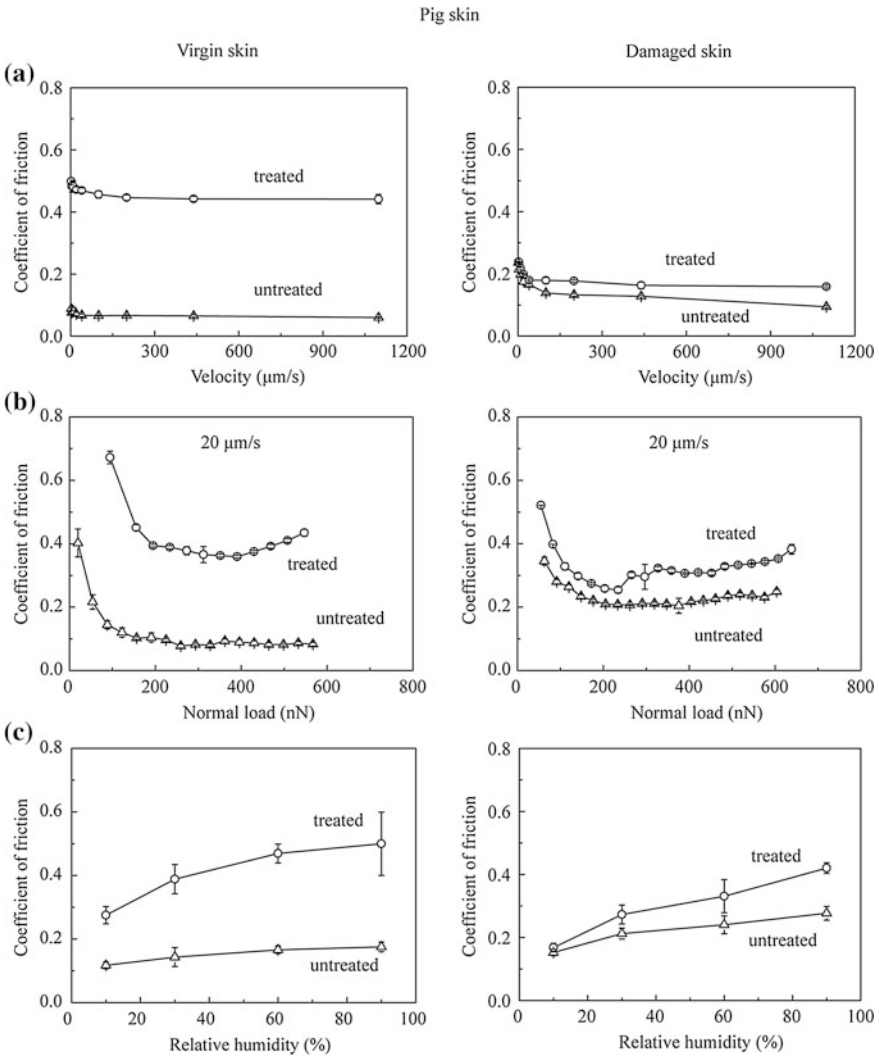

Fig. 7.10 Effect of **a** velocity, **b** normal load and **c** relative humidity on the coefficient of friction on the nanoscale for virgin pig skin, damaged skin, treated virgin skin, and treated damaged skin (Bhushan et al. 2012)

7.2.3 *Macroscale Friction and Effect of Velocity, Normal Load, and Number of Cycles*

Figure 7.12 shows the coefficient of friction of the four pig-skin samples on macroscale friction (Bhushan et al. 2012). Trends and the values of the coefficient of friction are similar to those of the rat skin. Figure 7.13 shows the effect of velocity,

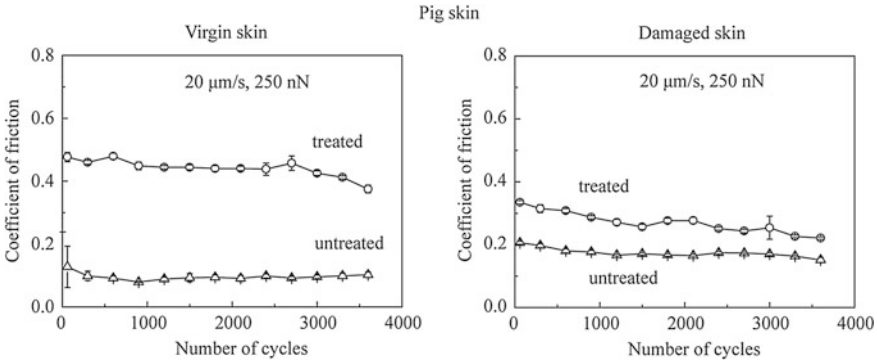

Fig. 7.11 The coefficient of friction on the nanoscale as a function of the number of cycles for virgin pig skin, damaged skin, treated virgin skin, and treated damaged skin (Bhushan et al. 2012)

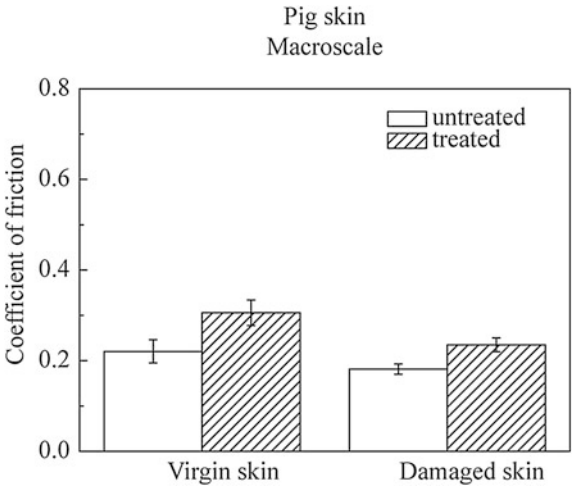

Fig. 7.12 Coefficient of friction on the macroscale for virgin pig skin, damaged skin, treated virgin skin, and treated damaged skin (Bhushan et al. 2012)

normal load, and number of cycles on macroscale friction (Bhushan et al. 2012). The coefficient of friction does not show a significance change with the increasing velocity. The coefficient of friction decreases as the normal load increases. The coefficient of friction remains constant with an increase in the number of cycles. Again trends are similar to those for the rat skin.

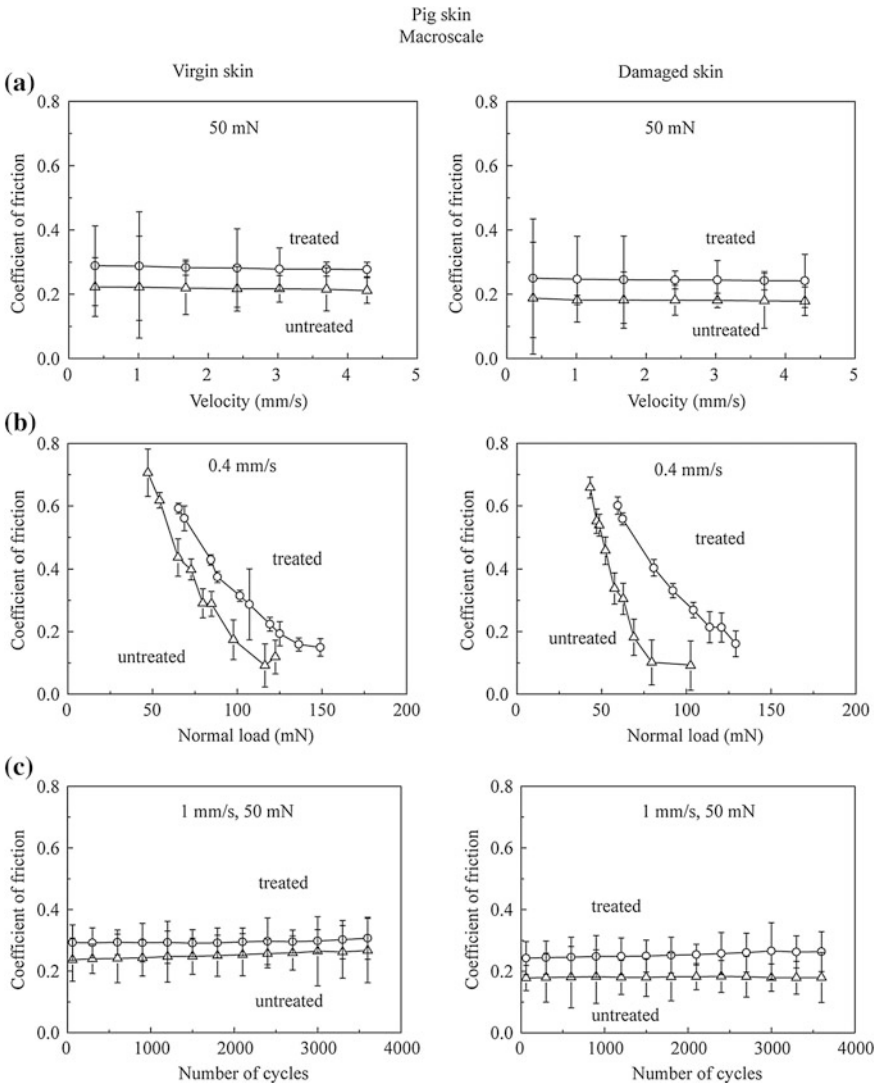

Fig. 7.13 Effect of **a** velocity, **b** normal load and **c** number of cycles of rubbing on the coefficient of friction on the macroscale for virgin pig skin, damaged skin, treated virgin skin, and treated damaged skin (Bhushan et al. 2012)

7.3 Nanomechanical Properties of Rat and Pig Skin

Nanomechanical properties of rat and pig skin were measured by using a nanoindenter. The load-displacement curves for rat and pig skin are presented in Fig. 7.14a (Bhushan et al. 2012). Under the same displacement control, the load

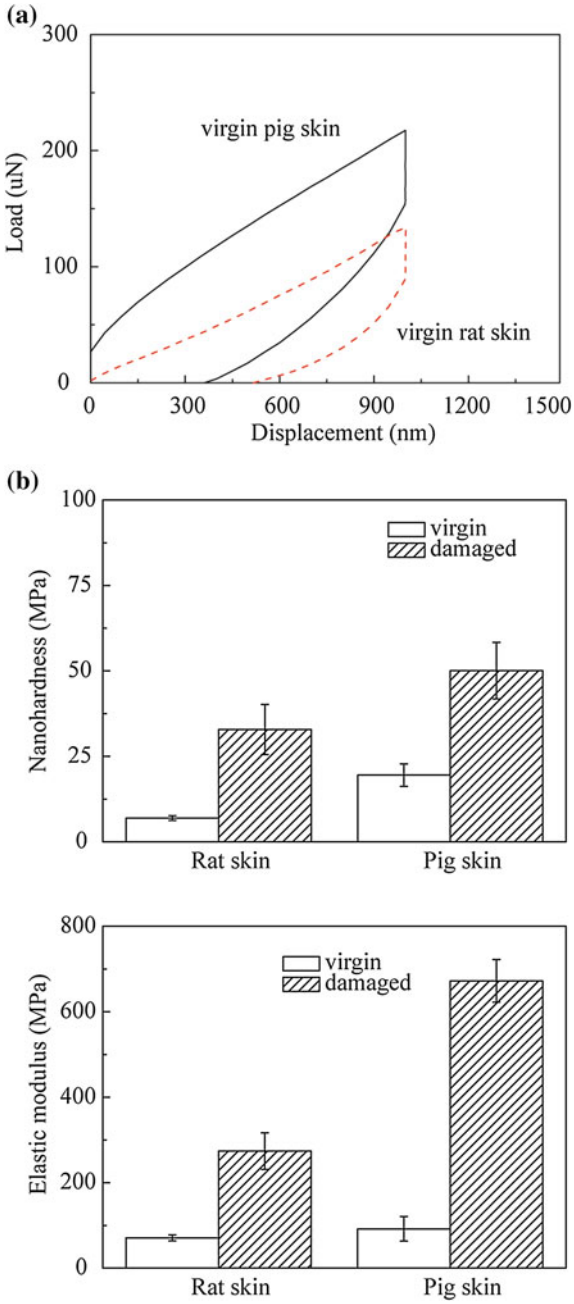

Fig. 7.14 **a** Load-displacement curves and **b** nanohardness and elastic modulus data for rat and pig skin (Bhushan et al. 2012)

required for a given displacement for pig skin is larger than that for the rat skin, which means the pig skin is harder than rat skin. The nanohardness and elastic modulus data are presented in Fig. 7.14b (Bhushan et al. 2012).

Table 2.1 summarizes the mechanical properties data for virgin pig and rat skin (Bhushan et al. 2012). Both the nanohardness and elastic modulus of pig skin samples are higher than those of rat skin samples, and those of the damaged skin are higher than virgin skin for both rat and pig skin. The differences between the damaged skin and virgin skin for pig skin are greater than those for rat skin.

7.4 Summary

In this chapter, friction and wear resistance (durability) of virgin and damaged rat skin and pig skin with and without a common cream treatment have been studied (Bhushan et al. 2012). The effect of velocity, normal load, and relative humidity on the coefficient of friction was studied on the nano- and macroscale. The wear resistance (durability) of skin samples was also studied by repeated cycling tests. Nanomechanical properties of rat skin and pig skin were measured. The major conclusions are as follows:

- For rat skin and pig skin, damaged skin has a larger roughness than virgin skin. After treatment with skin cream, the roughness decreases.
- The contact angle value of virgin rat skin and pig skin is lower than that of damaged skin. The contact angle decreases after treatment.
- The coefficient of friction of virgin pig skin is larger than that of virgin rat skin on the nanoscale.
- For both rat and pig skin samples, the coefficient of friction of damaged skin on the nanoscale is larger than that of virgin skin. After treatment, the coefficient of friction increases.
- For rat skin and pig skin samples, when the velocity increases, the coefficient of friction on the macroscale decreases.
- For rat skin and pig skin samples, at the beginning, as the normal load increases, the coefficient of friction on the nanoscale decreases. After a certain value of the normal load, the coefficient of friction of untreated skin samples remains constant, while that of treated skin samples shows a slight increase.
- As the relative humidity increases, the coefficient of friction of untreated rat skin and pig skin on the nanoscale does not increase much.
- On the macroscale, the coefficient of friction is larger than on the nanoscale.
- On the macroscale, the coefficient of friction of damaged skin is comparable to that of virgin skin. After treatment, the coefficient of friction increases.
- On the macroscale, the velocity and number of cycles do not have an obvious effect on the coefficient of friction. When the normal load increases, the coefficient of friction decreases.

- The virgin rat skin has lower nanohardness and elastic modulus than that of virgin pig skin. The damaged skin properties are higher than those of the virgin skin for both rat skin and pig skin.

References

Bhushan, B. (1996). *Tribology and Mechanics of Magnetic Storage Devices* (2nd ed.). New York: Springer.

Bhushan, B. (2013a). *Principles and Applications of Tribology* (2nd ed.). New York: Wiley.

Bhushan, B. (2013b). *Introduction to Tribology* (2nd ed.). New York: Wiley.

Bhushan, B., Chen, S., & Ge, S. (2012). Friction and durability of virgin and damaged skin with and without skin cream treatment using atomic force microscopy. *Beilstein Journal of Nanotechnology, 3*, 731–746.

Chen, N., & Bhushan, B. (2006). AFM studies of conditioner thickness distribution and binding interactions on hair surface. *Journal of Microscopy, 221*, 203–215.

Liu, H., & Bhushan, B. (2003). Nanotribological characterization of molecularly thick lubricant films for applications to MEMS/NEMS by AFM. *Ultramicroscopy, 97*, 321–340.

Lodge, R. A., & Bhushan, B. (2006). Surface characterization of human hair using tapping mode atomic force microscopy and measurement of conditioner thickness distribution. *Journal of Vacuum Science and Technology A, 24*, 1258–1269.

Tang, W., & Bhushan, B. (2010). Adhesion, friction and wear characterization of skin and skin cream using atomic force microscope. *Colloid Surface B, 76*, 1–15.

Part III
Synthetic Skin

Chapter 8
Nanotribological and Nanomechanical Characterization of Synthetic Skins With and Without Common Cream Treatment for Cosmetic Science

The nanotribological and nanomechanical data on two relatively inexpensive synthetic skins with and without common cream treatment are presented (Chen and Bhushan 2013). Synthetic skin-1 is commercially available Vitro-skin™. It contains both optimized protein and lipid components and is designed to have physical properties similar to human skin (Jermann et al. 2002). Synthetic skin-2 is a mixture of gelatin from porcine skin, glycerol, formaldehyde, prolipid, and water cast on a replica of human skin made of silicone (originally developed for dental implants) (Lir et al. 2007). Surface roughness, contact angle, adhesive force, friction force, and nanomechanical properties of the two synthetic skins were measured and compared with rat skin and pig skin. Next, a common skin cream (Vaseline Intensive Care Lotion) was applied to the synthetic skins and nanotribological and nanomechanical properties were compared with that of rat skin and pig skin.

8.1 Surface Roughness and Contact Angle for Rat Skin, Pig Skin, Synthetic Skin-1, and Synthetic Skin-2

Figure 8.1 shows topography maps and corresponding height profiles of the cross section indicated by the arrows on a 20 μm × 20 μm scan size for all skin samples (Chen and Bhushan 2013). The height profiles appear smoother for virgin skin compared with damaged skin, and for cream-treated skin compared with untreated skin. The RMS roughness and P-V distance data, which serve as quantified expressions of the surface characteristics, are shown in Fig. 8.2a, b, respectively (Chen and Bhushan 2013). Damaged skin has a higher roughness than virgin skin. After treatment with skin cream, the RMS roughness and P-V distance of virgin skin and damaged skin decreased. The reasonable explanation is that the skin cream can fill the gap between the cells of stratum corneum.

B. Bhushan, *Biophysics of Skin and Its Treatments*, Biological and Medical Physics, Biomedical Engineering, DOI 10.1007/978-3-319-45708-6_8

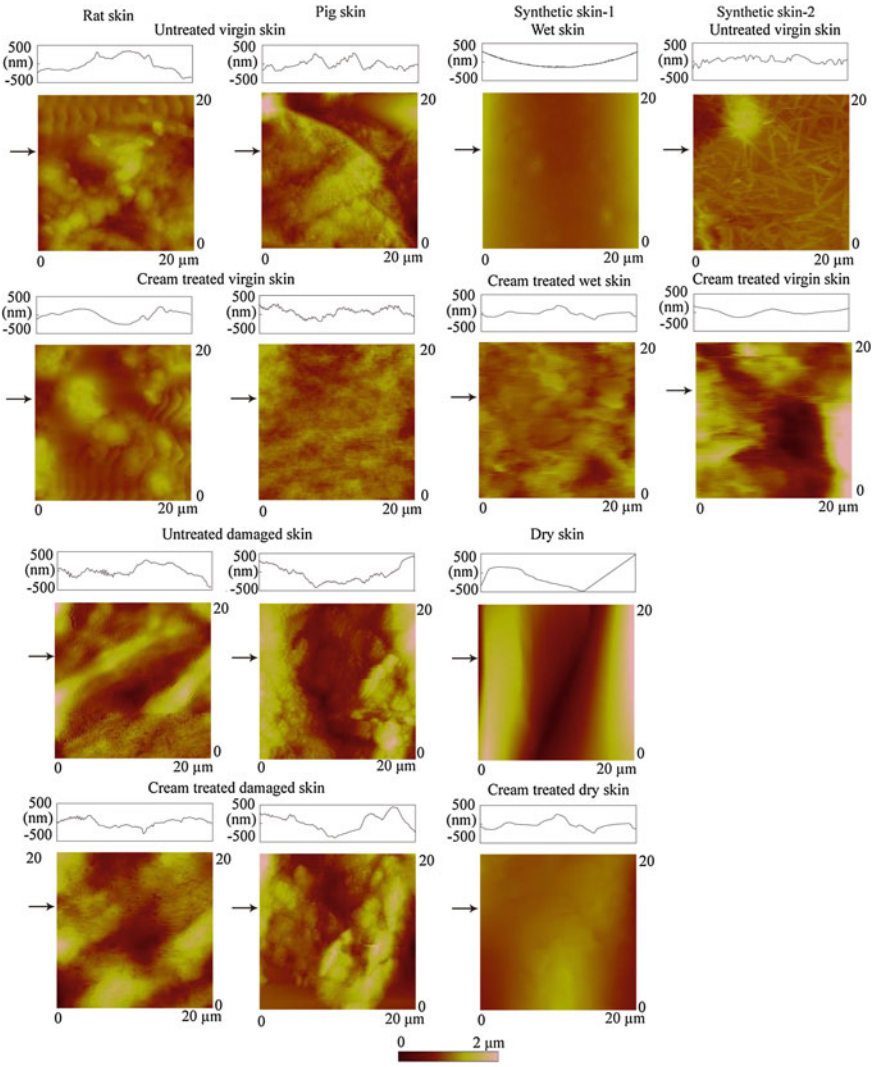

Fig. 8.1 AFM topography maps and roughness profiles taken at *arrows* indicated for virgin and damaged rat and pig skin (Bhushan et al. 2012), and wet and dry synthetic skin-1 and synthetic skin-2 treated with and without a common cream treatment (Chen and Bhushan 2013)

The contact angle data for all skin samples are shown in Fig. 8.2c (Chen and Bhushan 2013). The contact angle of virgin skin is lower than damaged skin due to physical and chemical changes to the skin surface. An increasing surface roughness may be partially responsible for an increase in contact angle of the damaged skin (Bhushan 2012). After treatment with skin cream, the contact angles of virgin and

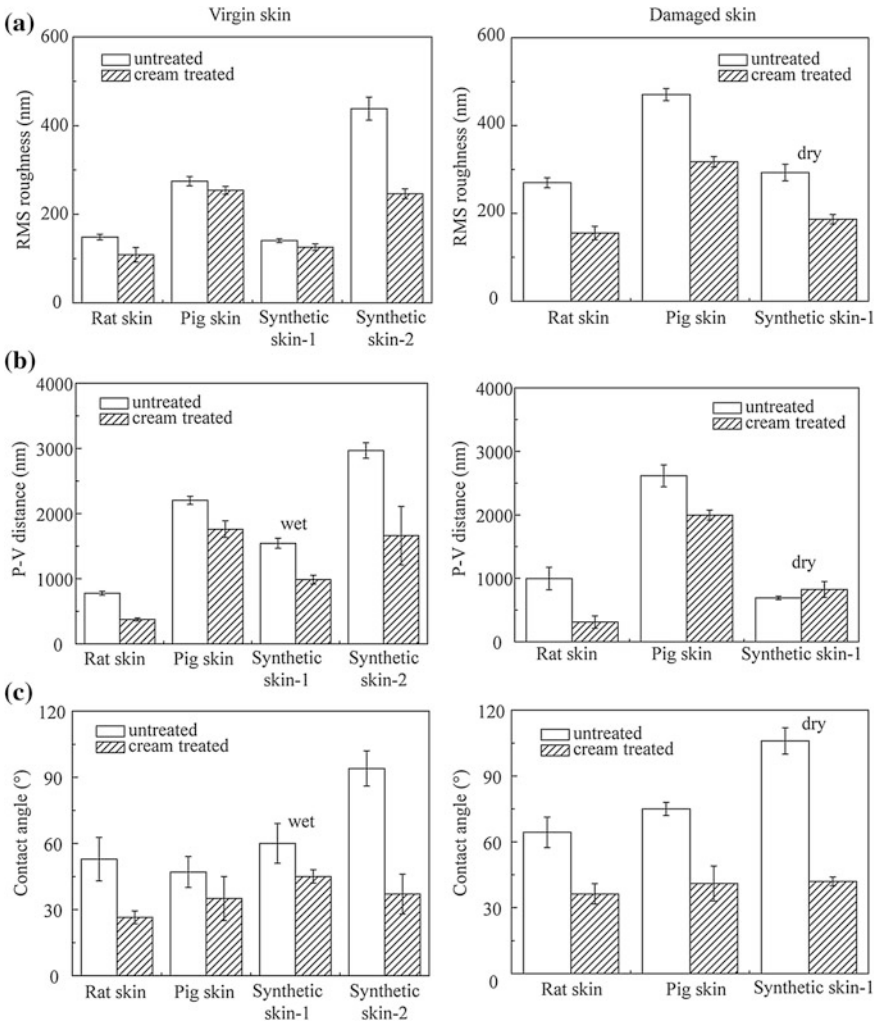

Fig. 8.2 **a** RMS roughness, **b** P-V distance, and **c** contact angle of virgin and damaged rat and pig skin, and wet and dry synthetic skin-1 and synthetic skin-2 treated with and without skin a common cream treatment (Chen and Bhushan 2013)

damaged skin decreased. The hydrophilic groups in skin cream, such as hydroxyl group, amines group, and carboxyl group in the humectants, increase the surface hydrophilicity and lead to a lower contact angle. Based on the roughness and contact angle data, the values of the two synthetic skins are on the same order as that of rat and pig skin.

8.2 Coefficient of Friction, Adhesive Force and Film Thickness for Rat Skin, Pig Skin, Synthetic Skin-1, and Synthetic Skin-2

Figure 8.3a presents the coefficient of friction of various skin samples (Chen and Bhushan 2013). For rat and pig skin, the coefficient of friction of damaged skin is higher than that of virgin skin. As discussed by Bhushan et al. (2012), damaged skin has a larger surface roughness, larger number of asperities (Bhushan 2013a, b), and lower thickness of natural lipids on the surface. For synthetic skin-1, the coefficient of friction of wet synthetic skin-1 is lower than dry synthetic skin-1, which is probably because of the decreasing surface roughness after the dry synthetic skin-1. The coefficient of friction increases for all the skin samples after treatment. Cream treatment moistens and softens the skin, which leads to a greater ductility and larger real area of contact. Larger contact area and formation of meniscus bridges are responsible for higher friction in cream-treated skin (Tang and Bhushan 2010; Chen and Bhushan 2013).

Figure 8.3b shows the film thickness of all samples (Chen and Bhushan 2013). For the virgin skin, the film represents natural lipids and condensed contaminant films, including water vapor. For all virgin skin, the film thicknesses are comparable. For the damaged skin, the film thickness of the dry synthetic skin-1 is larger than damaged rat and pig skin. The film thickness of damaged rat and pig skin are less than that of virgin rat and pig skin. The film thickness of all samples increases after treatment.

Figure 8.3c shows the adhesive force of all samples (Chen and Bhushan 2013). The trends are the same as for film thickness.

8.3 Adhesive Force and Film Thickness Maps for Rat Skin, Pig Skin, Synthetic Skin-1, and Synthetic Skin-2

Figures 8.4 and 8.5 shows the adhesive force and film thickness maps of the rat and pig skins and of wet and dry synthetic skin-1 and synthetic skin-2 with and without cream treatment, respectively (Chen and Bhushan 2013). After treatment with skin cream, the film thickness maps show that the cream film unevenly distributes on the skin surface, especially for synthetic skin-2 and pig skin. The bright region in the film thickness maps corresponded to a thicker cream film. It means that the adhesive force increases as the film thickness increases. The effect of cream film thickness on adhesive force has been studied, and the model of the film thickness dependence on adhesive force has been presented by Tang and Bhushan (2010). For the two

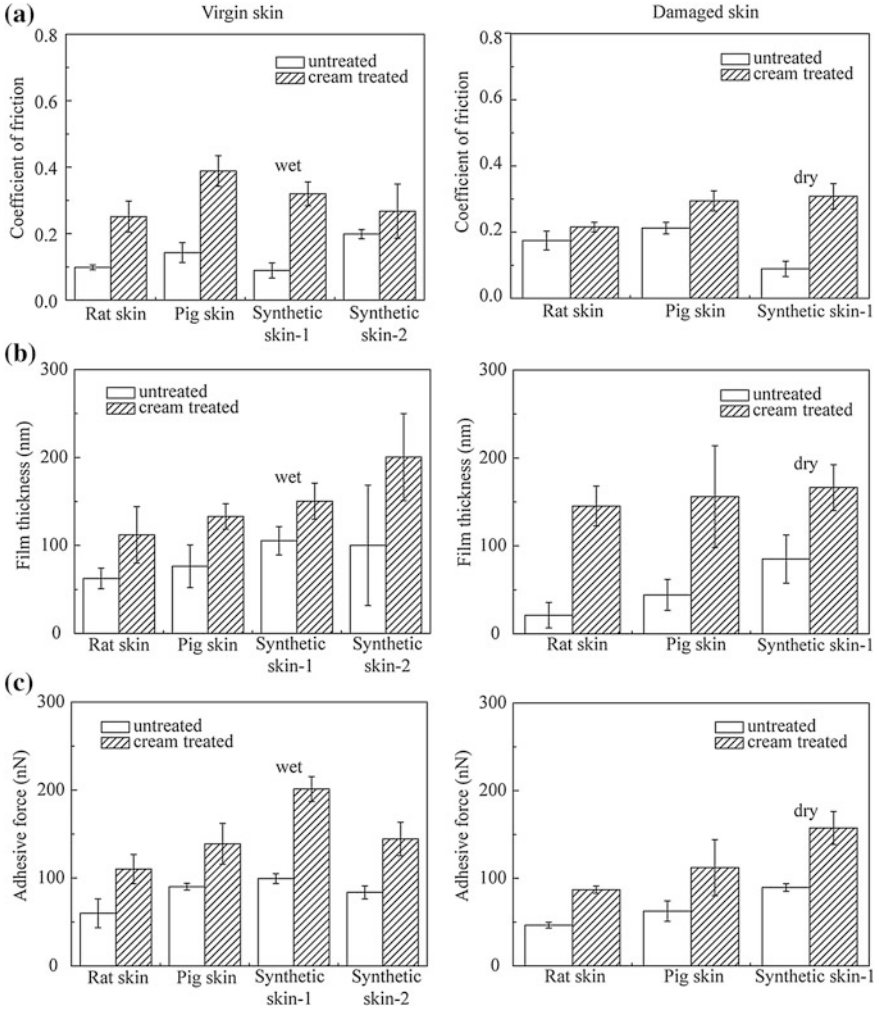

Fig. 8.3 **a** Coefficient of friction, **b** film thickness, and **c** adhesive force of virgin and damaged rat and pig skin and wet and dry synthetic skin-1 and synthetic skin-2 with and without a common cream treatment (Chen and Bhushan 2013)

synthetic skins, rat skin, and pig skin, after treatment with skin cream, the trends of film thickness and adhesive force are same, and both of them increase. The film thickness and adhesive force damaged rat and pig skin and dry synthetic skin-1 decrease compare with the virgin rat and pig skin and wet synthetic skin-1.

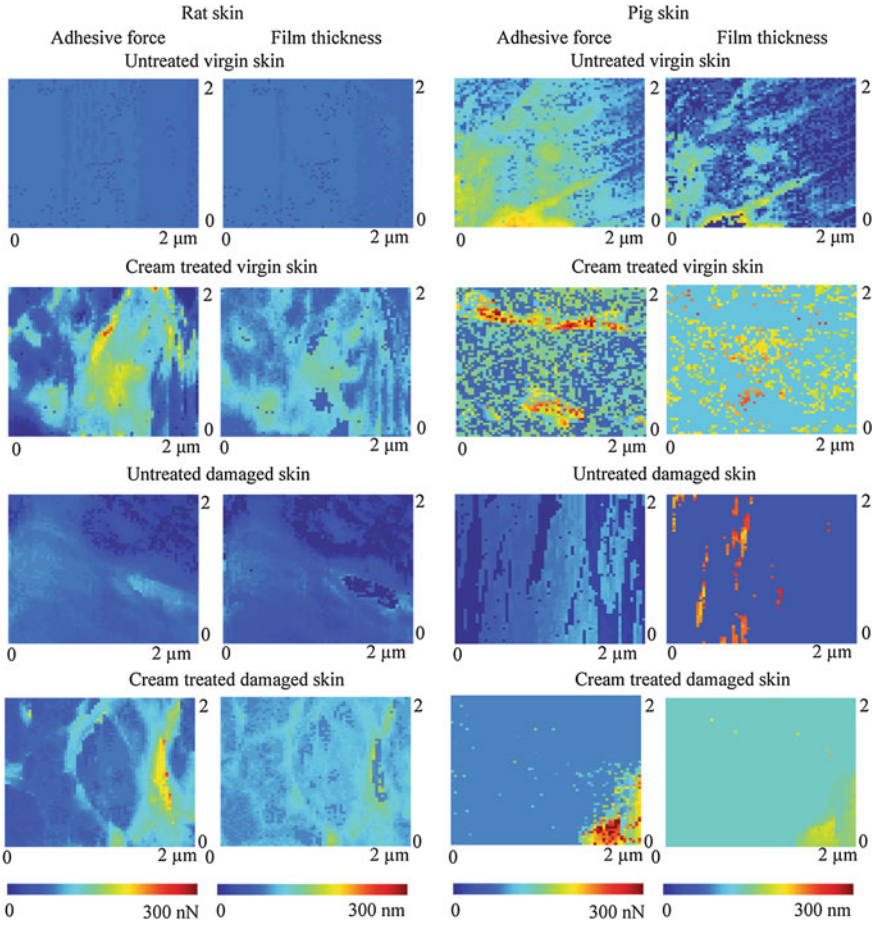

Fig. 8.4 Film thickness and adhesive force maps of virgin and damaged rat and pig skin with and without a common cream treatment (Chen and Bhushan 2013)

8.4 Nanomechanical Properties of Rat Skin, Pig Skin, Synthetic Skin-1, and Synthetic Skin-2

Nanomechanical properties of synthetic skin-1, synthetic skin-2, rat, and pig skin were measured by using a nanoindenter. The load-displacement curve of wet synthetic skin-1 is not presented because of its slipperiness. Instead, nanoindentation experiments on wet synthetic skin-1 were performed using a cycling load of 0.45 times of normal load ranging from 50 to 250 μN in 20 cycles in 60 s at a given step with a constant load segment of 1 s.

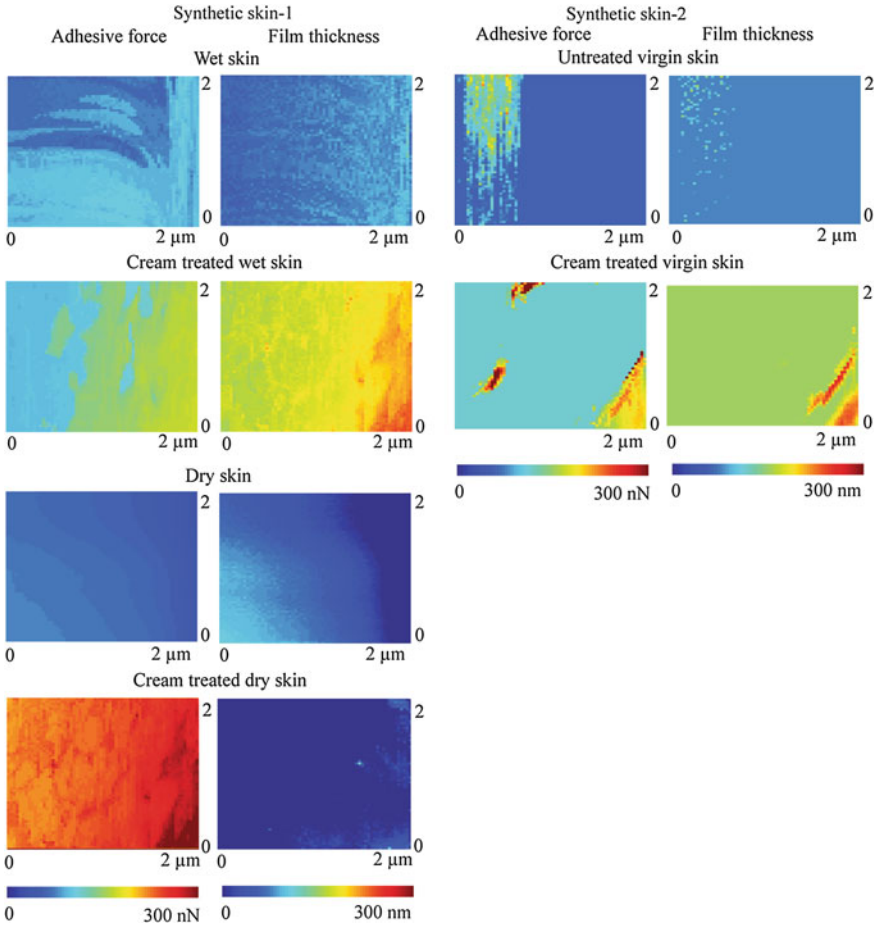

Fig. 8.5 Film thickness and adhesive force maps of wet and dry synthetic skin-1 and synthetic skin-2 with and without a common cream treatment (Chen and Bhushan 2013)

The load-displacement curves for two synthetic skins, rat, and pig skin are presented in Fig. 8.6a (Chen and Bhushan 2013). For virgin skin, under the same displacement control, the load required for a given displacement for synthetic skin-2 is larger than that for the virgin rat and pig skin, which means that synthetic skin-2 is a little harder than virgin rat and pig skin. For damaged skin under the same displacement control, the load required for a given displacement for pig damaged skin is larger than that for dry synthetic skin-1 and damaged rat skin. The nanohardness and elastic modulus data are presented in Fig. 8.6b (Chen and Bhushan 2013). The hardness of wet synthetic skin-1, virgin synthetic skin-2, virgin

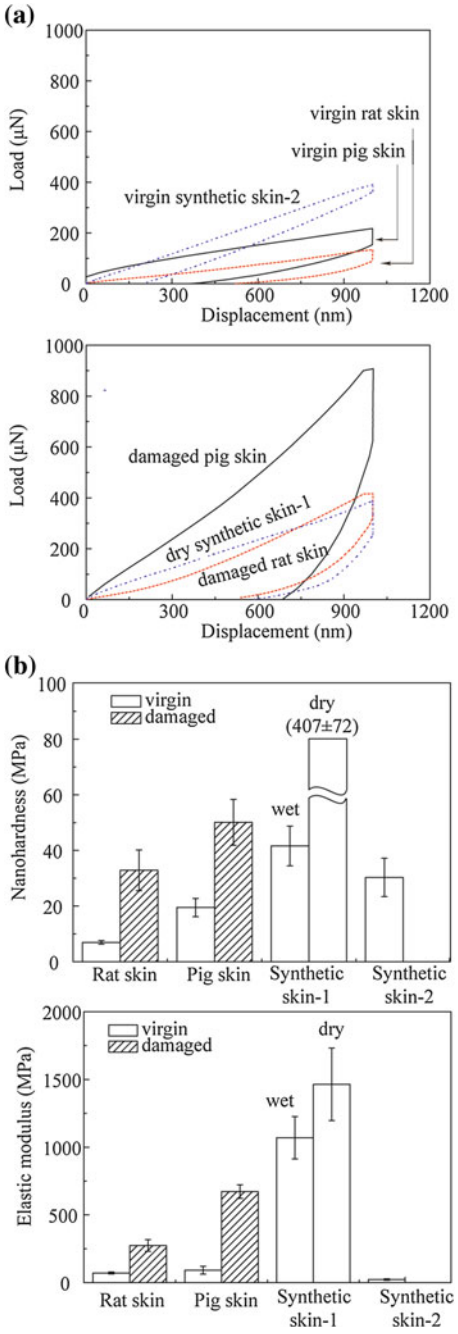

Fig. 8.6 **a** Load-displacement curves for virgin and damaged rat and pig skin and dry synthetic skin-1 and synthetic skin-2, **b** nanohardness and elastic modulus data for virgin and damaged rat and pig skin and wet and dry synthetic skin-1 and synthetic skin-2. Data for wet synthetic skin-1in Fig. 8.6a is not presented because of its slipperiness. Instead based on cycling load experiments, values of nanohardness and elastic modulus were obtained and presented in Fig. 8.6b (Chen and Bhushan 2013)

rat, and virgin pig skin are comparable. The elastic modulus of virgin synthetic skin-2 is lower than wet synthetic skin-1, virgin rat, and virgin pig skin. For damaged skin, the hardness and elastic modulus of dry synthetic skin-1 is larger than synthetic skin-2, rat, and pig skin. Overall, mechanical properties of synthetic skin-2 appear to be closer to that of rat and pig skin.

8.5 Summary

In this study, the surface roughness, contact angle, adhesive force, film thickness, elastic modulus, and hardness of two synthetic skins with and without skin cream treatment were studied using an AFM and a nanoindenter (Chen and Bhushan 2013). The data were compared with that of rat skin and pig skin. The major conclusions from this study are as follows:

- The presence of the cream film causes an increase of the surface film thickness, which leads to an increase of the adhesive force and friction force. The skin cream also reduces the surface roughness, increases the hydrophilic properties of skin, and softens the skin surface.
- The surface topography of the two synthetic skins is different from rat and pig skin as there are no hair follicles and hairs present on synthetic skin surface.
- In the case of virgin skin, the film thickness, adhesive force, coefficient of friction, RMS, P-V distance, and contact angle of the two synthetic skins, rat, and pig skin are comparable.
- The adhesive force, film thickness and coefficient of friction of the two synthetic skins, rat, and pig skin increase, and the RMS, P-V distance, and contact angle of the two synthetic skins and rat skin decrease.
- In the case of virgin skin, the hardness of wet synthetic skin-1, synthetic skin-2, rat, and pig skin are comparable.
- The elastic modulus of synthetic skin-2 is lower than wet synthetic skin-1, rat, and pig skin. For damaged skin, the hardness and elastic modulus of dry synthetic skin-1 is larger than synthetic skin-2, rat, and pig skin.

Based on surface and friction properties, the wet synthetic skin-1 and synthetic skin-2 are good simulations of virgin animal skins, and the dry synthetic skin-1 is comparable to the damaged rat and pig skin. However, the hardness of synthetic skin-2 is comparable to rat and pig skin, and can be a better simulation.

References

Bhushan, B. (2012). Nanotribological and nanomechanical properties of skin with and without skin cream treatment using atomic force microscopy and nanoindentation. *Journal of Colloid and Interface Science, 367*, 1–33.

Bhushan, B. (2013a). *Principles and Applications of Tribology* (2nd ed.). New York: Wiley.
Bhushan, B. (2013b). *Introduction to Tribology* (2nd ed.). New York: Wiley.
Bhushan, B., Chen, S., & Ge, S. (2012). Friction and durability of virgin and damaged skin with and without skin cream treatment using atomic force microscopy. *Journal of Nanotechnology, 3*, 731–746.
Chen, S., & Bhushan, B. (2013). Naonomechanical and nanotribological characterization of two synthetic skins with and without skin cream treatment using atomic force microscopy. *Journal of Colloid and Interface Science, 398*, 247–254.
Jermann, R., Toumiat, M., & Imfeld, D. (2002). Development of an in vitro efficacy test for self-tanning formulations. *International Journal of Cosmetic Science, 24*, 35–42.
Lir, I., Haber, M., & Dodiuk-Kenig, H. (2007). Skin surface model material as a substrate for adhesion-to-skin testing. *Journal of Adhesion Science and Technology, 21*, 1497–1512.
Tang, W., & Bhushan, B. (2010). Adhesion, friction and wear characterization of skin and skin cream using atomic force microscope. *Colloid Surface B, 76*, 1–15.

Part IV
Skin Tactile Perception

Chapter 9
Skin Vibrations Created During Touch

9.1 Introduction

Tactile perception, also known as "somatic sense" or "touch", is accomplished by scanning a surface with a finger. In many applications, such as when skin touches fabric, it is desirable for skin to perceive the other surface as smooth. In other situations, such as cosmetics application, it is desirable for the skin being touched to be perceived as smooth (Katz 1989; Hollins et al. 1998). To arrive at the perception that skin is smooth, our brains integrate data on skin's stretch, pressure, temperature, and vibrations during touching. During touching, interfacial friction results in vibrations carried by nerves to the brain, which are interpreted as the level of smoothness.

In skin cream research, a more direct measure of the degree of skin smoothness is to measure interfacial vibrations created during touch. It is known that skin cream affects skin surface and interfacial properties that affect skin vibrations (Scheibert et al. 2009). In this chapter, research on friction-induced vibrations on pig skin and synthetic skin are presented.

9.2 Experimental Apparatus and Procedure

A tribometer was used to rub the artificial finger on a skin sample surface in reciprocating mode as mentioned earlier in Chap. 3 (Bhushan 2013a, b). During the rubbing experiments, normal load and friction force were measured using semiconductor strain gauges mounted to a crossed I-beam configuration. An accelerometer sensor was mounted to measure vibration.

B. Bhushan, *Biophysics of Skin and Its Treatments*, Biological and Medical Physics, Biomedical Engineering, DOI 10.1007/978-3-319-45708-6_9

9.2.1 Artificial Finger

In order to characterize the vibration induced by a fingertip sliding on a skin surface, a plastic artificial fingertip that simulates the surface topography of a human finger was used, shown in Fig. 9.1. It was fabricated to mimic the shape and textures of a human right index fingertip. There are two main steps consisting of the production of the impression mold and the process of positive replica of the human index finger. A mold was made using a silicone impression material (Elite HD, Zhormack Clinical). A replica was made using liquid plastic (Smooth-On, Smooth-Cast 300 series). It has an elastic modulus of about 960 MPa, which is larger than that of skin, whose elastic modulus is on the order of 100 MPa (Bhushan et al. 2010). The artificial finger was attached to a pin holder at the edge of the cantilever beam with rapid glue (Araldite® Rapid).

9.2.2 Vibration Sensor Selection

There are various sensors with different frequency bandwidths that are used for tactile perception and measurement of vibrations produced during sliding (Ding and Bhushan 2016). Piezoelectric transducers (PZTs) are commonly used for vibration characteristics in the frequency range of several hundred kHz. As an example, they are used in sliding and indenting metals and ceramics (Bhushan 2011; Mo et al. 2013), and magnetic head-disk interfaces (Bhushan 1996; Bhushan and Forehand 1997).

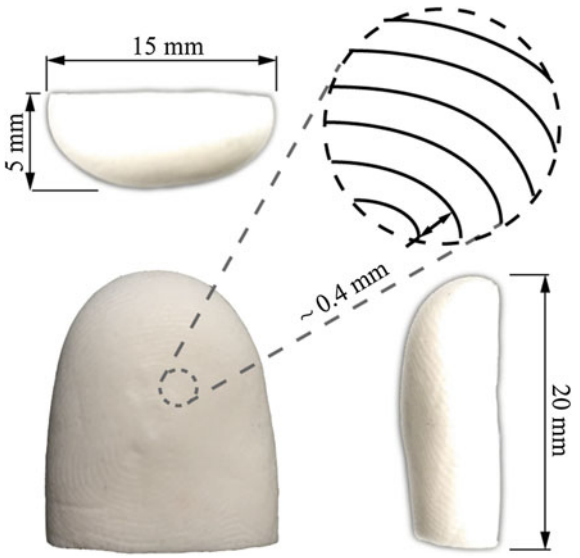

Fig. 9.1 Schematic of an artificial finger (Ding and Bhushan 2016)

The vibration frequency spectrum during rubbing of skin is expected to be 100–500 Hz (Bolanowski et al. 1988; Makous et al. 1995). For low frequency applications, such as in tactile perception with skin, a voice coil actuator (Fagiani et al. 2011) as well as a pressure sensitive finger have been used (Scheibert et al. 2009; Tang et al. 2015). In the latter, a commercial artificial finger (BioTac, Syn-Touch, Los Angeles, CA) employing a pressure sensor consists of a rigid core that contains all sensory transducers, covered by an elastomeric skin with a fingerprint. The space between the skin and core is filled with an incompressible, conductive fluid to give it a compliance that mimics human finger pads. Vibrations in the skin propagate through the fluid and are detected as dynamic (AC) signals by the hydroacoustic pressure sensor. In pressure studies, AC pressure was sampled at 2200 Hz and digitized with a resolution of 12 bits in the range of 0–3.3 V using onboard electronics inside the artificial finger.

In the research reported here, the artificial finger and sensing were separated. A record player needle can be placed on the side of the vibrating cantilever beam for measurement of low frequency vibrations in the lateral direction. In a record player, music is recorded on the side edges of grooved tracks. The needle touches against the edges and the pattern creates lateral vibrations leading to noise in the 100–300 Hz range (music). However, the needle provides resistance to lateral motion, adding to the intrinsic friction force and affecting vibrations. Instead, a capacitive type accelerometer capable of sensing less than 1 kHz was used, covering the expected frequency range of 100–500 Hz during the rubbing of skin (Ding and Bhushan 2016).

9.2.3 Description of Tribometer Apparatus and Procedure

A schematic of the experimental set-up is shown in Fig. 9.2 (Ding and Bhushan 2016). The artificial finger was fixed in a stationary holder and mounted at the end of a flexible cantilever beam. It was loaded against a reciprocating skin sample. The skin samples were mounted on a steel base. The normal load was applied by a microactuator. A Velmax reciprocating stage was used to provide the reciprocating motion. A Newport RSX-1M sample stage was installed on top of the reciprocating stage. It was installed on a 2-axis tilt platform (Newport 36 series), which has position resolution of 2 μm in both the horizontal and vertical directions. The reciprocating sliding device can provide linear motion with adjustable stroke length up to 50 mm and variable frequency up to 1.5 Hz (velocity 30 mm/s and stroke is 10 mm). Normal load and friction forces are measured with strain gauges mounted on the cantilever beam on a crossed I-beam structure. For high sensitivity, semiconductor strain gauges with a gauge factor of 115 were used. The beam structure was mounted on a vertical linear stage (Newport 462 series). A lab jack was used to lift the entire stage in the vertical direction. The system vibration was measured by a

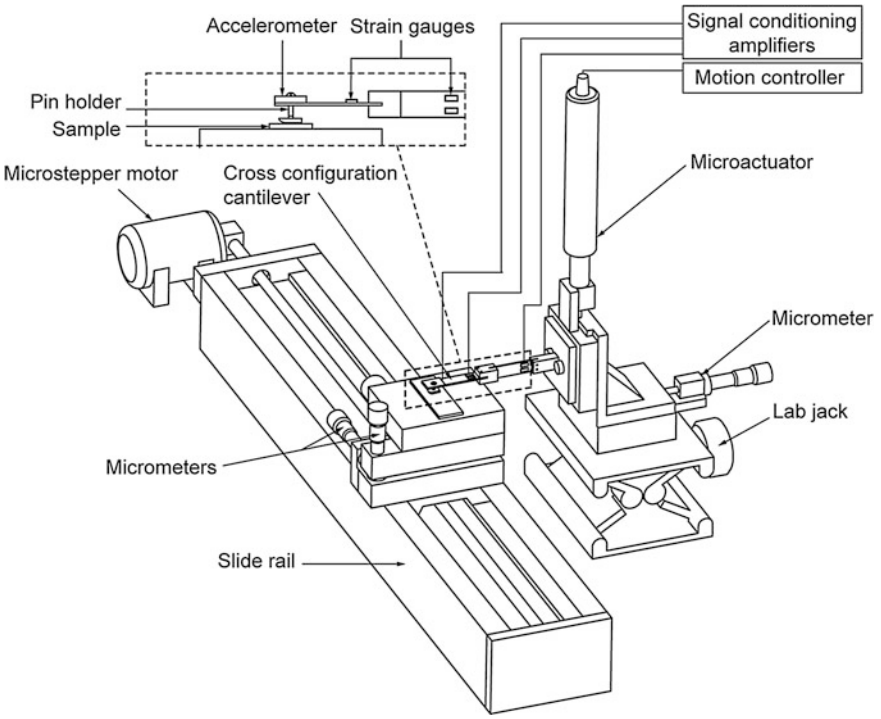

Fig. 9.2 Schematic of tribometer apparatus with a crossed I-beam strain-gage transducer and accelerometer (Ding and Bhushan 2016)

small, low profile (4 mm × 4 mm × 1.45 mm, mass 1.27 g), three-dimensional capacitive-type acceleration sensor (Analog Devices, ADXL335), which was screwed on a sensor holder at the top edge of the cantilever beam. The sensor uses three sets of cantilever beams inside the housing to provide measurements along three axes. The natural frequency of the beams were 5 kHz above the measured frequency. The accelerometer has a full-scale range of ±3 g, the bandwidth has a range of 0.5 Hz to 1.6 kHz in the x and y directions and 0.5–550 Hz in the z direction; and sensitivity at x, y, and z of 300 ± 0.001 mV/g.

Spectral analyses of the signals were carried out using Matlab version R2014b. Fast Fourier Transform (FFT) of the friction force and acceleration signals were obtained using the following relationship (Thomson and Dahleh 1998; Bendat and Piersol 2010),

$$FFT(f) = \int_{-\infty}^{\infty} \mathrm{e}^{-2\pi i f t} x(t) dt \tag{9.1}$$

where $FFT(f)$ is the Fast Fourier Transform of the variable $x(t)$, f is the frequency, and t is the time.

In order to determine correlation between friction force and acceleration, coherence function, $C_{xy}(f)$, was calculated using the following relationship (Bendat and Piersol 2010),

$$C_{xy}(f) = \frac{\left|P_{xy}(f)\right|^2}{P_{xx}(f)P_{yy}(f)} \tag{9.2}$$

where P_{xx} and P_{yy} are the power spectral density functions of x and y, respectively, and P_{xy} is the cross-power spectral densities of x and y. P_{xx} and P_{yy} can be obtained by taking FFT of the data (9.1) and squaring the results. P_{xy} is obtained by taking the FFT of the product of the two variables, x(t) and y(t).

Normal load, friction force, and accelerometer data were sampled at 4 kHz, considering a frequency measurement range of 0–1.6 kHz is sufficient to measure all the dominant frequencies of vibration in the present experimental conditions. These parameters were digitized with a resolution of 12 bits in the range of 3.5 V through Labview 7.1 software (National Instrument™) and onboard electronics.

All data from the strain gauge force sensors and the accelerometer were collected and saved by the Labview software, and then the spectrum analysis was obtained by FFT through the Matlab software. The correlation between friction and friction induced vibration for each test was obtained by magnitude squared coherence.

For each test with and without cream treatment, nominal normal load was 50 mN on the sample surface through the micrometer actuator. The reciprocating sliding velocity was 20 mm/s, and the scanning distance was 30 mm. Selected loads and velocities are believed to be typical conditions for a fingertip during rubbing of the skin surface. To study the effect of load, the load on the sample ranged from 50 to 200 mN. To study the effect of velocity, the velocity range was 10–30 mm/s. To study the effect of treatment time of the cream, the cream was applied and measurements were made after 0, 1, and 3 h of treatment time.

9.3 Results and Discussion

The data on friction force and acceleration signals and their FFT data, as well as coherence function for an artificial finger sliding on PMMA, pig skin, and synthetic skin are presented (Ding and Bhushan 2016). We first present data on PMMA with and without cream treatment as an engineering reference sample. We then present data on pig skin and synthetic skin. Finally, we present data on the effect of normal load, velocity, and cream treatment time.

9.3.1 PMMA, Pig Skin, and Synthetic Skin with and Without Cream Treatment

Figure 9.3 shows the friction force and acceleration data for the PMMA sample with and without cream treatment, as well as FFTs of both data and coherence functions (Ding and Bhushan 2016). Average value of the coefficient of friction (μ) is also listed in the friction force maps. The variation in friction force corresponds to variations in the normal load due to roughness. Selected data are summarized in Table 9.1. As expected, cream treatment reduces friction.

The data show that the frequency spectrum exhibits a dominant frequency of about 17 Hz for both untreated and treated samples, although surface topography changed after cream treatment. The coherence functions between friction forces and vibration accelerations were nearly 1 at this dominant frequency. Furthermore, the frequency of 17 Hz was found to be near the first natural frequency of the cross configuration cantilever structure strain gauge beam. The natural frequency was measured by hitting the end of the cantilever beam and recording friction and acceleration signals, and conducting their frequency spectral analysis. The second dominant frequency of the acceleration signals was about 110 Hz in Fig. 9.3a and about 90 Hz in Fig. 9.3b, and it decreases in amplitude (Ding and Bhushan 2016). These results indicate that cream treatment attenuated both the frequency and amplitude of friction-induced vibrations. The third dominant frequency in (a) is about 240 Hz. However, after cream treatment, the third signal disappears, Fig. 9.3b. Smoothness and lower friction of the sample with cream treatment sample is believed to be responsible for the decrease in amplitude of the acceleration signal. This is consistent with the observations by Cattaneo and Vecchi (2011) that smooth surfaces induced virtually no vibration, while rougher surface induced more vibrations. In contrast, the coherence function values for the cream treated sample were lower after the second dominant frequency of about 90 Hz. To sum up, the data shows that cream treatment of PMMA generated attenuated friction and surface smoothness.

Figure 9.4 shows the data on pig skin with and without cream treatment. Selected data are summarized in Table 9.1. As observed on PMMA, the first dominant frequency of the acceleration signals is 17 Hz. The second dominant frequency of about 90 Hz in (a) decreased to about 80 Hz with attenuated signal after cream treatment in (b), similar to what was observed for PMMA. However, the frequency between 17 and 90 and 110–200 Hz shows an increased amplitude, probably because, during sliding contact, the pig skin surface absorbed the skin cream, and the hydration made the skin smoother and more compliant (Table 5.1), leading to a larger contact area and friction. Large compliance is expected to increase the damping characteristics of the skin responsible for the attenuation in acceleration. Bhushan et al. (2010) have reported that root mean square (RMS) roughness of rat skin decreased from about 130 to about 70 nm and peak-to-valley (P-V) distance from 952 to 604 nm. Chen and Bhushan (2013) reported that RMS roughness of pig skin decreased from about 290–270 nm. This

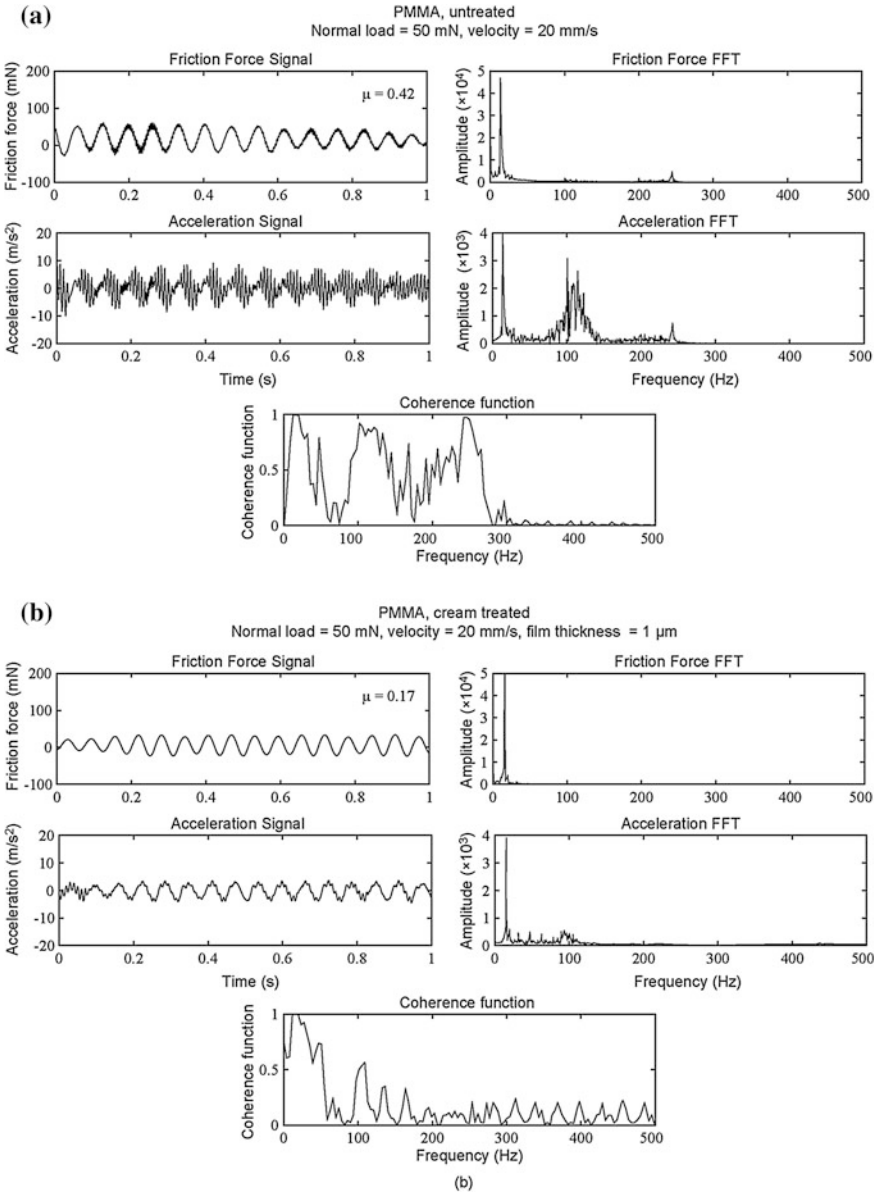

Fig. 9.3 Friction force and acceleration signals, and calculated FFT data and coherence function for **a** PMMA without cream treatment, and **b** PMMA with cream treatment with film thickness of 1 μm (Ding and Bhushan 2016)

Table 9.1 Average coefficient of friction and selected FFT data of samples (normal load = 50 mN, velocity = 20 mm/s, film thickness = 1 μm) (Ding and Bhushan 2016)

Sample		Average coefficient of friction	FFT dominant frequency (Hz)	FFT amplitude	
				Friction force ($\times 10^4$)	Acceleration ($\times 10^3$)
PMMA	Virgin	0.42	100	0.10	3.1
			240	0.70	0.80
	Cream treated	0.17	90	<0.01	0.60
			210	<0.01	0.05
Pig skin	Virgin	0.40	95	<0.01	4.0
			190	<0.01	0.20
	Cream treated	1.6	80	0.05	2.3
			170	0.05	0.60
Synthetic skin	Virgin	0.29	100	0.05	3.5
			200	0.05	0.60
	Cream treated	0.35	110	<0.01	1.5
			210	<0.01	0.10

represents smoothness as a result of cream treatment. The third dominant frequency of 240 Hz for PMMA without treatment is absent in pig skin. The magnitude of the coherence function for pig skin without treatment appears to be lower than that for smooth PMMA. To sum up, data shows a decrease in second dominant frequency and its amplitude, probably because of smoothness and compliance (increased damping) of the skin after cream treatment. There was also a correlation between friction and vibration signals.

Data for synthetic skin is shown in Fig. 9.5 and Table 9.1 (Ding and Bhushan 2016). All signal values, FFT amplitudes, and coherence function have trends similar to that of the pig skin.

Although three samples have different physiological and topographical features, data for all samples have the same trend. It is observed that cream treatment attenuates friction induced vibrations thereby improving tactile sensing. Attenuation in PMMA occurs due to reduced friction and in pig skin and synthetic skin seems to occur due to increasing damping. The coherence function of these signals showed that the vibration accelerations are closely correlated with friction forces at all dominant frequencies.

9.3.2 Effect of Normal Load and Velocity

Tactile perception may be affected by a change in normal load and velocity. Figure 9.6a, b shows the effect of normal load on the frequency spectra of the acceleration for pig skin with and without cream treatment (Ding and Bhushan

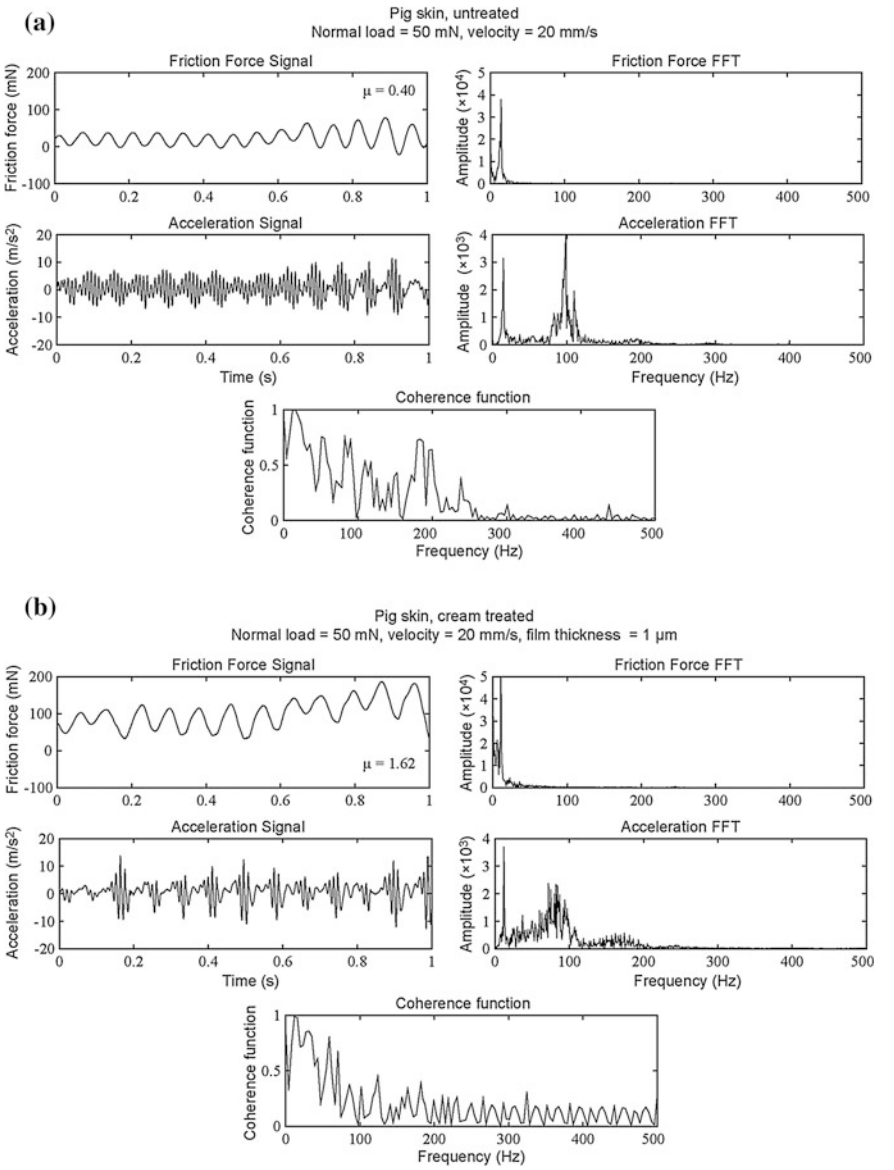

Fig. 9.4 Friction force and acceleration signals, and calculated FFT data and coherence function for **a** pig skin without cream treatment, and **b** pig skin with cream treatment with film thickness of 1 μm (Ding and Bhushan 2016)

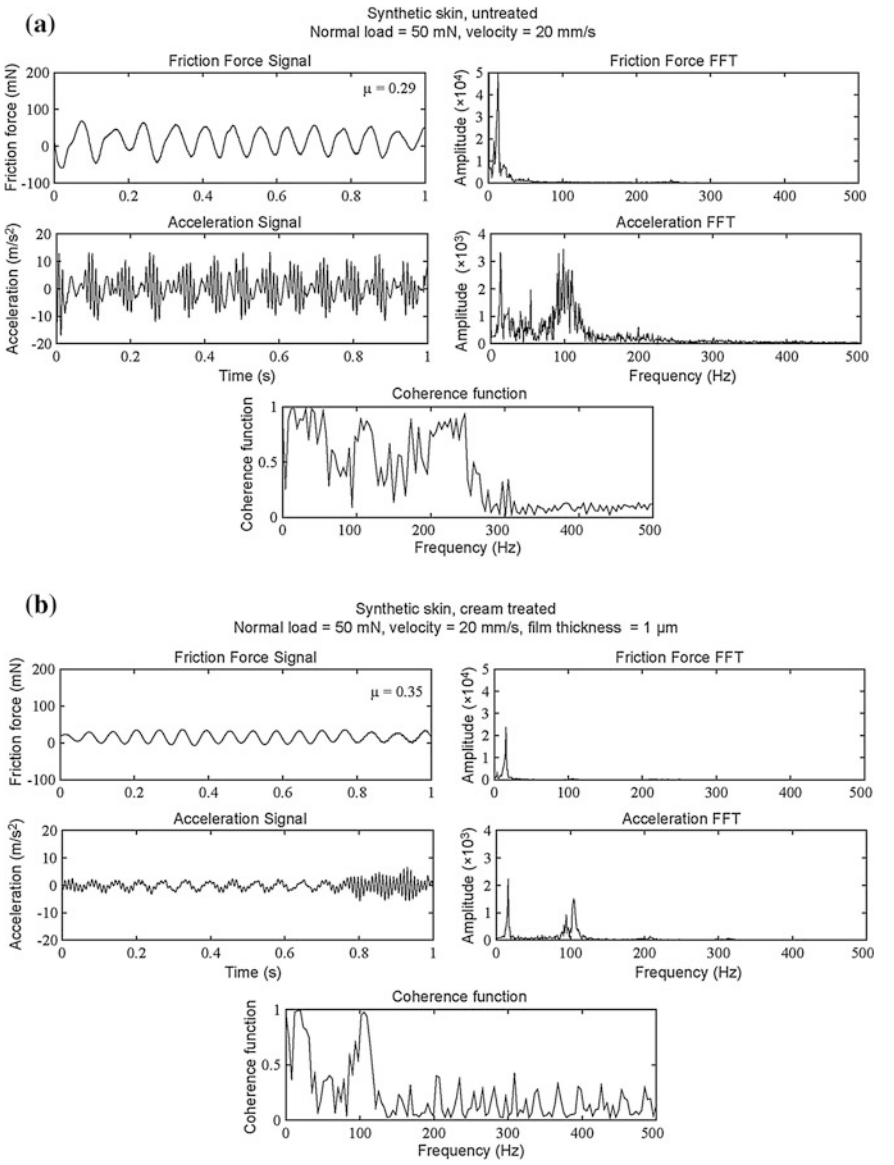

Fig. 9.5 Friction force and acceleration signals, and calculated FFT data and coherence function for **a** synthetic skin without cream treatment, and **b** synthetic skin with cream treatment with film thickness of 1 μm (Ding and Bhushan 2016)

2016). For pig skin with cream treatment, the data shows an increase in the normal load from 50 to 200 mN causes the frequency spectra to cover a large range and peak amplitudes to increase. The opposite trend is found for pig skin without cream treatment. This suggests that normal load is one of the factors affecting the tactile perception.

Figure 9.6c, d shows the FFT of acceleration measured for three scanning velocities on pig skin with and without cream treatment (Ding and Bhushan 2016).

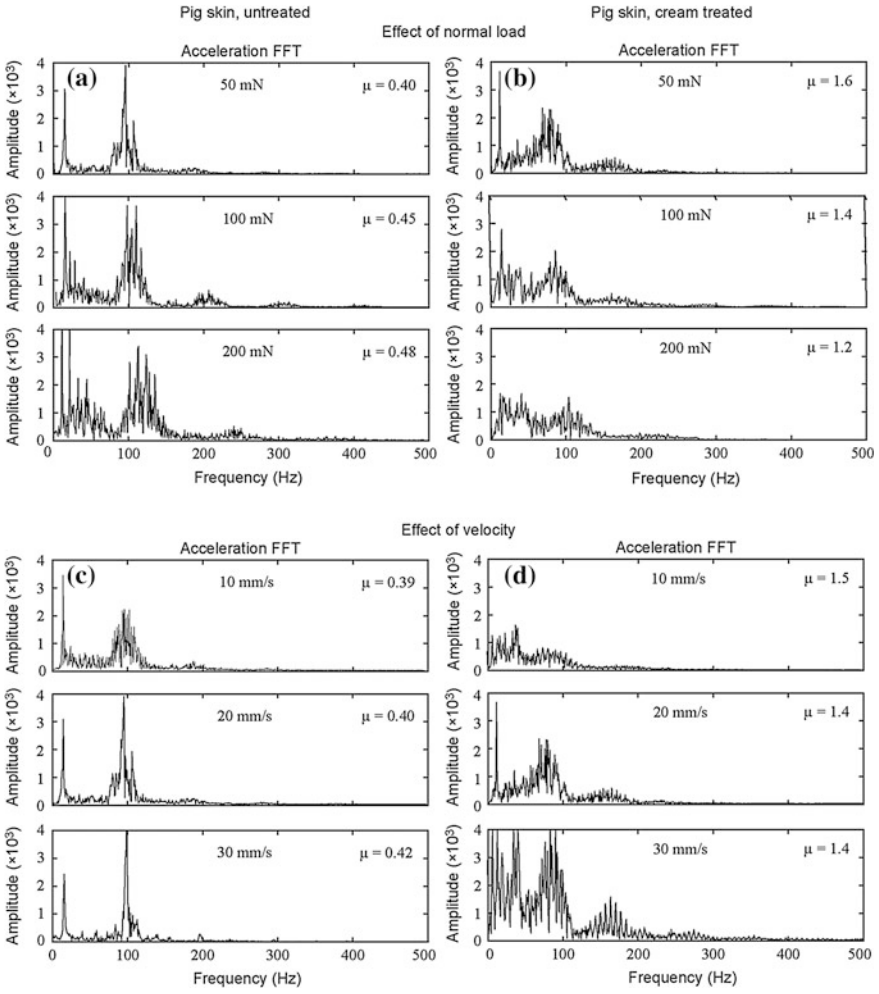

Fig. 9.6 Effect of normal load on FFT acceleration data for **a** pig skin without cream treatment, and **b** pig skin with cream treatment with scanning velocity of 20 mm/s and film thickness 1 μm, and effect of velocity on FFT acceleration data for **c** pig skin without cream treatment, and **d** pig skin with cream treatment with normal load 50 mN and film thickness of 1 μm (Ding and Bhushan 2016)

The data shows that increasing velocity from 10 to 30 mm/s causes trends similar to those found for increasing load. The results indicate that scanning velocity also affects tactile perception.

9.3.3 *Effect of Cream Treatment Time*

Skin cream is absorbed through the skin surface with time. Therefore, it is of interest how treatment time affects tactile perception. Figure 9.7 shows data for cream treatment time from 0 to 3 h (Ding and Bhushan 2016). The vibration spectra remains within the same frequency range, but the amplitudes of the peaks generally drop as a function of cream treatment time. This suggests that skin cream provides smoother tactile perception after 3 h treatment. In terms of percutaneous absorption, the compounds of the skin cream dissolve/partition into the surface lipids of the stratum corneum, making the surface more compliant. These interactions with skin can cause a drastic change in tactile perception within 3 h (Ding and Bhushan 2016).

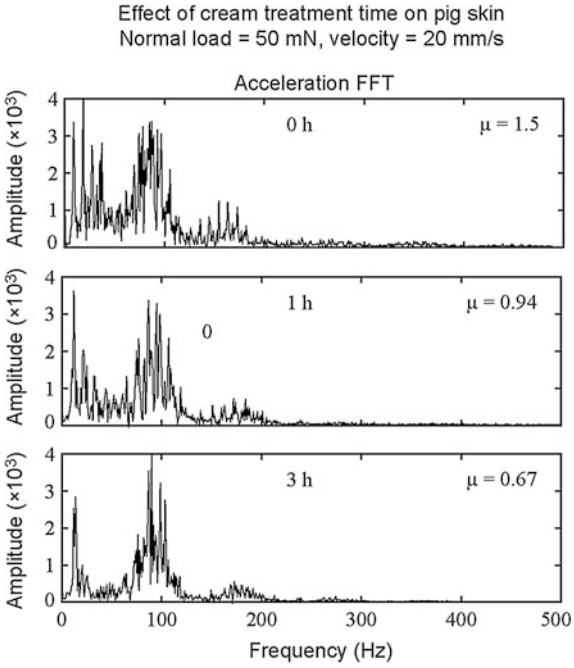

Fig. 9.7 Effect of cream treatment time on FFT acceleration data on pig skin with cream treatment with normal load of 50 mN, scanning velocity of 20 mm/s, and film thickness of 1 μm (Ding and Bhushan 2016)

9.4 Summary

Friction induced vibrations during rubbing of skin were measured to study changes in tactile perception of various skin samples. An artificial finger was rubbed against samples in a reciprocating mode, and friction and acceleration signals were measured and their coherence was analyzed (Ding and Bhushan 2016). Pig skin and synthetic skin samples with different surface topography and physical properties with and without cream treatment were investigated. A homogenous and smooth PMMA sample also was used as a baseline. Frequency spectra (FFT) were used to quantify tactile perception. Coherence function was calculated to study the correlation between friction force and vibration signals. The effect of normal load and velocity on pig skin with and without cream treatment and the effect of cream treatment time were studied. The conclusions from this study are as follows.

- After application of skin cream, the amplitude of the vibration is attenuated, which corresponds to smoother tactile perception. In the case of pig skin and synthetic skin with cream treatment, although friction increases, increased damping and compliance attenuates frequency.
- There was a correlation between friction force and vibration signals.
- Higher normal load and velocity for skin with cream treatment affect tactile perception. The frequency range remains the same, but amplitude decreases, which corresponds to an increase in perceived smoothness. The opposite is true for skin without cream treatment.
- Cream treatment time affects tactile perception. With longer cream treatment time, the frequency range remains the same, but amplitude decreases, which corresponds to an increase in perceived smoothness.

To sum up, a simple experimental setup using an artificial finger sliding against a reciprocating surface provides insight into tactile perception of skin.

References

Bendat, J. S., & Piersol, A. G. (2010). *Random Data* (4th ed.). New York: Wiley.

Bhushan, B. (1996). *Tribology and Mechanics of Magnetic Storage Devices* (2nd ed.). New York: Springer.

Bhushan, B. (2011). *Nanotribology and Nanomechanics I—Measurement Techniques and Nanomechanics, II—Nanotribology, Biomimetics, and Industrial Applications* (3rd ed.). Heidelberg, Germany: Springer.

Bhushan, B. (2013a). *Principles and Applications of Tribology* (2nd ed.). New York: Wiley.

Bhushan, B. (2013b). *Introduction to Tribology* (2nd ed.). New York: Wiley.

Bhushan, B., & Forehand, S. (1997). In situ instrumentation for localized wear studies of magnetic thin-film disks. *Proceedings of the Institution of Mechanical Engineers, Part J: Journal of Engineering Tribology, 211*, 249–262.

Bhushan, B., Tang, W., & Ge, S. (2010). Nanomechanical characterization of skin and skin cream. *Journal of Microscopy, 240*, 135–144.

Bolanowski, S. J., Gescheider, G. A., Verrillo, R. T., & Checkosky, C. M. (1988). Four channels mediate the mechanical aspects of touch. *The Journal of the Acoustical Society of America, 84*, 1680–1694.

Cattaneo, Z., & Vecchi, T. (2011). *Blind Vision: The Neuroscience of Visual Impairment*. Cambridge, Massachusetts: MIT Press.

Chen, S., & Bhushan, B. (2013). Naonomechanical and nanotribological characterization of two synthetic skins with and without skin cream treatment using atomic force microscopy. *Journal of Colloid and Interface Science, 398*, 247–254.

Ding, S., & Bhushan, B. (2016). Tactile perception of skin and skin cream by friction induced vibrations. *Journal of Colloid and Interface Science, 481*,131–143.

Fagiani, R., Massi, F., Chatelet, E., Bertier, Y., & Akay, A. (2011). Tactile perception by friction induced vibrations. *Tribology International, 44*, 1100–1110.

Hollins, M., Bensmaïa, S. J., & Risner, S. R. (1998). The Duplex theory of tactile texture perception. In S. Grondin & Y. Lacouture (Eds.), *Proceedings of the Fourteenth Annual Meeting of the International Society for Psychophysics* (Fechner Day 98.) (pp. 115–120). Quebec, Canada: The International Society for Psychophysics.

Katz, D. (1989). *The World of Touch* (L. E. Krueger & Lawrence Erlbaum Associates, Inc., Trans.). Hillsdale, New Jersey.

Makous, J. C., Friedman, R. M., & Vierck, J. (1995). A critical band filter in touch. *Journal of Neuroscience, 15*, 2808–2818.

Mo, J. L., Wang, Z. G., Chen, G. X., Shao, T. M., Zhu, M. H., & Zhou, Z. R. (2013). The effect of groove-textured surface on friction and wear and friction-induced vibration and noise. *Wear, 301*, 671–681.

Scheibert, J., Leurent, S., Prevost, A., & Debrégeas, G. (2009). The role of fingerprints in the coding of tactile information probed with a biomimetic sensor. *Science, 323*, 1503–1506.

Tang, W., Zhang, J., Chen, S., Chen, N., Zhu, H., Ge, S., et al. (2015). Tactile perception of skin and skin cream. *Tribology Letters, 59*, 24.

Thomson, W. T., & Dahleh, M. D. (1998). *Theory of Vibration with Applications* (5th ed.). Upper Saddle River, New Jersey: Prentice Hall.

Part V
Closure

Chapter 10
Overall Summary and Outlook

Skin is the outer layer covering a human or animal body. Its function is to protect the body from physical and environmental assaults, and to provide sensation, heat regulation, water resistance, and other functions. Environmental conditions, such as dry and cold weather, can reduce the moisture content of skin and lead to dry, rough, itchy skin. As skin goes through daily activities, it is damaged. Skin also ages with time, resulting in changes in skin properties.

For healthy and beautiful human skin, skin care products such as skin cream are used to create a smooth, soft, and moist flexible surface by altering the tribological and mechanical properties of the skin surface. This changes the tactile perception when treated skin touches a surface. Friction, adhesion and wear during sliding between the treated surface and the rubbing surfaces need to be optimized. Skin cream is used to improve skin health and its tactile perception. Some important factors affecting the smooth feel and repair of the skin surface include rheology of skin cream as a function of cream thickness and strain rate, and the binding interaction between skin cream and skin surface and operating environment.

Pig skin resembles human skin in general, and is a common substitute for human skin for pharmaceutical and cosmetic research. Rat skin has also been used. Synthetic skins are also of interest for pharmaceutical and cosmetic research. Various synthetic formulations are commercially available.

Nanotribological and nanomechanical properties of virgin and damaged animal skin, as well as synthetic skins with and without cream treatment and the role of operating environment have been studied using an AFM and nanoindentation. Macrotribological properties also have been studied to examine scale effects. Tactile perception studies have been carried out to understand tactile sensing mechanisms. The following are the key findings:

- Skin cream reduces the surface roughness and increases the hydrophilic properties of skin.
- The cream film unevenly distributes on skin surface.

B. Bhushan, *Biophysics of Skin and Its Treatments*, Biological and Medical Physics, Biomedical Engineering, DOI 10.1007/978-3-319-45708-6_10

- Skin cream moistens and softens the skin surface, which leads to greater ductility and a larger real area of contact, resulting in higher adhesion and friction. The presence of skin cream also increases friction due to meniscus and viscous effects.
- Higher viscosity results in higher friction and longer durability.
- Cream treatment reduces charge build up on the skin surface. Relative humidity facilitates charge dissipation.
- Synthetic skin provides a good simulation for the skin and can be used in cosmetic research.
- After application of skin cream, the amplitude of the vibration is attenuated, which corresponds to smoother tactile perception. In the case of pig skin and synthetic skin with cream treatment, although friction increases, increased damping and compliance attenuates frequency.
- There is a correlation between friction force and vibration signals.
- Cream treatment time affects tactile perception. With longer cream treatment time, the frequency range remains the same, but amplitude decreases, which corresponds to an increase in perceived smoothness.

As an outlook, more work is needed to obtain correlation between skin friction and vibration characteristics. Further research is needed to develop synthetic skins that provide a more realistic human skin model for laboratory research and the development of beauty care products.

Appendix A
Primer to Tribology

A.1 Introduction

Tribology is defined as the science and technology of interacting surfaces in relative motion, and of related subjects and practices. It includes the studies of adhesion, friction, wear, and lubrication (Bhushan 1996, 2001, 2013a, b). Since physical and chemical properties affect interfacial phenomena, the field of tribology includes the study of these properties. These include surface films, surface roughness, mechanical properties, and rheology of lubricants.

All surfaces are rough on the micro- to nanoscale. Even cleaved mica or graphite are rough on the atomic scale. High points on the surfaces are referred to as asperities, hills, or mountains (also called peaks in 2-D, and summits in 3-D), and low points are referred to as valleys. The number of asperities on an engineering surface can range from a few to several million or more. At an interface, contact occurs on a large number of asperities ranging from one such as during metal cutting at high loads, to several million or more in the case of rather smooth surfaces, Fig. A.1 (left).

Asperities contacts lead to local elastic/plastic/viscoelastic deformation to support the applied load. Deformations are a function of local mechanical properties and surface roughness. During sliding, friction and wear are governed by interactions at a large number of asperity contacts. It should also be recognized that surface physical and chemical properties change continuously during sliding, which makes it difficult to understand changes in friction and wear in a dynamic process. Materials and sometimes solid/liquid/vapor lubricant films are selected to provide desired friction and wear properties (Bhushan and Gupta 1991).

To develop a fundamental understanding of the interfacial process, it is of interest to simulate a single asperity contact. This can be done by using a sharp tip sliding on one of the engineering surfaces of interest, Fig. A.1 (right). Once we understand the single asperity contact, we can extend this understanding to better understand a complex engineering interface involving a number of asperities.

B. Bhushan, *Biophysics of Skin and Its Treatments*, Biological and Medical Physics, Biomedical Engineering, DOI 10.1007/978-3-319-45708-6

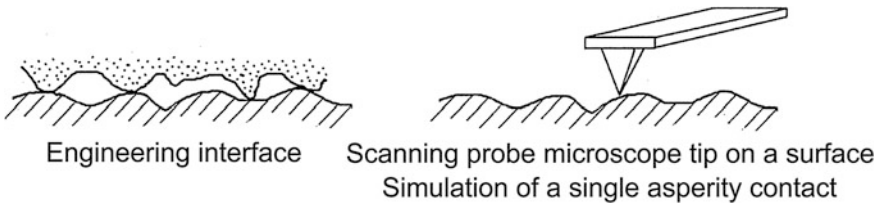

Fig. A.1 Schematics of an engineering interface (*left*) and atomic force microscope tip in contact with an engineering surface (*right*) (Bhushan 2011, 2013a, b)

An atomic force microscope (AFM) uses a sharp tip with a radius ranging typically from 5 to 50 nm. It is brought into contact for research at loads on the order of 1 nN or less. During contact, picoasperities present even on a carefully prepared sharp tip cone come into contact with several asperities on the surface of interest. Typically, the number of contacts can be 5–10. Once one understands friction and wear of a simulated single-asperity contact, this understanding can be used to understand interfacial phenomena on a large scale involving a large number of asperities. These so-called nanotribological studies are of importance in a fundamental understanding of interfacial phenomena on a small scale and to provide a bridge between macro- and nanoscales (Bhushan et al. 1995; Bhushan 1999, 2010a, 2011). Given that scale size affects interfacial phenomena, friction and wear properties would be scale dependent. Therefore, one needs to take into account scale effects when translating data and trends on macro- to nanoscales and vice versa.

In this Appendix, we present a primer to tribology organized as shown in Fig. A.2 (Bhushan 2013a, b). We start with solid surface characterization. Then, two surfaces are brought into static contact and we discuss deformation of asperity contacts. Next, we separate two surfaces orthogonal to the interfacial plane and discuss the adhesive force required to separate two surfaces. Next, we introduce lateral motion and discuss the friction force required to initiate and maintain sliding. Next, we discuss interface temperatures generated by high frictional heat density at the asperity contacts. Then, we discuss wear mechanisms. Finally, we discuss fluid film lubrication and boundary lubrication used to control friction and wear if materials themselves cannot.

A.2 Solid Surface Characterization

A solid surface, or more exactly, a solid-gas or solid-liquid interface, has a complex structure and complex properties dependent upon the nature of solids, the method of surface preparation, and the interaction between the surface and the environment (Bhushan 2013a, b). Properties of solid surfaces are crucial to surface interaction.

The solid surface consists of several zones having physico-chemical properties peculiar to the bulk material itself. In addition to work-hardened or deformed layer

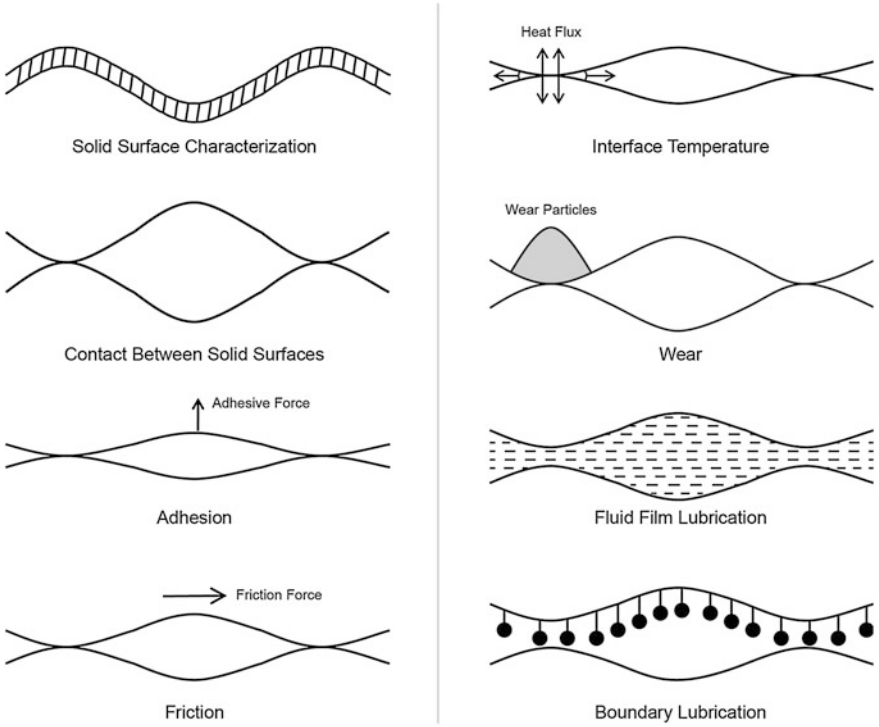

Fig. A.2 Outline of the primer to tribology

during machining, the layers are formed by physisorption, chemisorption, and/or chemical reaction. For the effect of adsorbed films, even a monolayer is significant in surface interaction.

In addition to surface films, solid surfaces contain irregularities or deviations from the prescribed geometrical form, without regard to method of formation. No machining method, however precise, can produce a molecularly flat surface on conventional materials. Even cleaved mica or graphite contain atomic scale roughness. The surfaces contain irregularities of various grades ranging from shape deviations to irregularities on the order of interatomic distances. For technological applications, both macro- and micro/nanoroughness of the surfaces (surface topology or surface texture) are important.

A.2.1 Surface Films Characterization

Surface films need to be characterized. Imaging techniques include optical microscopy, scanning electron microscopy (SEM), transmission electron microscopy (TEM), and field ion microscopy (FIM), as well as scanning tunneling microscopy

(STM) and atomic force microscopy (AFM) (Bhushan 2011). For detailed physical and chemical characterization, various surface analytical techniques are used. These can be classified based on radiation detected—electron, ion, X-ray photon, other photons, and electromagnetic fields (Bhushan 1996). Commonly used techniques for structural analyses include X-ray diffraction and electron diffraction. Commonly used techniques for chemical analyses include Auger electron spectroscopy (AES), energy dispersive analysis of X-rays (EDAX), X-ray photon spectroscopy (XPS), Fourier transform infrared spectroscopy (FTIR), mass spectrometry (MS), X-ray fluorescence, and secondary ion mass spectroscopy (SIMS) (Bhushan 1996).

A.2.2 Surface Roughness Characterization

A.2.2.1 Average Roughness Parameters

Surface roughness most commonly refers to the variations in the height of the surface relative to a reference plane. It is measured either along a single line profile or along a set of parallel line profiles (surface maps). It is usually characterized by one of the two statistical height descriptors:

1. CLA (center-line average) or AA (arithmetic average) designated as R_a, and
2. The standard deviation or variance (σ), or RMS (root mean square) designated as Rq.

A second measure of surface roughness is an extreme-value descriptor, R_t or maximum peak-to-valley height (simply, P-V distance).

To mathematically describe roughness parameters, we first define center line or mean line as the line such that the area between the profile and the mean line above the line is equal to that below the mean line.

$$m = \frac{1}{L}\int_0^L z dx = \frac{\sum_{i=1}^{N} z_i}{N} \tag{A.1}$$

where N is the number of points. R_a is the arithmetic mean of the absolute values of vertical derivation from the mean line through the profile.

$$R_a = CLA = AA = \frac{1}{L}\int_0^L |z - m| dx = \frac{\sum_{i=1}^{N} |z_i - m|}{N} \tag{A.2}$$

σ is the square root of the arithmetic mean of the squares of the vertical deviation from the mean line.

$$\sigma^2 = \frac{1}{L}\int_0^L (z-m)^2 dx = \frac{\sum_{i=1}^{N}(z_i - m)^2}{N} = Rq^2 - m^2 \qquad \text{(A.3)}$$

P-V distance is the vertical distance between the highest peak or summit and the lowest valley.

It should be noted that the average roughness parameters just described are primarily concerned with the relative departure of the profile in the vertical direction only. They do not provide any information about the slopes, shapes, and sizes of the asperities or about the frequency and regularity of the occurrence. For a complete characterization of a surface profile, spatial functions such as autocovariance function or power spectral density function, should be included.

A.2.2.2 Roughness Measurement Techniques

The most commonly used roughness measurement techniques include mechanical stylus profiler, noncontact optical profiler, and scanning tunneling microscope/atomic force microscope (STM/AFM). Table A.1 provides a comparison of various properties of these instruments. These all have vertical resolution down to 0.1–1 nm or less. Stylus and optical profilers provide lateral resolution on the order of 0.1–0.5 μm, whereas STM/AFM can provide atomic-scale resolution. Optical profilers are noncontact, which may be of interest for soft surfaces such as elastomers and skin, and for applications in which any scratching is not allowed, such as high-quality optical lenses. Scan size in stylus and optical profilers can be several mm x several mm, whereas in STM/AFM, it is typically on the order of 100 nm × 100 nm.

Figure A.3 shows an example of surface maps/profiles of a glass-ceramic disk obtained using three measurement techniques. It should be noted that when plotting

Table A.1 Comparison of commonly used roughness measurement methods

Method	Resolution		Cost/ease of use	Limitations
	Spatial	Vertical		
Mechanical stylus profiler	0.1–0.5 μm	0.1–1 nm	~$100k, easy to use	Contact type. Can damage the sample, large scan size—several mm
Noncontact optical profiler	~0.5 μm	0.1–1 nm	~$120k, relatively easy to use	Requires some optical reflection, noncontact, large scan size—several mm
Scanning tunneling microscope	0.2 nm	0.02 nm	~$150k, requires training	Requires electrically-conducting surfaces, atomic resolution, scan size ~100 μm × 100 μm
Atomic force microscope	0.2–1 nm			Scan size—~100 μm × 100 μm

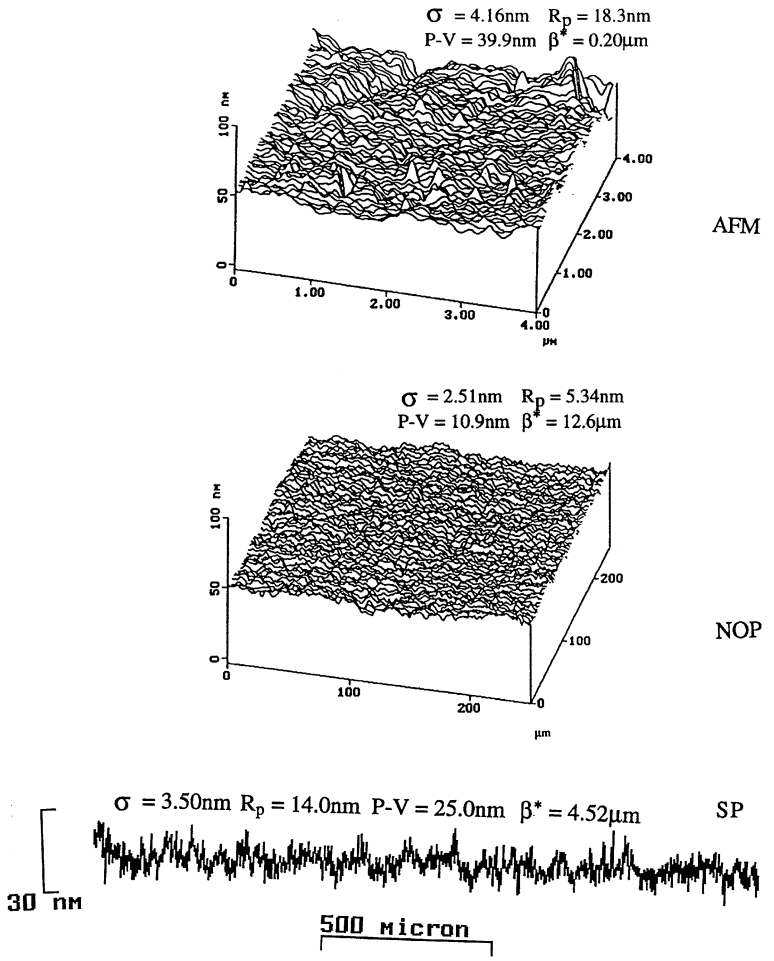

Fig. A.3 Surface roughness plots of a glass-ceramic disk measured using an atomic force microscope (spatial resolution ~1 nm), noncontact optical profiler (spatial resolution ~1 μm), and stylus profiler (tip radius ~0.2 μm) (Bhushan 2013a, b)

roughness data, the vertical axis is generally magnified by about three orders of magnitude or more with respect to the horizontal axis in order to magnify the roughness features. Since lateral resolutions of the three instruments are different, profiles/maps and magnitudes of roughness parameters are also different. Although the roughness is intrinsic to the surface, the measured roughness is extrinsic. There is no unique scale of measurement of interest, and roughness at scales relevant to the application should be used.

A.3 Contact Between Solid Surfaces

When two nominally flat surfaces are placed in contact, surface roughness causes contact to occur at discrete contact spots (junctions), Fig. A.4. Contact size ranges from the atomic scale to several hundred microns. The sum of the areas of all the contact spots constitutes the real (true) area of contact, or simply contact area. For most materials for an applied load, this will be only a small fraction of the apparent (nominal) area of contact, typically several orders of magnitude lower. As a result, local stresses would be substantially higher than the nominal stresses, typically several orders of magnitude higher. The real area of contact is a function of the surface roughness, mechanical properties, and interfacial loading conditions (Bhushan 2013a, b).

A.3.1 Analysis of the Contacts

Local deformation of contacts occurs by elastic, elastic/plastic, and/or viscoelastic deformation. It can be analyzed by elastic and elastic-plastic deformation analyses. An analysis of a single asperity contact is rather straightforward. For most cases with multiple-asperity contacts, statistical or numerical analyses are used (Bhushan 2013a, b).

For a single asperity contact with a spherical asperity on the each of the two mating surfaces, with composite radius R, composite elastic modulus E^*, hardness

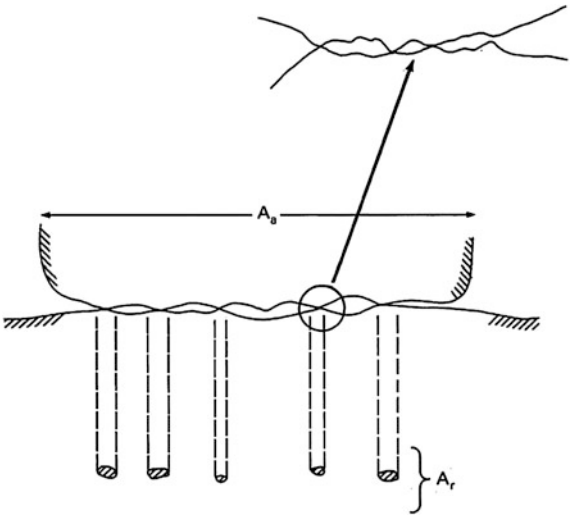

Fig. A.4 Schematic of an interface, showing the apparent and real areas of contact. Typical size of an asperity contact ranges from submicron to a few microns. Inset shows the details of a contact on a submicron scale (Bhushan 2013a, b)

of the softer material H, and nominal load W, the real area of contact for elastic contacts (A_{re}) and for plastic contacts (A_{rp}) is given as

$$A_{re} = \pi\left(\frac{3WR}{4E^*}\right)^{2/3} \tag{A.4a}$$

$$A_{rp} = \frac{W}{H} \tag{A.4b}$$

The plastic deformation is initiated at the subsurface at a location where maximum shear stress exceeds the yield stress in shear, and then extends to the surface, Fig. A.5. The location of the maximum shear stress depends on the size, mechanical properties, and coefficient of friction.

For a multiple asperity contact with spherical asperities of composite summit radius R_p and composite standard deviation of summit heights σ_p with several assumptions is given as

$$A_{re} \sim \frac{3.2W}{E^*\left(\sigma_p/R_p\right)^{1/2}} \tag{A.5a}$$

$$A_{rp} \sim \frac{W}{H} \tag{A.5b}$$

where whether the contact is elastic or plastic is dependent upon a parameter known as the plasticity index ψ

$$\psi = \frac{E^*}{H}\left(\frac{\sigma_p}{R_p}\right)^{1/2} \tag{A.6}$$

with $\psi < 0.6$, elastic and $\psi > 1$, plastic

For a single asperity contact in elastic contact, real area of contact is proportional to $W^{2/3}$ and for all other cases, it is proportional to W.

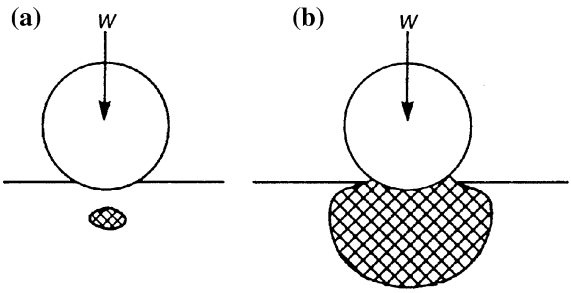

Fig. A.5 Indentation of an elastic-perfectly plastic solid by a spherical indenter; **a** onset of plasticity below the surface, and **b** at a higher load, full plasticity is reached and the plastic flow extends to the free surface

A.3.2 Measurement of the Real Area of Contact

Since the sizes of contacts range from the atomic scale to several hundred microns and are randomly distributed, it is extremely difficult to measure contact size distribution with any accuracy. Optical interference techniques have been used with little success (Bhushan 2013a, b).

A.4 Adhesion

When two surfaces are brought into contact, adhesion or bonding across the interface can occur (Bhushan 2013a, b). A finite normal force, called adhesive force, is required to pull the two solids apart, Fig. A.6. The ratio of the normal tensile force W' required for separation (normally referred to as adhesive force) to the normal compressive load W initially applied, is referred to as the coefficient of adhesion, μ',

$$\mu' = \frac{W'}{W} \tag{A.7}$$

W' typically increases linearly with an increase of W, and μ' generally increases with duration of static contact and separation rate.

A.4.1 Solid–Solid Contact

Proximity of the asperities results in an adhesive joint caused by interatomic attractions. Adhesion is considered to be either physical or chemical in nature.

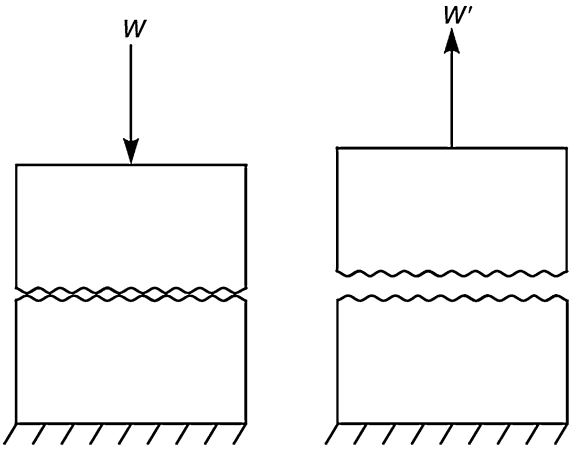

Fig. A.6 Schematic of the normal pull of two solid bodies; W is the compressive normal load applied for a certain duration, and W' is the tensile normal load needed to separate surfaces

A chemical interaction involves strong covalent bonds, ionic or electrostatic bonds, or metallic bonds. Physical interaction involves weak hydrogen bonds and van der Waals bonds as a result of intermolecular forces.

A.4.2 Liquid-Mediated Contact

A small quantity of liquid at the interface can result in a liquid-mediated contact. Any liquid that wets or has a small contact angle (hydrophilic) on a surface will condense from vapor on the surface in the form of annular-shaped capillary condensate in the contact zone, Fig. A.7a. The liquid film may also be deliberately applied for lubrication or other purposes. In the presence of a thin liquid film, adhesive bridges or menisci form around the contacting and near-contacting asperities due to surface energy effects.

The menisci formed with a wetting liquid are concave shaped and the liquid pressure (Laplace pressure) inside the meniscus is negative, which results in adhesion between the two bodies. Menisci can significantly increase adhesion. During separation of two surfaces, a so-called meniscus force is required to overcome adhesion. In addition, the viscosity of the liquid causes an additional attractive force, a rate-dependent viscous force during separation. Thus,

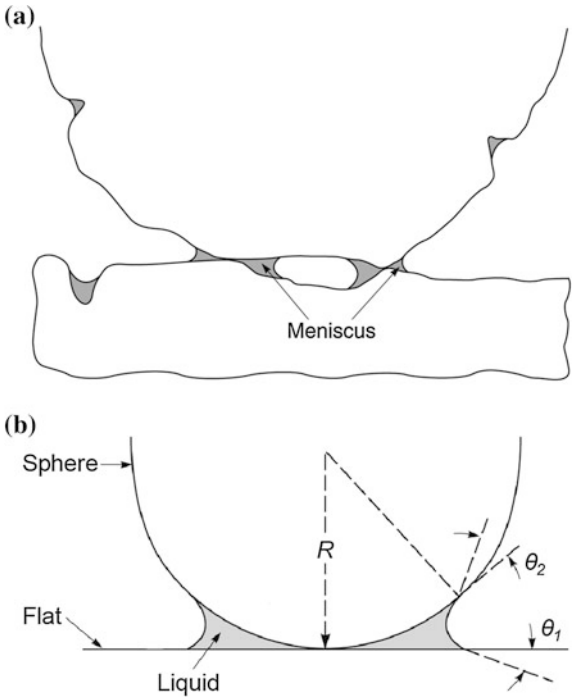

Fig. A.7 **a** Schematic of condensation from liquid vapor on the surfaces at the interface, and **b** meniscus formation from a liquid condensate at the interface for a sphere in contact with a flat surface (θ_1 and θ_2 are the liquid contact angles with flat and spherical surfaces, respectively)

liquid-mediated adhesive force (F_{ad}) consists of meniscus force (F_m) due to surface tension and a rate-dependent viscous force (F_v),

$$F_{ad} = F_m(t) + F_v(t) \tag{A.8}$$

As an example, for a simple case of a spherically topped asperity of radius R in contact with a flat surface with a liquid meniscus at the interface (Fig. A.7b), meniscus force is given as

$$F_m = 2\pi R\gamma(\cos\theta_1 + \cos\theta_2) \tag{A.9}$$

where γ is the liquid surface tension and θ_1 and θ_2 are liquid contact angles with the flat surface and spherical asperity, respectively. Note that F_m increases with γ and the shape of asperities.

Viscous force for a liquid-mediated contact is given as

$$F_v = \beta\frac{\eta}{t_s} \tag{A.10}$$

where β is a constant, η is the dynamic viscosity of the liquid, and t_s is inversely related to acceleration or velocity of the interface during start-up. η is strongly dependent upon the separation rate.

A.5 Friction

Friction is the resistance to motion during sliding or rolling that is experienced when one solid body moves tangentially over another with which it is in contact, Fig. A.8a (Bhushan 2013a, b). The resistive tangential force at the interface, which acts in a direction opposite to the direction of motion, is called the friction force.

There are two main types of friction that are commonly encountered: dry or "Coulomb" friction and fluid friction with a fluid film present at the interface. Rolling friction is generally a couple of orders of magnitude lower than the sliding friction, such as encountered between wheels and the road in a moving automobile.

A.5.2 Coefficient of Friction

Friction force is approximately proportional to the nominal load,

$$F = \mu W \tag{A.11}$$

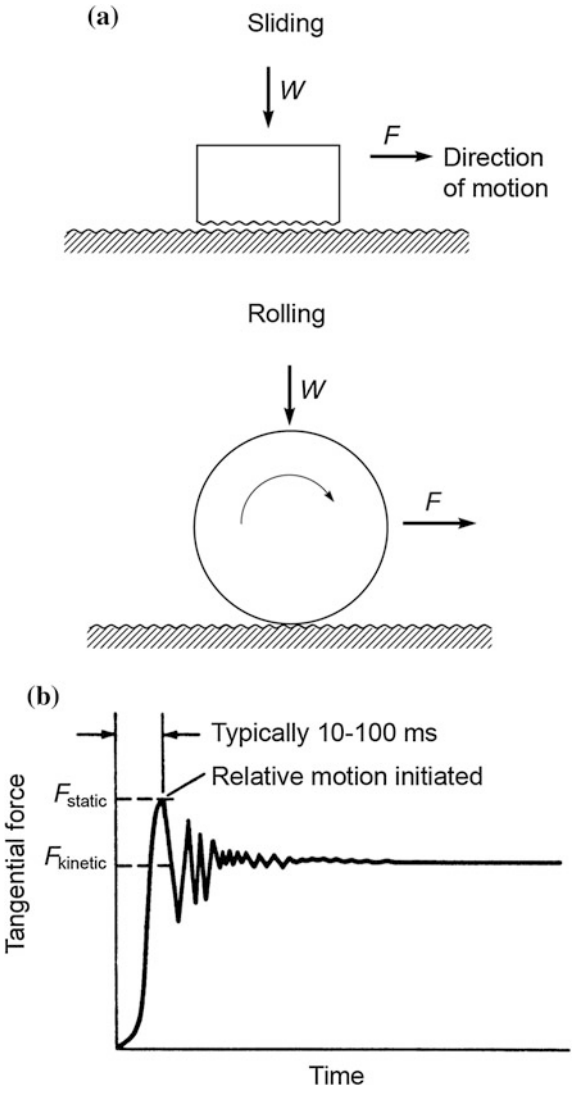

Fig. A.8 **a** Schematic of a body sliding on a surface and a body rolling on a horizontal surface; W is the normal load and F is the friction force, and **b** tangential force as a function of time or displacement; F_{static} is the static friction force required to initiate motion and $F_{kinetic}$ is the kinetic friction force required to sustain motion

where μ is nondimensional and is called the coefficient of friction. The force required to initiate sliding is referred to as static friction force (F_s), and the force required to maintain sliding is referred to as kinetic or dynamic friction force (F_k), Fig. A.8b. The static friction force is either higher than or equal to the kinetic friction force. It is generally desired that the coefficient of friction of a sliding interface should be less than 0.3–0.5.

A.5.2 Basic Mechanisms of Sliding Friction

There are two dominant sources of friction—adhesion and deformation. As indicated earlier, proximity of asperities results in adhesion. During sliding, the interfacial bonds need to be broken, and if the bonds are stronger than that of the material locally underneath, shearing occurs in one of the respective bodies, Fig. A.9a. Based on classical theory of adhesion, the friction force for a dry contact because of adhesion, F_a,

$$F_a = A_r \tau_a \tag{A.12}$$

and for a contact with a partial liquid film,

$$F_a = A_r[\alpha\tau_a + (1-\alpha)\tau_l] \tag{A.13a}$$

and

$$\tau_l = \frac{\eta V}{h} \tag{A.13b}$$

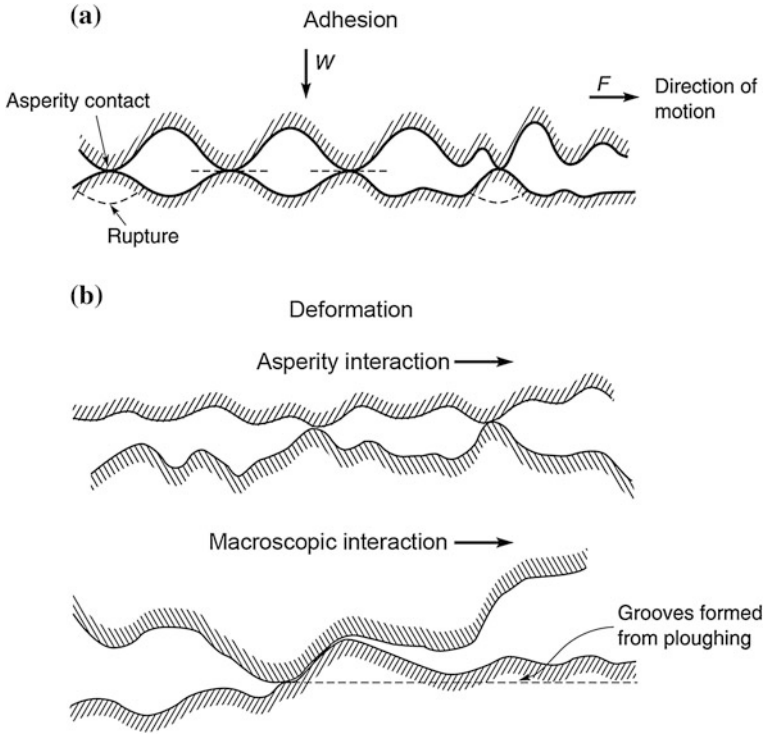

Fig. A.9 **a** Schematic of two rough surfaces in a sliding contact, and **b** schematic of asperity interaction and macroscopic interactions of two rough surfaces in sliding contact

where τ_a and τ_l are the average shear strengths of the dry contact and of the liquid film, respectively, α is the fraction of the unlubricated area, η is the dynamic (absolute) viscosity of the liquid, V is the relative sliding velocity, and h is the liquid film thickness.

Deformation occurs by two types of interactions during sliding: microscopic interaction where primarily plastic deformation and displacement of the contacting surface asperities are required, and macroscopic interaction where the asperities of the harder or rougher body plow grooves in the surface of the softer or smoother body via plastic deformation or fracture, Fig. A.9b. The plowing component of deformation friction increases with an increase of surface roughness and/or hardness mismatch.

A.6 Interface Temperature of Sliding Surfaces

In any sliding operation, most of the frictional energy input is generally used up in plastic deformation, and is directly converted to heat in the material close to the interface, Fig. A.10 (Bhushan 2013a, b). The heat is dissipated over asperity contact areas; therefore, heat dissipated per unit area is large. This can lead to generation of surface temperatures on the order of tens to hundreds of °C, even on the order of one thousand °C in heavily loaded contacts, such as in metal cutting. Duration of the asperity contact is related to asperity size and sliding velocity, which typically ranges from a few ns to a few ms. Thus, temperature flashes are generated at contact spots, typically over a micron to a few microns in diameter with a few ns to a few ms in duration during the life of a given contact. These temperature flashes shift from one place to another during sliding. The temperature rise increases with an increase in the coefficient of friction, normal load, sliding velocity, and is inversely related to the thermal properties of the sliding surfaces.

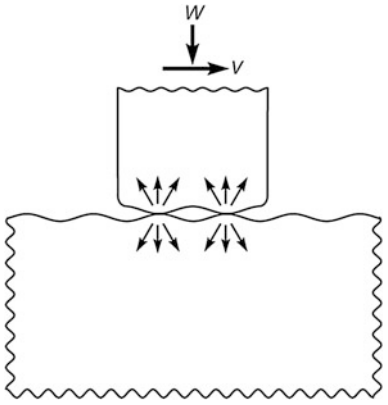

Fig. A.10 Schematics of two bodies in sliding contact with frictional heat dissipated at the asperity contacts

A.7 Wear

Wear is the surface damage or removal of material from one or both of two solid surfaces in a sliding, rolling, or impact motion relative to each other (Bhushan 2013a, b). During relative motion, first, material on the contacting surface may be displaced so that properties of the solid body, at least at or near the surface, are altered, but little or no material is actually lost. Later, material may be removed from a surface and may result in the transfer to the mating surface or may break loose as a wear particle. In the case of transfer from one surface to another, the net volume or mass loss of the interface is zero, although one of the surfaces is worn (with a net volume or mass loss).

Wear damage precedes the actual loss of material, and it may also occur independently. It should be emphasized that even microscopic damage due to material displacement on a given body with no net change in volume or mass, also constitutes wear.

A.7.1 Types of Wear Mechanisms

Wear occurs by mechanical and/or chemical means and is generally accelerated by thermal means (frictional heating). There are several distinct wear mechanisms. There are two dominant friction mechanisms—adhesive wear and abrasive wear.

Adhesive wear occurs when the interfacial bond is stronger than that of the material locally underneath and shearing occurs in one of the respective bodies resulting in material transfer, Fig. A.11a. This transfer is followed by a loss of material from the interface. Based on the classical theory of wear, volume of wear v is given as

$$v = \frac{kWx}{H} \tag{A.14}$$

where k is a nondimensional wear coefficient, x is the sliding distance, H is the hardness of the softer material, and k represents the probability of formation of wear debris in a given asperity encounter. The value of k ranges typically from 10^{-8} to 10^{-4} for mild wear, and from 10^{-4} to 10^{-2} for severe wear.

Abrasive wear occurs by two-body or three-body contact, Fig. A.11b. In two-body wear, the harder or rougher of the two surfaces plows into the mating surface. In three-body wear, small particles of abraded material or foreign particles are caught between the two surfaces and abrade one or both of the surfaces. In the case of two-body abrasive wear, the wear rate increases with an increase of surface roughness. The wear rate in three-body abrasion is lower than that of two-body abrasion, since some rolling of interacting particles occurs during sliding.

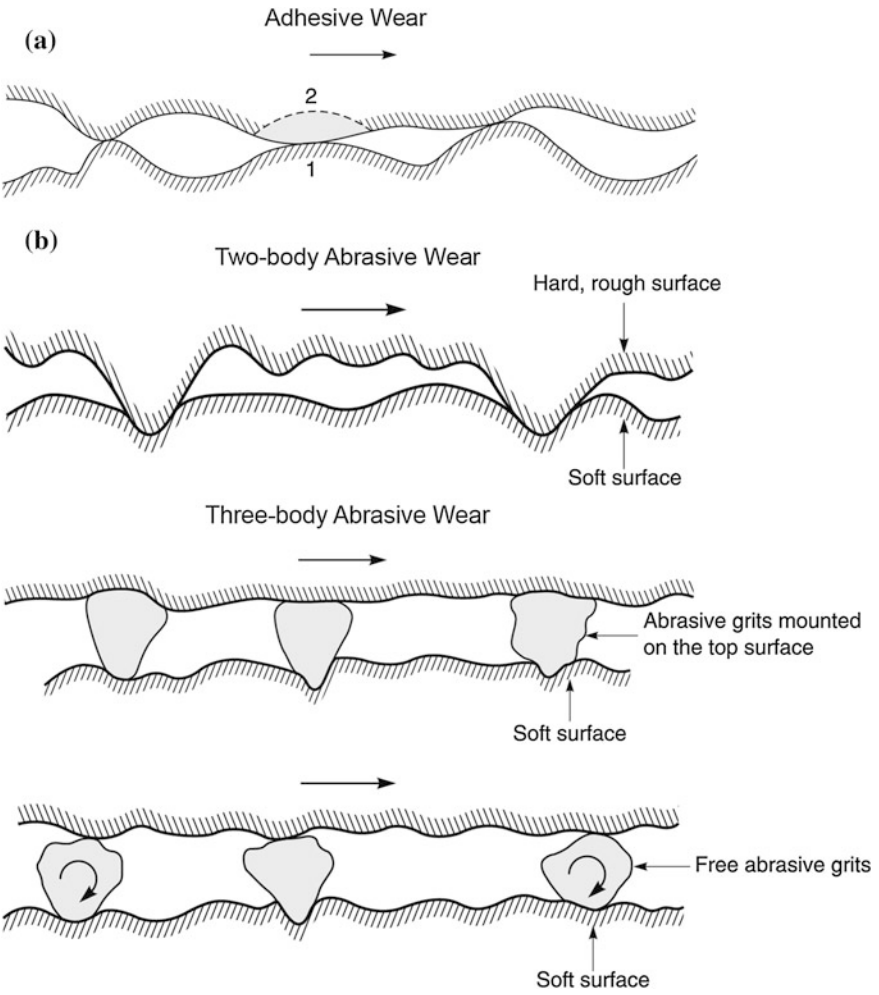

Fig. A.11 **a** Schematic showing two possibilities of break (1 and 2) during shearing of an interface, and **b** schematics of a rough, hard surface (*top*) or a surface mounted with abrasive grits sliding on a softer surface (*middle*), and free abrasive grits caught between the surfaces with at least one of the surfaces softer than the abrasive grits (*bottom*)

A.8 Fluid-Film Lubrication and Boundary Lubrication

Sliding between clean solid surfaces generally results in high friction and wear. Any solid particles or surface films present in the operating environment reduce friction and wear. However, the presence of such films cannot be guaranteed, and furthermore, they degrade with use. In order to design interfaces with low friction and wear, solid particles or fluid films are needed if materials alone cannot provide the

desired properties (Bhushan and Gupta 1991; Bhushan 2013a, b). These lubricant films can be as thin as a couple of nm (e.g., in magnetic storage devices) to hundreds of μm (e.g., in automotive applications) to several mm (e.g., in earth moving equipment). With solid lubrication, μ as low as 0.05 can be realized and with fluid film lubrication, μ as low as 0.001 can be realized. Fluid films can be liquid or gaseous, and even water or air can act as a lubricant.

Fluid films can be introduced at the interface by hydrostatic, hydrodynamic, or boundary lubrication (Bhushan 2013a, b). In hydrostatic lubrication, a thick fluid film is produced by introducing high-pressure fluid through orifices using a pump. The benefit is that a fluid film can be maintained regardless of the operating speed. However, it requires a pump and fluid-cleaning equipment, which adds weight and cost.

The other regimes of lubrication can be found in the Stribeck curve, shown in Fig. A.12, and include hydrodynamic lubrication, elastohydrodynamic lubrication,

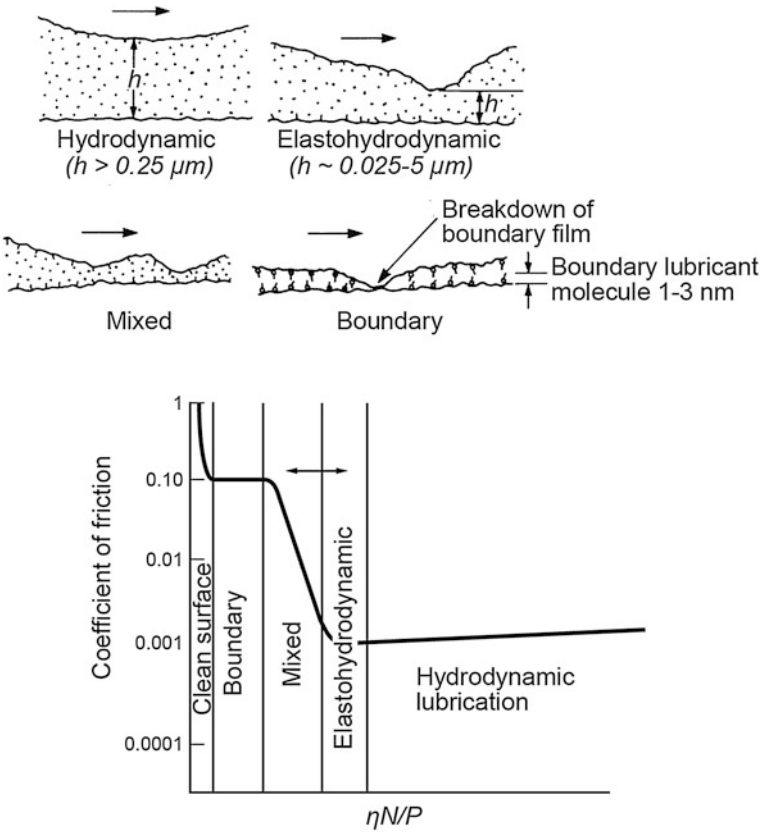

Fig. A.12 Coefficient of friction as a function of $\eta N/P$ (*Stribeck curve*) showing different lubrication regimes observed in a fluid lubrication without an external pumping agency. η is the dynamic viscosity of the fluid, N is the rotational speed, and P is the normal pressure

mixed lubrication, and boundary lubrication. In hydrodynamic lubrication, as a bearing with a convergent shape in the direction of motion starts to move in the longitudinal direction from rest, a thin layer of fluid is pulled through because of viscous entrainment, and is then compressed between the bearing surfaces, creating a sufficient (hydrodynamic) pressure to support the load without any external pumping agency, Fig. A.13. A coefficient of friction as low as 0.001 can be realized. These bearings are called self-acting bearings. Hydrodynamic lubrication is sometimes called ideal lubrication because pumps or other equipment are not required to clean the lubricant, unlike hydrostatic lubrication.

The magnitude of the hydrodynamic pressure is dependent upon the shape of the convergent channel, sliding speed, and fluid viscosity. Fluid viscosity is strongly dependent upon the pressure, temperature, and shear rate of the fluid.

Elastohydrodynamic lubrication (EHL) is a subset of hydrodynamic (HD) lubrication. In EHL, the elastic deformation of the contacting solids plays a significant role in the HD lubrication process.

The other extreme regime is boundary lubrication. Boundary lubrication is the condition in which the solid surfaces are so close together that the surface interaction dominates and low friction and wear protection is provided by formation of boundary films on the surface by mitigating solid-solid contact, Fig. A.14. As the load increases, speed or the fluid viscosity decreases, the hydrodynamic film to support the external load cannot be formed, and many of the asperities touch and others are separated by the fluid film. These films are formed by physisorption, chemisorption, and/or chemical reaction. Even a monolayer of absorbed molecules may provide some protection against wear. These films are continuously replenished during sliding. The degree of protection is dependent upon the polarity of liquids and solids. The coefficient of friction in boundary lubrication is on the order of 0.1.

It should be noted that boundary lubrication is also needed in hydrodynamic and elastohydrodynamic lubrication during starting/stopping until a thicker fluid film is developed at operating speeds.

Liquid lubricants used include both natural organic and synthetic organic types, Table A.2. The most commonly used are mineral oils (petroleum oils), a family of

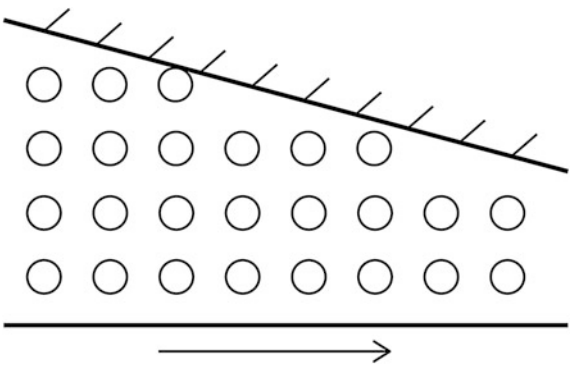

Fig. A.13 Schematic of a convergent channel in a hydrodynamic bearing

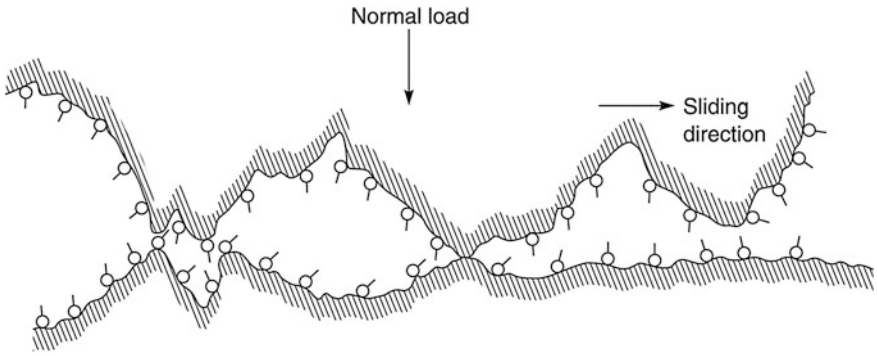

Fig. A.14 Schematic of two surfaces separated by a boundary layer of lubricant

Table A.2 Types of liquid lubricants and operating conditions limitations

Natural organics	Synthetic organics
Animal fat	Synthetic hydrocarbons
Vegetable oils	Esters
Mineral (petroleum oils)	Silicones
(Thermal stability $\sim$135 °C, vapor pressure $\sim 10^{-6}$–10^{-2} torr)	Silanes
	Polyphenyl ethers
	Perfluoropolyethers (Thermal stability $\sim$370 °C, and vapor pressure $\sim 10^{-12}$ torr)

natural organics, that exhibit thermal stability only to $\sim$135 °C and vapor pressure of 10^{-6} to 10^{-2} torr. They are excellent lubricants in relatively low load, low speed, and low temperature applications. Synthetic organics are used for more extreme conditions – high loads, speeds, and temperature, and lower vacuum pressures. As an example, perfluoropolyethanes have thermal stability to $\sim$370 °C and vapor pressure of $\sim 10^{-12}$ torr. They are used in vacuum grease, magnetic storage devices, and various microdevices that require extreme stability and are required to operate at extreme operating conditions

References

Bhushan, B. (1996). *Tribology and mechanics of magnetic storage devices* (2nd ed.). New York: Springer.

Bhushan, B. (1999). *Handbook of micro/nanotribology* (2nd ed.). Boca Raton, Florida: CRC Press.

Bhushan, B. (2001), *Modern tribology handbook, vol. 1—Principles of tribology; vol. 2—Materials, coatings, and industrial applications*. Boca Raton, Florida: CRC Press.

Bhushan, B. (Ed.). (2010). *Springer handbook of nanotechnology* (3rd ed.). Heidelberg, Germany: Springer.

Bhushan, B. (2013a). *Principles and applications of tribology* (2nd ed.). New York: Wiley.
Bhushan, B. (2013b). *Introduction to tribology* (2nd ed.). New York: Wiley.
Bhushan, B., & Gupta, B. K. (1991). *Handbook of tribology: Materials, coatings, and surface treatments*. New York: McGraw-Hill Book Company.
Bhushan, B., Israelachvili, J. N., & Landman, U. (1995). Nanotribology: Friction, wear and lubrication at the atomic scale. *Nature, 374*, 607–616.
Bhushan, B. (2011). *Nanotribology and nanomechanics I—Measurement techniques and nanomechanics, II—Nanotribology, biomimetics, and industrial applications* (3rd ed.). Heidelberg, Germany: Springer.

Subject Index

Note: Page numbers followed by *f* and *t* refer to figures and tables, respectively

B. Bhushan, *Biophysics of Skin and Its Treatments*, Biological and Medical Physics, Biomedical Engineering, DOI 10.1007/978-3-319-45708-6